THE DEVELOPMENT OF A HIGH PERFORMANCE LASER DOPPLER VELOCIMETER FOR FLUID MECHANICS AND ACOUSTICS RESEARCH APPLICATIONS

by

Neil McLay WILSON. B.Tech., B.Sc.

A thesis submitted for examination for the degree of

Master of Applied Science

University of Adelaide

Mechanical Engineering Department

July 1977.

TABLE OF CONTENTS

TABLE OF CONTENTS (Cont'd) Page

SUMMARY

It is the purpose of this present study to delineate the design criteria and operating principles of a high speed, digital laser Doppler velocimeter that is suitable for a large number of applications in fluid mechanics and acoustics research.

The shortcomings of existing techniques for the measurement of fluid and surface velocities are discussed and the advantages of laser Doppler systems are investigated. Relevant theoretical considerations are presented, with particular reference to the capabilities and limitations of light scattering techniques. A comprehensive review of the currently available methods for optical frequency biasing forms the basis for the development of a high diffraction efficiency acousto-optic cell. The essential and desirable characteristics of a high performance LDV are established and incorporated into the design and construction of a digital signal processing system that uses time domain analysis for the demodulation of velocity and real time information. The system is shown to offer solutions to the serious problems of directional aliasing; signal biasing; spectral broadening and signal dropout and is used with a modified Michelson interferometer to detect the surface velocity of a mechanically driven mirror.


LASER DOPPLER VELOCIMETER
accumul.
discrete
start
stop
reset
auto stop
O.T.O.B
LASER DOPPLER VELOCIMETER
POWER SUPPLY

STATEMENT

This thesis contains no material which has been accepted for the award of any other degree or diploma in any university and, to the best of my knowledge and belief, contains no material previously published or written by another person, except where due reference is made in the text.

ACKNOWLEDGEMENTS

There are many people whom I wish to thank for their assistance and guidance during the course of this project.

In particular, my supervisors, Drs. G.L. Brown and D.A. Bies, were a continual source of inspiration and enthusiastic encouragement. Their assistance, on so many occasions, was readily forthcoming and always in a sense of helpful criticism and direction. Professor H.H. Davis initially provided the opportunity for me to do this research and Professor S.E. Luxton, on appointment as Head of the Department, continued to provide the departmental assistance that was so necessary for the successful completion of the work.

Without the expertise and generous support of the electronics workshop, the project would have required a significantly longer time for completion and would have produced an instrument well below the standard achieved. My particular thanks are therefore directed to Messrs. H. Bode, P. Walker and G. Osborne of the Mechanical Engineering Department Electronics Workshop.

I am also grateful to Mr. A. Davis for the development and construction of the acousto-optic cell driver and for the assistance and advice that he willingly offered during the construction phase of the LDV.

In the latter stages of the project, Dr. C.J. Abell gave me invaluable assistance through helpful discussion and suggestion and companionship through those times when all seemed lost. For this I will always be indebted.

To Helen and my family, as always, I owe the greatest debt.

NOMENCLATURE

a - constant

a_r - receiver aperture radius

c - speed of light

d - fringe spacing; grating spacing

d_p - particle diameter

$\underset{\sim}{e}_i, \underset{\sim}{e}_s$ - incident, scattered light beam unit vectors

$\underset{\sim}{e}_{s_n}$ - n^{th} order scattered light beam unit vector (Fig.13)

f - frequency; focal length of a lens

f_a - acoustic frequency

f_b - bias frequency

f_D - Doppler frequency

f_i, f_s - frequency of incident, scattered light beam

f_m - modulating frequency

f_n - frequency of n^{th} order diffracted beam

f_o - laser frequency

g - Landé g factor

h - height of acoustic beam; Planck's constant

i_1, i_2 - intensity functions

j' - quantum number

$\underset{\sim}{k}_i, \underset{\sim}{k}_s$ - incident, scattered wave vectors; incident, scattered photon momentum vectors

ℓ - length of focal volume; length of laser cavity; solenoid length.

ℓ' - focal volume dimension (Fig.12); quantum number.

ℓ_a - effective probe length

ℓ_m - molecular mean free path

ℓ_r - minimum probe length

m_j' - total angular momentum quantum number

n - diffracted order; no. of particles; percentage error; no. of turns.

NOMENCLATURE (Cont'd)

p - phase retardation; elasto-optic coefficient (79)

p_1; $p_{>1}$ probabilities

r - pinhole radius; disc radius

s - Laplacian operator

s, s', s'_1, s'_2, s'_r - dimensions (Fig.8)

t - time; focal volume thickness

v - velocity

v_a - acoustic velocity

$\underset{\sim}{v}_p$ - particle velocity vector

v_f - fluid velocity; fringe velocity

w - beam width

x_1, x_2 - dimensions (Fig.8)

A - receiving optics aperture

D - e^{-1} diameter of unfocused laser beam

E_1, E_2 - intensities of the two incident beams

E_i, E_s - incident, scattered beam intensities

E_o, E_p - intensity at the centre, at a point p in the focal volume.

F - Gaussian F number

$\underset{\sim}{H}$ - magnetic field intensity

I - coil current

I_o - unattenuated laser intensity

I_θ - scattered beam intensity at an angle θ

$J_n(a)$ - Bessel ftn.

K - propogation constant of sound waves; Cunningham const.

$\underset{\sim}{K}_a$ - incident phonon wave vector.

K_s - scattering coefficient

NOMENCLATURE (Cont'd)

$\underset{\sim}{L}_i$ - orbital angular momentum vector.

M - figure of merit; constant.

N - no. of wavefronts; Avogadro's no. ; no. of cycles.

N_p - no. of scattering particles.

P - hydrostatic pressure

P_a - acoustic power

R - gas constant

R_r - receiver distance from scattering volume

$\underset{\sim}{S}_i$ - spin angular momentum vector.

T - absolute temperature; measurement interval.

$\bar{V}$ - mean velocity

V_c - size of the focal volume

W - acoustic beam width

Z - const.

α, β, γ - angular notation

β - modulation index

δ - radius of beam waist

δ_s - radius of scattered beam waist

ε - error due to particle inertia

η - refractive index; viscosity

η_1 - constant

θ - angle of incidence

θ_B - Bragg angle

θ_n - n^{th} order diffraction angle.

λ - optical wavelength

λ_i, λ_s - incident, scattered wavelengths.

$\underset{\sim}{\mu}$ - nett magnetic moment vector

μ_B - Bohr magneton.

NOMENCLATURE (Cont'd)

ν - kinematic viscosity

ν_o - laser frequency

ρ - density

ρ_p, ρ_f - particle, fluid density

τ_{min} - minimum time of flight

ϕ - angle of inclination of $\underset{\sim}{v}_p$; phase angle

ψ_i, ψ_s - incident, scattered wave functions.

ω - angular frequency.

ω_D - angular Doppler frequency

ω_i, ω_s - incident, scattered beam angular frequencies

ω_m - maximum angular turbulence frequency.

ΔA - dimension (Fig. 8)

ΔE - induced change in atomic energy levels.

Δf_c - laser cavity half width

Δf_D - Doppler spectral broadening; Doppler frequency deviation.

Δf_{Ne} - He-Ne laser half line width

Δs - half the length of the focal volume (Fig.8).

$\overline{\Delta x^2}$ - particle Brownian motion

Δy - fringe separation

$\Delta \nu$ - Zeeman frequency shift

$\Delta \Omega$ - solid angle subtended by receiving aperture.

κ - geometric constant

Λ - acoustic wavelength.

Ω - solid angle of acceptance.

CHAPTER ONE

VELOCITY MEASUREMENT IN FLUID MECHANICS AND ACOUSTICS RESEARCH

SUMMARY:

In fluid mechanics and acoustics research, localised, instantaneous velocity information has, hitherto, been obtained by means of hot-wire, differential pressure and piezo-electric devices. The problems associated with the application of these instruments to a number of important, current investigations are reviewed in this chapter and it is concluded that, even with the use of fast analogue circuitry and "state of the art" data acquisition systems, commonly encountered phenomena frequently preclude the use of conventional methods of measurement.

Laser Doppler velocimetry (LDV) is proposed as a system embodying a number of the essential characteristics of an ideal velocity measuring instrument, however analyses in this and subsequent chapters indicate that, while offering significant advantages over traditional techniques in some areas, the LDV cannot completely avoid disparagement. Some of these important advantages and disadvantages are summarised in tabular form as a comparative study of laser Doppler, hot-wire and piezo-electric accelerometer techniques.

1.1 CONVENTIONAL TECHNIQUES

For many years, the two general fields of fluid mechanics and acoustics have been the subject of a great deal

of experimental research. The measurement of velocity is of paramount importance in this research and extensive effort has been directed towards the development of instruments capable of determining localised, instantaneous velocity information. Hot wire and film anemometers and differential pressure devices have been used extensively in fluid mechanics, while the mainstay for acoustics research into surface vibrations has been the piezo-electric accelerometer.

These techniques have proved their utility in the investigation of fluid and acoustic phenomena, but their application to a number of current research problems is restricted by several inherent limitations. For example, while it was considered adequate to determine the temporal mean and standard deviation of a fluctuating velocity signal from a hot-wire in a turbulent flow, hot-wire anemometry had little requirement for very high frequency response circuitry or fast analogue to digital conversion systems. However, as suggested by Laufer (1975), such techniques are not sufficient to completely describe the nature and mechanics of turbulent flow. Recognizing this limitation, a great deal of work has been done with hot wires using very fast analogue circuits and high speed data acquisition systems. Although this has enabled a far more detailed analysis of time-series velocity data, other difficulties associated with the use of hot wires remain.

Similarly in acoustics, large, massive surfaces may be investigated by an accelerometer placed in contact with the surface with little fear of probe interaction. However, recent work in such fields as biological acoustics indicate

a requirement for a very sensitive, non contact measuring device that is capable of measurements in otherwise inaccessible regions. Time-averaged and real-time laser holography have been successfully used in such applications but, in general, suffer from the stringent requirement for non-random vibrations with displacements in excess of one half wavelength of incident light.

It is clear, therefore, that in both fluid mechanics and acoustics research, traditional techniques for velocity measurements are not adequate for all applications. In acoustics, we require an instrument capable of measuring non periodic velocities of surfaces that may be located in dangerous, corrosive, hot or inaccessible regions. A smaller discrimination than $\lambda/2$ is often required for high frequency components and the obviation of the need for transducer calibration would be a significant practical advantage. Such an instrument would, for example, be invaluable in the measurement of machine cutting tool vibrations; lateral or longitudinal vibrations of rotating bearings; structurally transmitted noise from boiler walls; and the behaviour of very thin diaphragms.

Recent fluid mechanics projects in the study of polymer flows, multiphase flows and atmospheric turbulence have similarly indicated the need for an alternative to hot wire anemometry. Material probe interaction in vortices and the unsuitability of hot wires for separated flows and supersonic velocities also inhibit the investigation of many important phenomena. The main disadvantages in the use of the (more popular) constant temperature hot wire

anemometer (CTHWA) are its non-linear response; requirement for calibration; directional ambiguity; and likelihood of flow disruption. Although the probes need not be calibrated if only qualitative or correlation measurements are required and the velocity components may, with difficulty, be resolved with multiple wire configurations, significant interaction and cross talk will result from placing the probes too close together. This characteristic interaction prohibits both the determination of two or more velocity components at the same point in the flow and the measurement of fluid velocity at any point close downstream from a material probe.

These disadvantages, together with the unsuitability of the CTHWA for flows with significant temperature perturbations and the fragile nature of thin wires suggest that, although hot wire anemometry remains useful for many applications, an alternative technique is required.

1.2 LASER DOPPLER VELOCIMETRY

The concepts of optical heterodyning and the Doppler frequency shift in light energy scattered from a moving particle or surface have been widely known for many years. However, it required the development of the continuous wave gas laser as a coherent light source with a very narrow bandwidth for these two phenomena to be successfully combined for the determination of fluid or surface velocities over large distances. Since Yeh and Cummins (1964) published their work on localized fluid flow measurement using laser Doppler methods, a very large number of LDV devices and techniques have been developed and reported. Such devices

possess a number of essential features of the ideal instrument for the examination of the structure of turbulent fluid flow. Foremost amongst these features of the LDV are; non interaction with the moving source; ability to make absolute velocity measurements without calibration; applicability to subsonic, supersonic and temperature varying flows and excellent frequency response and spatial resolution capabilities. Furthermore, the LDV is the only instrument that is capable of removing directional ambiguity in velocity signals without imposing a translational velocity to the transducer, relative to the flow. A number of techniques for achieving this through frequency biasing are discussed in Chapter 3.

In spite of these significant advantages over the CTHWA, the LDV is not the perfect solution. In considering an LDV system it is necessary to recognize the requirements for high quality optical components and vibration free mounting surfaces. Finite spectral broadening due to transmission and receiving apertures and low signal to noise ratios are also a problem in signal processing. Demodulation of the Doppler signal, particularly when derived from a discontinuous source, is very difficult and may lead to significant errors in interpretation. When used in acoustics applications, the vibrating surface must have a sufficiently high reflectivity while fluid flow investigations may require seeding of the flow with scattering sources of a suitable size.

Comparative studies on the performance of hot wire and laser Doppler systems have been published by a number of authors. One such study is presented in Table 1 and an analysis of these characteristics clearly indicates that for

a number of currently important applications, the LDV offers significant advantages over the use of hot wire techniques. Similarly, LDV and piezo-electric accelerometer methods for acoustic applications may be compared and Table 2 shows some of the highly desirable characteristics of the LDV for acoustic and vibration measurements. It is these advantages of the LDV that have prompted major investigations into the use and optimization of laser Doppler techniques for modern fluid mechanics and acoustics research.

TABLE 1

A Comparative Study on the Performance of a Hot Wire Anemometer and Symmetrical Laser Doppler Velocity Meter in Turbulence Characterization.

(From Mazumder, 1972)

	Hot Wire Anemometer	Symmetrical Laser Doppler Velocity Meter
System equation	$V = \sqrt{A+BU^m}$ (nonlinear) V = volts (output); U = velocity; A, B and m are constant in a small velocity interval. In general, A, B and m are functions of Reynolds No., gas density, conductivity, temp., etc.	f = KU (linear) f = frequency (Doppler shift) K = constant; U = velocity. Velocity measurements are not generally affected by the properties of the flow medium.
Calibration	Must be calibrated.	Provides a method for absolute measurement of velocity.
Sensing Volume	Wire dia ≃ 4μ, ℓ = 1.5mm; probe dia. = 3 mm (typical).	d ≃ 5μ; ℓ = 600μ (using corrected optics).
Interaction with the flow medium	Disturbs flow field.	No significant interaction.
Limits of measurement.	Measurement of velocity generally limited to 20 cm/sec to 150 m/sec for air.	Can be used both in subsonic and supersonic flow region.
Temperature limit	Normally designed for max fluid temp of 250°C.	Can be used at fluid temp up to 1000°C or higher depending on the Brownian motion of the aerosol particles.
Contamination	Corrosion and contamination affects calibration.	Scattering aerosol (range 0.5μ to 2μ dia) must be present within the fluid medium.
Frequency response	Upper frequency limit may be extended to approx. 50KHz with appropriate electronic circuitry.	Frequency response of a laser Doppler system is much higher compared to the highest turbulence frequency in fluid flows. However, scattering particle inertia may become significant in the regions of high local accelerations in supersonic flows.

TABLE 1 (Cont'd)

	Hot Wire Anemometer	Symmetrical Laser Doppler Velocity Meter
Directional ambiguity of 180° in velocity measurement.	Present	Can be eliminated by using a frequency biasing technique.
Noise Level	Generally equivalent to 0.5% turbulence intensity level at moderate velocity.	Approximately equivalent to 0.5% turbulence intensity, primarily caused by instrumental frequency broadening.
Remote measurement	Not possible	Remote sensing possible.

TABLE 2

Comparative Study of LDV and Piezo-electric Accelerometer Techniques in Acoustic and Vibration Measurements.

	Laser Doppler Velocimeter	Piezo-electric Accelerometer.
System Operation	Frequency to voltage conversion gives direct measurement of surface velocities.	Pressure fluctuations due to surface acceleration produce a fluctuating voltage on the crystal electrodes. Velocity is obtained by integration of this waveform.
Calibration	Absolute method.	Requires calibration.
Sensor Location	1. May be focussed onto a very small area. $A \simeq 300 \times 10^{-12} m^2$ 2. Simultaneous measurement at more than one point is difficult. 3. Non contact method: suitable for remote measurements.	1. Averages over the whole area of crystal surface. 2. Any number of transducers may be used simultaneously. 3. Contact method. Not suitable for harsh environments.
Loading	No significant loading effects.	Transducer may load the vibrating surface.
Temperature Limit.	May be used on hot surfaces, but optical filtering may be required.	Selected materials, e.g. lead zirconate, may be used at temperatures well in excess of 100°C.
Directional Ambiguity	Requires frequency biasing mechanism or similar technique.	Inherently bidirectional response.
Frequency Response	Frequency response is well in excess of acoustic range.	Typically 1 Hz to 25KHz (B+K model # 4344)
Sensitivity	Depends upon optical configuration and laser wavelength. $f_D = \frac{1}{\lambda_i}(\underset{\sim}{e}_s - \underset{\sim}{e}_i) \cdot \underset{\sim}{v}_p$	3mV/g; with a maximum acoustic sensitivity of 0.01g. (B+K model # 4344)

CHAPTER TWO

LDV METHODS, LIMITATIONS AND CAPABILITIES

SUMMARY:

With the development of laser Doppler velocimetry as a powerful measurement technique in fluid mechanics and acoustics, many valuable contributions have been made to the theory of light scattering and optical heterodyning. A resume of the important results of these investigations is included in this chapter in order that a basis for the design of a high performance LDV may be established.

The light scattering mode geometries are developed with a standardised notation to indicate the similarity in the results for the three commonly used configurations. These, in turn, are shown to be particular solutions of a generalised expression for the distribution of light in the focal volume. Criteria for the determination of the effective focal volume dimensions are derived with particular reference to the critical nature of the size and location of the receiving optics pinhole aperture.

Spectral broadening of the Doppler signal is discussed in terms of optimum particle specifications; finite aperture broadening; finite signal lifetime and velocity gradients in the focal volume. It is shown that even if the scattering particle size is strictly controlled and the receiving aperture is decreased to a minimum, the conditions for reducing the spectral broadening due to the two remaining sources

are mutually contradictory. The proposed compromise solution, i.e. a fringe crossing detector that requires a scattering particle to intersect a minimum number of interference fringes is shown to alter the effective focal volume dimensions which, in turn, may lead to the possibility of directional aliasing if the interference fringes in the focal volume are stationary. When the fringes are set in motion by means of an optical biasing technique, a similar analysis demonstrates that the maximum detectable particle velocity may be severely restricted if the biasing frequency is too low.

All of these conditions and restrictions are shown in subsequent chapters to weigh heavily in the consideration and design of the operating parameters for an LDV system.

2.1 OPTICAL HETERODYNING

In wave vector notation, the Doppler frequency shift that results from the scattering of a monochromatic light beam from a moving object may be expressed by:-

$$f_D = \frac{1}{2\pi} (\underset{\sim}{k}_s - \underset{\sim}{k}_i) \cdot \underset{\sim}{v}_p \qquad (1)$$

where $\underset{\sim}{v}_p$ is the instantaneous velocity of the object; $\underset{\sim}{k}_s$ and $\underset{\sim}{k}_i$ are, respectively, the wave vectors of the scattered and incident light beams; and f_D is the Doppler frequency shift. If $\underset{\sim}{e}_s$ and $\underset{\sim}{e}_i$ are the corresponding unit vectors for the scattered and incident light beams and λ_s and λ_i represent the scattered and incident optical wavelengths, equation (1) may be written as:-

$$f_D = \frac{1}{2\pi} \left(\frac{2\pi}{\lambda_s} \cdot \underset{\sim}{e}_s - \frac{2\pi}{\lambda_i} \cdot \underset{\sim}{e}_i\right) \cdot \underset{\sim}{v}_p \qquad (2)$$

Since, for non relativistic motion, $|v_p| << c$, where c is the velocity of light; $\frac{c}{f_D} >> \lambda_i$, hence $\lambda_s \simeq \lambda_i$ and equation (2) may be simplified to:-

$$f_D = \frac{1}{\lambda_i} (\underset{\sim}{e}_s - \underset{\sim}{e}_i) \cdot \underset{\sim}{v}_p \qquad (3)$$

In addition, $f_D = f_s - f_i$, where f_s and f_i are respectively the frequencies of the scattered and incident light beams, so the frequency of the scattered light energy, f_s, may be determined for any scattering process and can be expressed as:-

$$f_s = f_D + f_i = \frac{1}{\lambda_i} (\underset{\sim}{e}_s - \underset{\sim}{e}_i) \cdot \underset{\sim}{v}_p + f_i \qquad (4)$$

Although this analysis applies to all non-relativistic motion, the lack of resolution of spectrometric and other techniques prohibits the direct measurement of the wavelength or frequency shift in many applications of practical interest. The solution to this problem is the principle of optical heterodyning where the difference in scattered and incident frequencies is detected by means of a square law detector.

The incident and scattered light beams can be represented by the functions $\psi_i(t) = E_i \cos \omega_i t$ and $\psi_s(t) = E_s(t) \cos (\omega_s t + \phi)$ respectively; where ω_i and ω_s are the incident and scattered angular frequencies and ϕ is an arbitrary phase angle. If the two beams are incident on a photodetector with a square law response, the resulting photo-current is given by:-

$$i(t) = a \left| \psi_i(t) + \psi_s(t) \right|^2 \qquad (5)$$

where a is a constant and i(t) is the instantaneous current.

Expanding equation (5);

$$i(t) = a|E_i \cdot \cos \omega_i t + E_s(t) \cdot \cos (\omega_s t + \phi)|^2$$

i.e. $$i(t) = a[E_i^2 \cdot \cos^2 \omega_i t + E_s^2(t) \cdot \cos^2(\omega_s t + \phi) + 2E_i E_s(t) \cos (\omega_i t) \cos (\omega_s t + \phi)]$$

hence $$i(t) = a[\frac{1}{2} E_i^2 + \frac{1}{2} E_s^2(t) + \frac{1}{2} E_i^2 \cos 2\omega_i t + \frac{1}{2}E_s^2(t) \cos 2(\omega_s t + \phi) + E_i E_s(t)\cos(\omega_i t + \omega_s t + \phi) + E_i E_s(t) \cos (\omega_i t - \omega_s t - \phi)]$$

If it is assumed that $|E_i| >> |E_s|$ and that the bandwidth of the detector is well below the optical frequencies ω_i and ω_s, an effective average of the high frequency terms in this expansion will enable the detector current to be approximated by;

$$i(t) = a[\frac{1}{2} E_i^2 + E_i E_s(t) \cos (\omega_i t - \omega_s t - \phi)] \quad (6)$$

The first term in equation (6) is dependent only upon the amplitude of the incident beam and therefore contributes to the DC component of the detector current. The remaining term is dependent upon the amplitudes of both the incident and scattered beams and also has an AC component, the angular frequency of which is equal to the difference in frequencies of the scattered and incident beams. The output waveform is therefore a sinusoid of frequency f_D superimposed on an offset voltage determined by the incident light intensity. This difference frequency is directly proportional to the transverse component of the particle velocity and it is the function of the LDV detector circuit to demodulate and interpret the Doppler frequency as velocity data.

2.2 MODE GEOMETRIES

As indicated by equation (3), the magnitude of the Doppler frequency shift is a function of scattered and incident beam orientation. This interrelationship has resulted in the development of a very large number of ingenious optical configurations and light collection techniques, all of which may by classified according to the resulting light intensity distribution within the focal volume. Analyses such as those presented by Durst and Whitelaw (1971) generally distinguish the following three modes of operation:-

(a) Reference Mode (local oscillator heterodyning)

(b) Fringe Mode (differential heterodyning)

and (c) Doppler Mode (symmetrical heterodyning)

which are schematically represented in Figure (1)

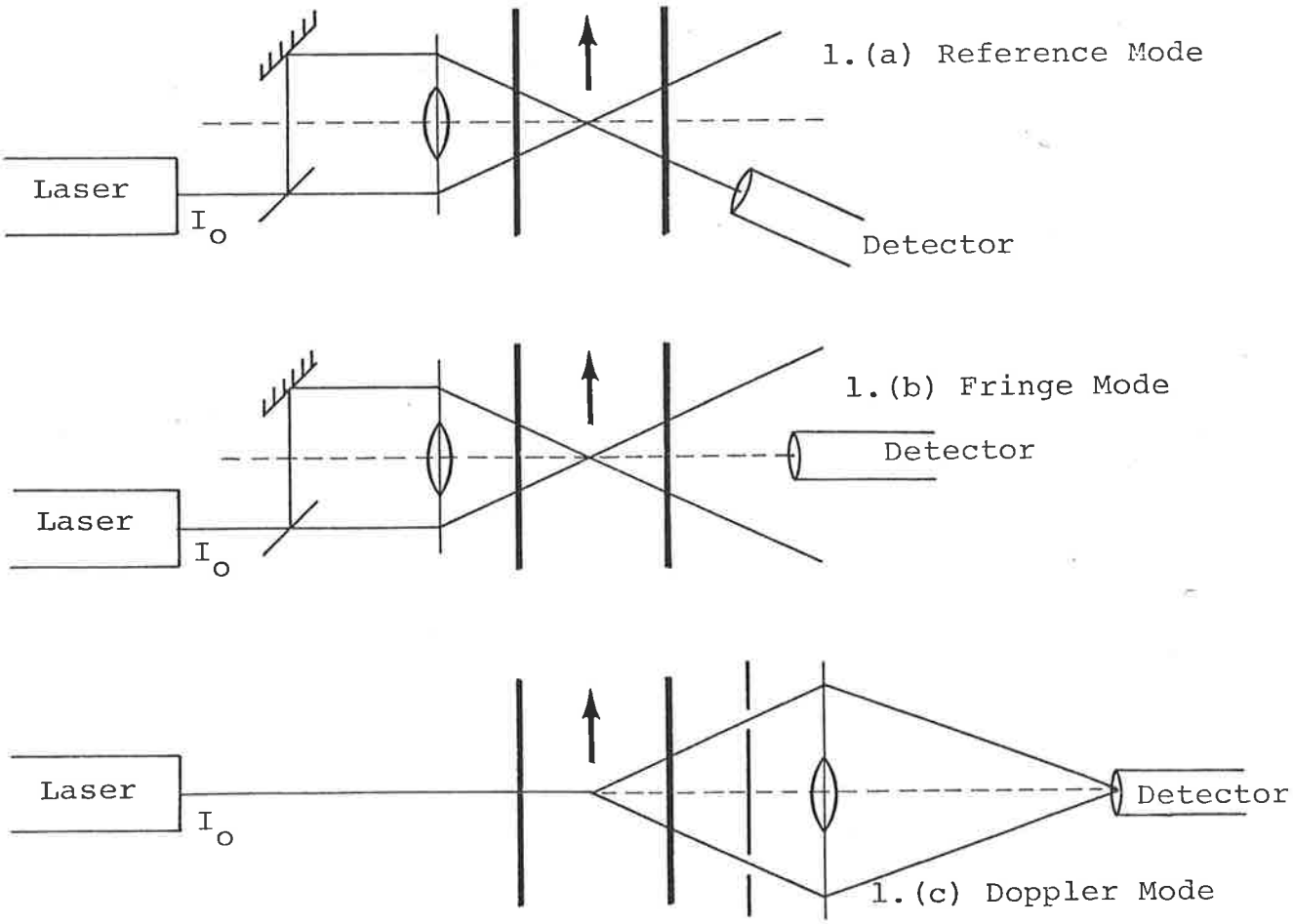

Figure 1. Mode Geometries

2.2.1. Reference Mode Geometry

When the LDV is used in the reference mode, the original laser beam, I_o, is split into an intense (typically 0.95 I_o) scattering beam and a weak (typically 0.05 I_o) reference beam which are focussed to a common point in the flow. The photodetector is placed in line with the reference beam and detects both the reference beam and light from the scattering beam that is scattered in the reference direction. Optical mixing of these two light sources results in a Doppler signal that is a function of both the velocity component of the scattering particle and the position of the photodetector.

The reference mode geometry is illustrated in Figure (2a) where $\underset{\sim}{e}_{i_1}$ and $\underset{\sim}{e}_{i_2}$ represent the unit vectors for the scattering beam (#1) and reference beam (#2) respectively and $\underset{\sim}{e}_{s_1}$ represents the unit vector for the scattered light from beam #1 in the direction of the reference beam.

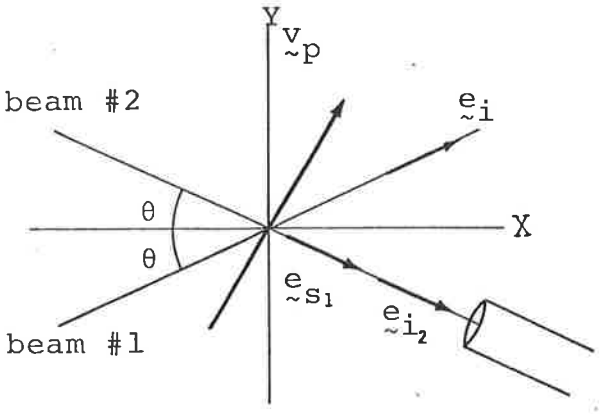

Fig. 2a.

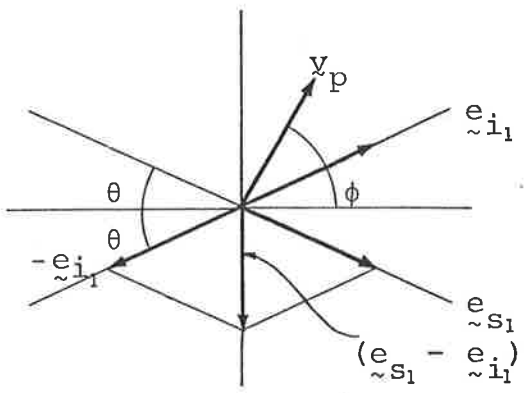

Fig. 2b.

Figure 2. Reference Mode Geometry

For this configuration, the Doppler frequency is given by:-

$$f_D = f_{s_1} - f_{i_2} \qquad (7)$$

where f_{s_1} is the frequency of the scattered light from beam #1 and f_{i_2} is the frequency of the incident light from beam #2. Application of equation (4) to this configuration yields:

$$f_{s_1} = \frac{1}{\lambda_i} (\underset{\sim}{e}_{s_1} - \underset{\sim}{e}_{i_1}) \cdot \underset{\sim}{v}_p + f_{i_1} \qquad \text{and hence}$$

$$f_D = \frac{1}{\lambda_i} (\underset{\sim}{e}_{s_1} - \underset{\sim}{e}_{i_1}) \cdot \underset{\sim}{v}_p + (f_{i_1} - f_{i_2})$$

From the geometry of Figure (2b),

$$(\underset{\sim}{e}_{s_1} - \underset{\sim}{e}_{i_1}) \cdot \underset{\sim}{v}_p = -2 \sin\theta \cdot v_p \cdot \cos(\phi + 90).$$
$$= +2 \cdot v_p \cdot \sin\theta \cdot \sin\phi$$
$$= 2v_{p_y} \cdot \sin\theta$$

therefore $$f_D = \frac{2 \cdot v_{p_y}}{\lambda_i} \cdot \sin\theta + (f_{i_1} - f_{i_2}) \qquad (8)$$

The significance of the $(f_{i_1} - f_{i_2})$ term in equation (8) is the basis of the directional ambiguity problem that is inherent to laser Doppler techniques. If the incident frequencies of both beams are the same; $f_{i_1} = f_{i_2}$ and equation (8) reduces to:

$$f_D = \frac{2 \cdot v_{p_y}}{\lambda_i} \cdot \sin\theta \qquad (9)$$

Provided that the velocity component in the y direction, v_{p_y}, is always positive ($0 < \phi < 180^o$) the Doppler frequency derived from equation (9) is positive. If, however, a flow reversal is experienced and v_{p_y} becomes negative ($180^o < \phi < 360^o$) equation (9) yields a negative Doppler frequency:

$$f_D = \frac{-2 v_{p_y}}{\lambda_i} \cdot \sin\theta$$

Since the photodetector current is proportional to the absolute difference between the two input frequencies, equation (9) is more accurately written as:-

$$f_D = \left| \frac{2 \cdot v_{p_y}}{\lambda_i} \cdot \sin \theta \right| \qquad (10)$$

and the LDV is therefore seen to be incapable of resolving the sign of the velocity component. In oscillatory or high turbulence flows, such a restriction would be prohibitive and it is for these applications that a bias frequency needs to be provided.

Referring to equation (8), if $f_{i_1} \neq f_{i_2}$ then the flow reversal just described would result in a frequency variation with respect to a bias frequency, f_b (equal to the difference between f_{i_1} and f_{i_2}). Equation (8) is therefore modified to:

$$f_D = (f_{i_1} - f_{i_2}) \pm \frac{2v_{p_y}}{\lambda_i} \cdot \sin \theta$$

or

$$f_D = f_b \pm \frac{2v_{p_y}}{\lambda_i} \cdot \sin \theta \qquad (11)$$

and the system is now capable of resolving the directional ambiguity.

A number of different techniques for providing a suitable bias frequency for this method of removing the directional ambiguity are described in Chapter 3. It should also be noted, however, that recent work, such as that of Müller (1974), suggests an alternative method to the bias frequency technique whereby two photodetectors are used to determine the flow direction by a comparison of the phase difference in the two heterodyned signals.

2.2.2 Fringe Mode Geometry

Using the same notation, the fringe mode configuration illustrated in Figures (1b) and (3) may be similarly analysed.

As was the case in reference mode, the LDV in fringe mode uses a focal volume formed by the intersection of two light beams. In this case, the intensities of both beams are approximately equal and the focal volume may be considered to consist of a series of interference bands of consecutive light and dark fringes. As the particles following the flow enter the focal volume and cross the fringes, the light is scattered from both the incident beams and is detected by a photosensitive device placed at any convenient location. One of the main advantages of the fringe mode operation is the independence of observed Doppler frequency and photodetector location. This independence is indicated by the following analysis of Figure (3).

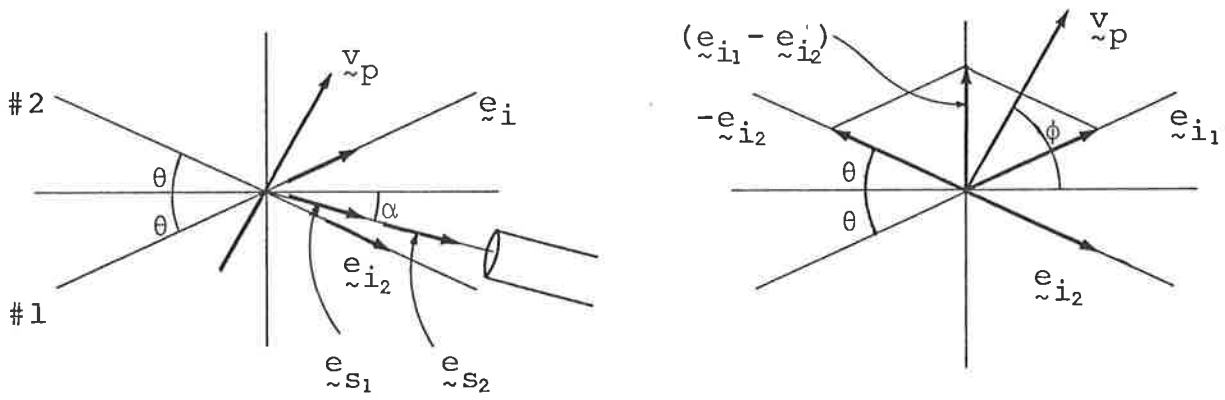

Fig. 3a. Fig.3b.

Figure 3. Fringe Mode Geometry

For fringe mode, from Figure (3a) and equation (4),

$$f_D = f_{s_2} - f_{s_1} \tag{12}$$

where $f_{s_2} = \frac{1}{\lambda_i} (\underset{\sim}{e}_{s_2} - \underset{\sim}{e}_{i_2}) \cdot \underset{\sim}{v}_p + f_{i_2}$

and $$f_{s_1} = \frac{1}{\lambda_i} (\underset{\sim}{e}_{s_1} - \underset{\sim}{e}_{i_1}) \cdot \underset{\sim}{v}_p + f_{i_1}$$

Therefore; $$f_D = \frac{1}{\lambda_i} (\underset{\sim}{e}_{s_2} - \underset{\sim}{e}_{i_2}) \cdot \underset{\sim}{v}_p + f_{i_2} - \frac{1}{\lambda_i} (\underset{\sim}{e}_{s_1} - \underset{\sim}{e}_{i_1}) \cdot \underset{\sim}{v}_p - f_{i_1}$$

but $\underset{\sim}{e}_{s_1} \equiv \underset{\sim}{e}_{s_2}$, hence

$$f_D = \frac{1}{\lambda_i} (\underset{\sim}{e}_{i_1} - \underset{\sim}{e}_{i_2}) \cdot \underset{\sim}{v}_p + (f_{i_2} - f_{i_1})$$

or $$f_D = \frac{1}{\lambda_i} (\underset{\sim}{e}_{i_1} - \underset{\sim}{e}_{i_2}) \cdot \underset{\sim}{v}_p + f_b \qquad (13)$$

From Figure (3b),

$$(\underset{\sim}{e}_{i_1} - \underset{\sim}{e}_{i_2}) \cdot \underset{\sim}{v}_p = 2 \sin\theta \cdot v_p \cdot \cos (90 - \phi).$$

hence $$f_D = \frac{1}{\lambda_i} \cdot 2 v_p \sin \phi \cdot \sin \theta + f_b \qquad (14)$$

For the same reasons as were advanced for the previous analysis, the most general form of equation (14) is given by:

$$f_D = f_b \pm \frac{2 \cdot v_{p_y} \sin \theta}{\lambda_i} \qquad (15)$$

which is identical to equation (11) for the reference mode configuration. It should now be noted, however, that the Doppler frequency expressed in equation (13) is independent of the scattering angle and hence the position of the photo-detector. This independence and the provision of maximum signal to noise ratio for single particle scattering constitute the major practical advantages of the fringe mode configuration.

2.2.3 Doppler Mode Geometry

For the Doppler mode configuration, the focal volume is illuminated with a single intense beam and the detector receives light from two apertures in a field stop. This technique is illustrated in Figures (1c) and (4) and may be

analysed in the following way:

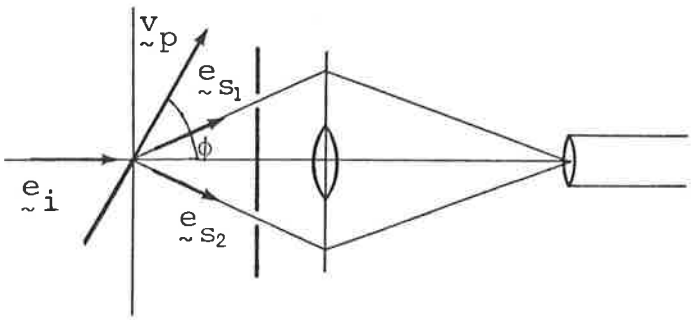

Fig. 4a.

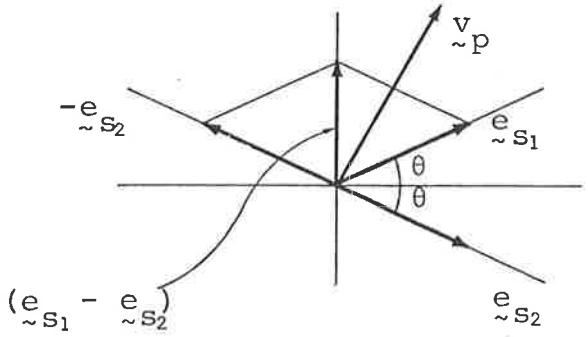

Fig. 4b.

Figure 4 Doppler Mode Geometry

From Figure (4a),

$$f_D = f_{s_1} - f_{s_2} \qquad (16)$$

$$= \frac{1}{\lambda_i}(\underset{\sim}{e}_{s_1} - \underset{\sim}{e}_i)\cdot\underset{\sim}{v}_p + f_i - \frac{1}{\lambda_i}(\underset{\sim}{e}_{s_2} - \underset{\sim}{e}_i)\cdot\underset{\sim}{v}_p - f_i$$

$$\therefore \quad f_D = \frac{1}{\lambda_i}(\underset{\sim}{e}_{s_1} - \underset{\sim}{e}_{s_2})\cdot\underset{\sim}{v}_p$$

but $(\underset{\sim}{e}_{s_1} - \underset{\sim}{e}_{s_2})\cdot\underset{\sim}{v}_p = 2\sin\theta\cdot v_p\cdot\cos(90-\phi)$, from Figure 4b,

hence $f_D = 2\cdot v_p\cdot\frac{\sin\phi}{\lambda_i}\cdot\sin\theta$

i.e. $$f_D = \frac{2v_{p_y}}{\lambda_i}\cdot\sin\theta \qquad (17)$$

It can be seen from this analysis that the observed Doppler frequency is a function of the scattering angle, θ, and hence will be dependent upon the position of the photodetector and the apertures in the field stop. The Doppler mode also differs from the reference and fringe configurations in that only one incident beam is used and hence no fringe pattern is established in the focal volume. This implies that no bias frequency can be imposed on the Doppler signal and hence the technique is incapable of detecting bidirectional flows. For applications where this is not important, however, the simplicity and ease of alignment of the Doppler mode constitute significant practical advantages.

Although the systems described above have been analysed for the forward scattering mode, back scattering configurations, where the light is collected at an angle greater than 90^{o} from the incident beam direction, are also commonly used. These techniques are useful for long range anemometry and for applications where access to only one side of the test section is available. The major disadvantage with back scattering techniques is a reduction of the signal strength by up to two orders of magnitude over a comparable forward scattering system.

2.3 DISTRIBUTION OF LIGHT IN THE FOCAL VOLUME.

As described by Durst and Whitelaw (1971), the light intensity distribution in the region of interference between two focused Gaussian light beams may be described by the function:-

$$E_p^2 = E_o^2 \left[1 + \left(\frac{E_2}{E_1}\right)^2 + 2 \left(\frac{E_2}{E_1}\right) \cdot \cos \left(\frac{4\pi}{\lambda} y \sin\theta\right) \exp \left(-\frac{y^2}{\delta^2}\right)\right] \quad (18)$$

where E_p is the light intensity at any point P in the volume.

E_o is the light intensity at the geometric centre of the volume

E_1, E_2 are the intensities of the two incident beams.

y is the distance of P from the central axis

and θ is the half angle between beams.

Assuming diffraction limited optics, δ, the radii of the beam waists at the e^{-1} points for each of the beams in the focal plane may be determined from diffraction theory and expressed as:

$$\delta = \frac{\lambda f}{\pi D} \quad (19)$$

where f is the focal length of the lens

D is the e^{-1} diameter of the unfocussed laser beam

and λ is the incident wavelength.

Since the beam edges occur at approximately 2D, the Gaussian f number for the lens may be defined as

$$F = \frac{f}{2D} \tag{20}$$

and equation (19) may alternatively be written as:

$$\delta = \frac{2 \cdot \lambda \cdot F}{\pi} \tag{21}$$

The region of intersection is illustrated schematically as the polygon ABCD in Figure (5), where O is the geometric centre and $\underset{\sim}{e}_1$ and $\underset{\sim}{e}_2$ are the unit vectors in the direction of the two light beams.

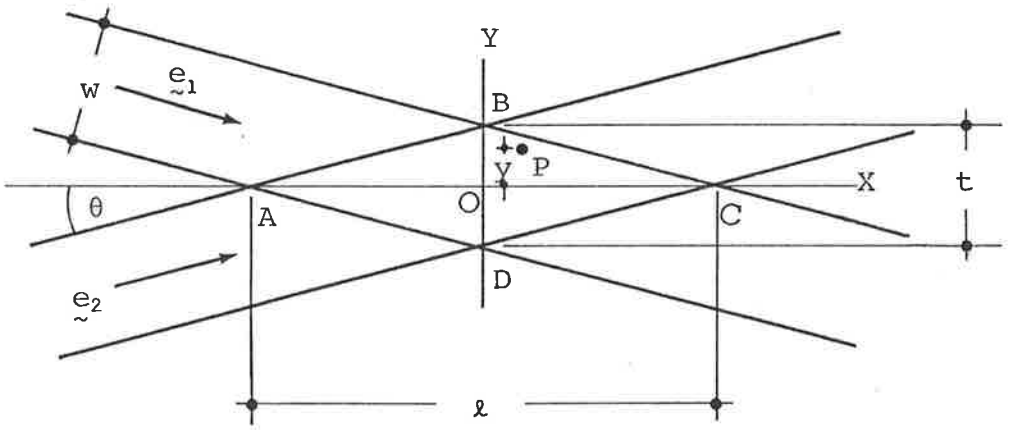

Figure 5. Region of Intersection

Solution to equation (18) has been sought for the three special conditions when:

(a) $E_1 = E_2$; i.e. the incident beams are of equal intensity and equation (18) simplifies to:

$$E_p^2 = 4\, E_o^2 \cos^2\left(\frac{2\pi}{\lambda} \cdot y \sin\theta\right) \cdot \exp\left(-\frac{Y^2}{\delta^2}\right) \tag{22}$$

For this condition, the fringe pattern has maximum contrast and is illustrated in Figure (6a). The separation between

fringes is given by the relationship:

$$d = \Delta y = \frac{\lambda}{2\sin\theta} \tag{23}$$

and this configuration constitutes the fringe pattern for laser Doppler systems operating in the fringe mode.

(b) $E_1 >> E_2$; For this condition, the fringe pattern is still present but is much less clearly defined than for the fringe mode above. The spatial separation of the fringes is still given by equation (23) but a scattering particle that traverses the focal volume will, for this configuration, produce a small fluctuating signal, superimposed on a relatively large DC component. This corresponds to the reference beam mode where E_1 is the scattering beam and E_2 the reference beam.

The intensity distribution for the reference mode is illustrated in Figure (6b).

(c) $E_2 = 0$. If only one beam is present, equation (18) reduces to:

$$E_p^2 = E_o^2 \cdot \exp\left(-\frac{y^2}{\delta^2}\right) \tag{24}$$

which is the expression derived by Durst and Whitelaw (1969) for the light intensity distribution in the focal volume of a lens for an incident beam with Gaussian distribution. This distribution is shown in Figure (6c) from which it is obvious that no interference fringe pattern is established. A scattering particle that traverses this focal volume will produce a Doppler frequency only when heterodyning occurs between scattered beams in two different directions. This configuration is used by instruments operating in the Doppler mode.

Although the light distribution within the focal volume is different for each of the three modes described, the nature of the Doppler signal derived from a scattering particle is similar. As the particle traverses the focal volume, the heterodyne process produces a "Doppler burst", schematically represented in Figure 7, where the envelope curve results from the Gaussian intensity distribution of the light in the focal volume and the carrier signal constitutes the Doppler frequency for the moving particle.

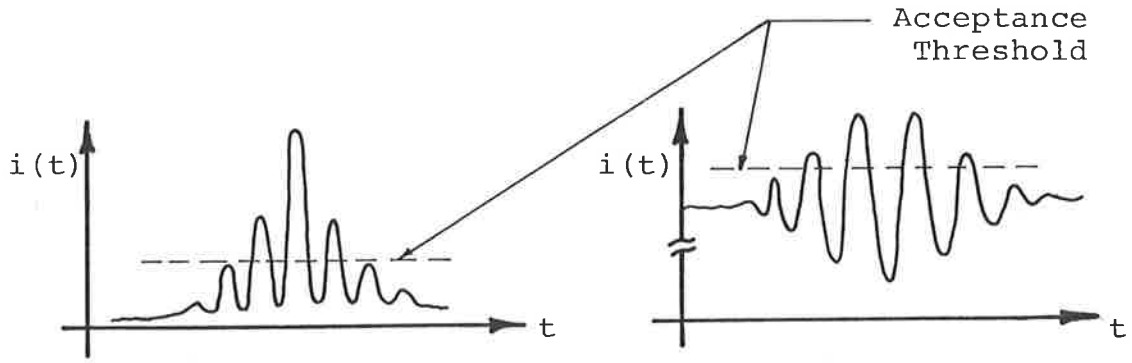

Fig. 7a. Fig. 7b.

Figure 7: Typical Doppler Signals.

In the case of the reference and fringe modes, where interference fringes "exist" in the focal volume, each period of the Doppler signal may be considered as corresponding to the motion of the particle through an interference fringe. Determination of the Doppler frequency and a knowledge of the fringe spacing will therefore immediately yield the normal component of the particle velocity. For the Doppler mode, the particle velocity is determined from the geometry of Figure (4) and the application of equation (17).

2.4 FURTHER OPTICAL CONSIDERATIONS

2.4.1 Focal Volume Size

Although it was claimed in Table 1 that the sensing volume of the LDV and hot wire anemometer were comparable, these small measurement volumes may only be achieved for the LDV by an appropriate selection of transmitting and receiving optical components.

Assuming that the focusing of the laser beams at the focal volume is diffraction limited, equation (19) defines the beam radii at the e^{-1} points as $\delta = \frac{\lambda f}{\pi D}$. If a total beam diameter of 4δ is assumed to include all of the light energy, the dimensions of the region of intersection of Figure (5) are determined as follows:

$$\begin{aligned} \omega &= 4\delta \\ \ell &= \frac{\omega}{\sin\theta} = \frac{4\delta}{\sin\theta} \\ t &= \frac{\omega}{\cos\theta} = \frac{4\delta}{\cos\theta} \end{aligned} \qquad (24)$$

As a typical example, for $\lambda = 632.8$nm; $f = 75$ mm; $D = 2$ mm and $\theta = 2^{o}$;

$\delta = 7.55\mu$m; $\ell = 865\mu$m; $t = 30\mu$m

Since the calculation was for the total light energy in the two incident beams, the effective focal volume will, in practice, be smaller than these dimensions. This results from the requirement to set some form of acceptance threshold on the Doppler burst in order to exclude the random noise that is detected during the period when no scattering particle is traversing the focal volume. This implies that only the centre-most portion of the focal volume is used for actual

signal detection and the effective dimensions of the region of intersection are thereby reduced.

Although limitation of the region of intersection is a very useful way of reducing the effective probe volume, this technique cannot be used for the Doppler mode and will not prevent spectral broadening due to Doppler scattering from the incident beams outside of the region of intersection. It is clear, therefore that a further restriction on the sensing volume is necessary and that this restriction must be provided by an appropriate selection of the receiving optical components.

Figure (8) shows a typical configuration for the collection of scattered light over an aperture with a maximum radius of (A+ΔA) at a distance s from the focal volume.

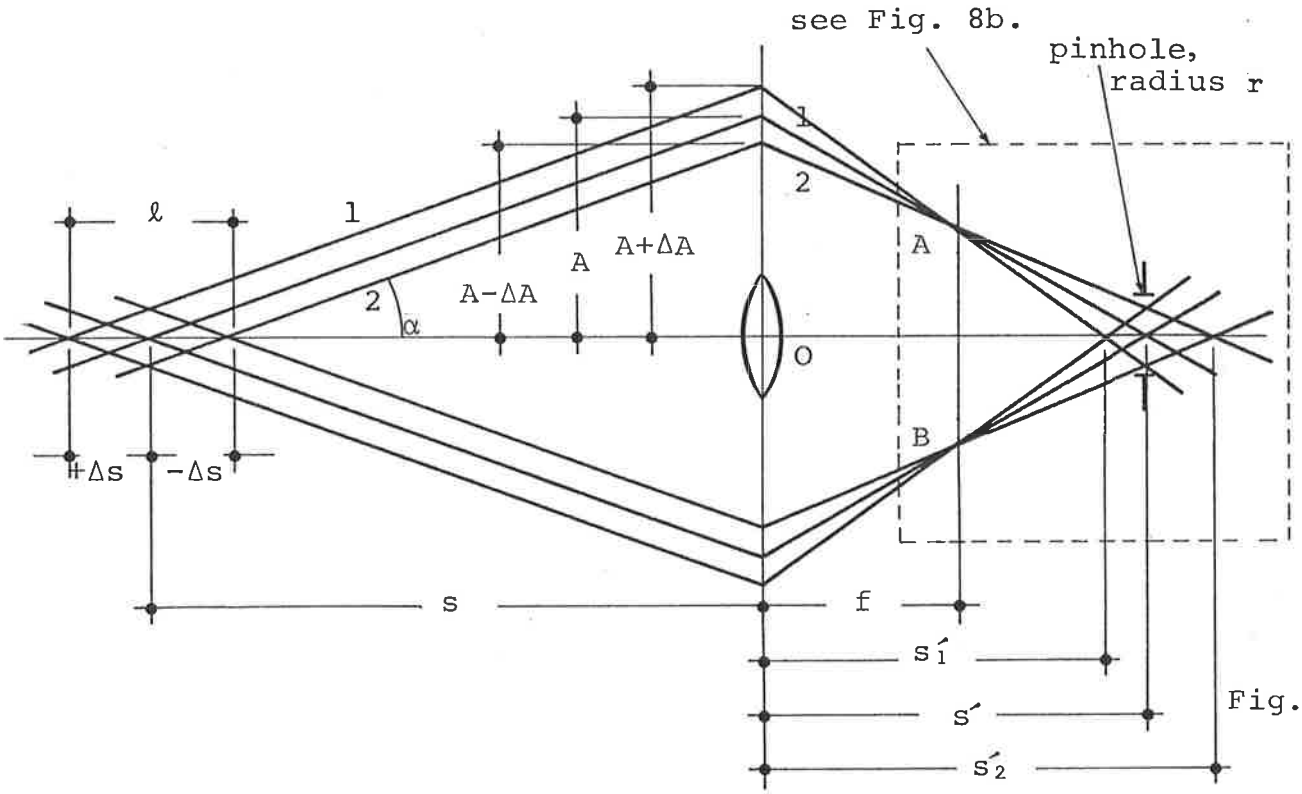

Fig.8a

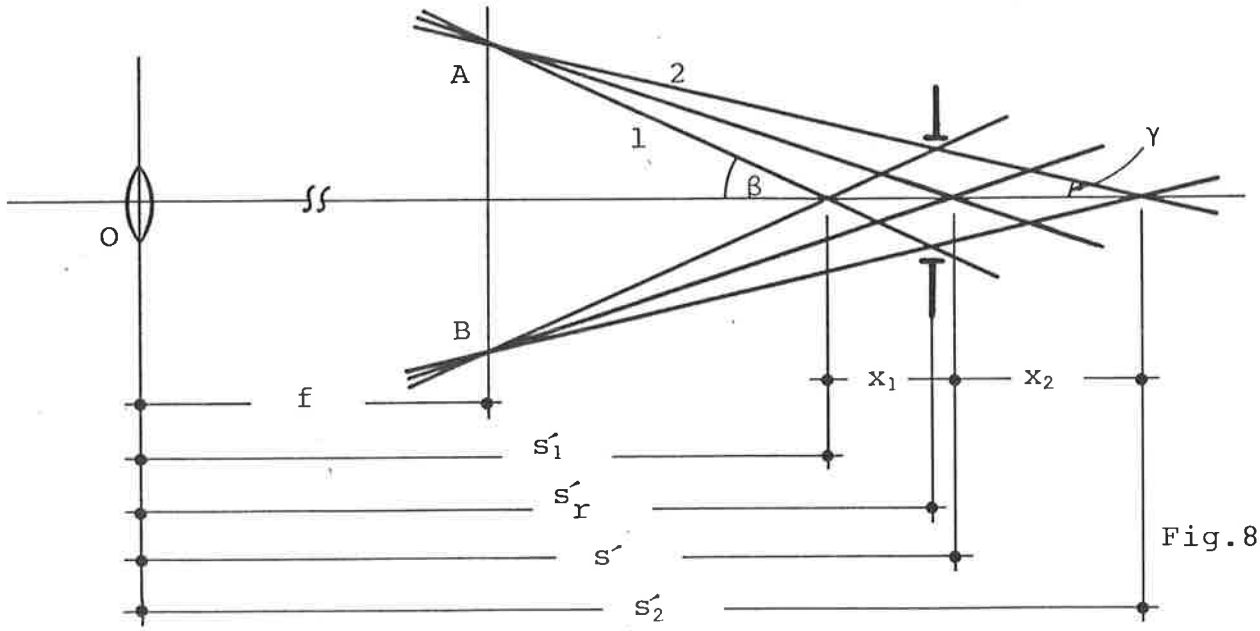

Fig.8b.

Figure 8. Receiving Optics

Assuming no spherical aberration in the lens at the origin O, the effect of the pinhole of radius r placed at a distance s_r in the image space is to restrict the object field in the paraxial direction to the region (s+Δs) to (s-Δs). Any ray emanating from the focal volume and passing through the maximum aperture of radius A+ΔA will also pass through the pinhole. A ray emanating from any other point in the object space will not pass through the pinhole restriction.

Using the lens formula for thin lenses and the geometry of Figures (8a) and (8b), the following relationships can be established:-

$$\frac{1}{s} + \frac{1}{s'} = \frac{1}{f}$$

$$\frac{1}{s+\Delta s} + \frac{1}{s'_1} = \frac{1}{f} \qquad (25)$$

$$\frac{1}{s-\Delta s} + \frac{1}{s'_2} = \frac{1}{f}$$

$$\text{and} \quad \tan\alpha = \frac{A}{\ell} = \frac{A+\Delta A}{s+\Delta s} = \frac{A-\Delta A}{s-\Delta s}$$

$$\tan\beta = \frac{r}{x_1} = \frac{A+\Delta A}{s_1'} \qquad (26)$$

$$\tan\gamma = \frac{r}{x_2} = \frac{A-\Delta A}{s_2'}$$

These equations may be rearranged to give:

$$x_1 = \frac{rs_1'}{A+\Delta A} \; ; \qquad x_2 = \frac{rs_2'}{A-\Delta A}$$

where $s_1' = \frac{f(s+\Delta s)}{s+\Delta s-f}$ and $s_2' = \frac{f(s-\Delta s)}{s-\Delta s-f}$

However $(s_2' - s_1') = (x_1 + x_2)$; hence

$$\frac{f(s-\Delta s)}{(s-\Delta s-f)} - \frac{f(s+\Delta s)}{(s+\Delta s-f)} = \frac{r}{(A+\Delta A)} \cdot \frac{f(s+\Delta s)}{(s+\Delta s-f)} + \frac{r}{(A-\Delta A)} \cdot \frac{f(s-\Delta s)}{(s-\Delta s-f)}$$

But $$\frac{(s+\Delta s)}{(A+\Delta A)} = \frac{(s-\Delta s)}{(A-\Delta A)} = \frac{1}{\tan\alpha}$$

$\therefore$

$$\frac{(s-\Delta s)}{(s-\Delta s-f)} - \frac{(s+\Delta s)}{(s+\Delta s-f)} = \frac{r}{\tan\alpha}\left[\frac{1}{(s+\Delta s-f)} + \frac{1}{(s-\Delta s-f)}\right] \qquad (27)$$

Expansion and simplification of equation (27) yields

$$\Delta s = \frac{r}{\tan\alpha} \cdot \frac{(s-f)}{f} \qquad (28)$$

hence the total length of the focal volume will be given by:-

$$\ell = \text{focal volume length} = \frac{2r}{\tan\alpha} \cdot \frac{(s-f)}{f} \qquad (29)$$

Now $\tan\alpha = \frac{A}{s}$ and $\frac{f}{A} = F$, the Gaussian f number for the lens, hence:

$$\ell = \frac{2\,r\,s\,(s-f)}{A\,f} = \frac{2r\,s\,(s-f)F}{f} \qquad (30)$$

In addition to this limitation on the object field length, the effective focal volume may also be reduced in

thickness by considering diffraction limited optics for the receiving aperture. As for the incident beams, the minimum waist radius of the scattered beam is given by equation (19) as $\delta_s = \frac{\lambda f}{\pi D}$ at the e^{-1} points. The thickness of the effective scattering volume will therefore be limited to

$$t = \frac{4 \lambda f}{\pi 2A} \qquad (31)$$

where f is the focal length of the receiving lens and 2A is the diameter of the receiving aperture.

To evaluate equations (30) and (31) with the following typical figures:

F = 11, f = 3.5cm; r = 12.5μm; and s = 10 cm,

it can be seen that the length of the sensing volume is limited to:

$$\ell = \frac{2 r s (s-f) F}{f^2} = \frac{2x12.5x10(10-3.5)x11x10^{-6}}{(3.5)^2}$$

i.e. ℓ = 1.46 mm,

while the minimum possible thickness is given by:-

$$t = \frac{2 \cdot \lambda F}{\pi} = 4.43\mu m$$

It is clear therefore that the actual sensing volume for the LDV will be the area of overlap shown in Figure (9) and the dimensions will be determined by the smaller of the evaluations of equations (24), (30) and (31). These focal volume dimensions, for typical practical figures, compare favourably with the size of material probes.

From Figure (9), it is obvious that the optimum operating condition for the fringe and reference modes will occur when the object field restriction due to the pinhole just overlaps the region of intersection of the two incident

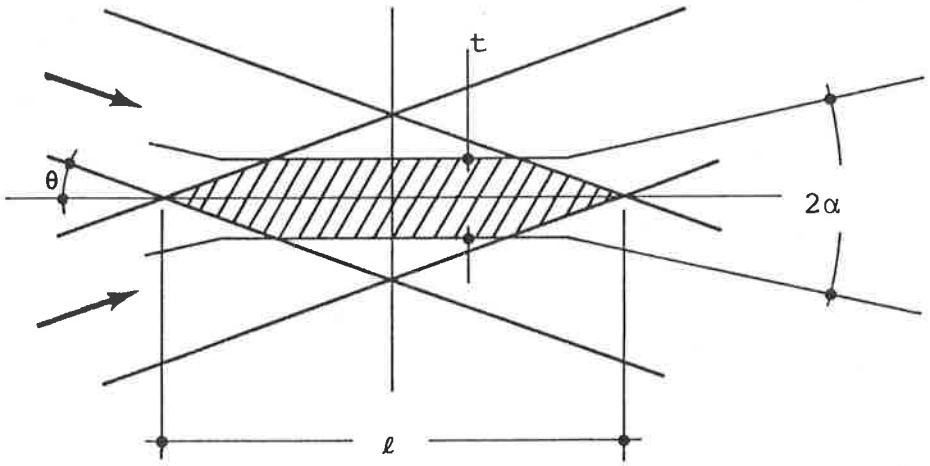

Figure 9. Effective Focal Volume Size

beams. For this to occur, the location of the pinhole in the image space is critical and, although from Figure (8b) it is obvious that it should be located at the position of minimum focus, the distance s'_r may be determined analytically from equations (25) and (26) by solving the set of simultaneous equations:

$$y = -\frac{(A-\Delta A)}{s'_2}\cdot x + (A-\Delta A)$$

$$y = \frac{(A+\Delta A)}{s'_1}\cdot x - (A+\Delta A)$$

when $y = r$ and $x = s'_r$.

Substituting the appropriate values of y and x,

$$r = -\frac{(A-\Delta A)}{s'_2}\cdot s'_r + (A-\Delta A) = \frac{(A+\Delta A)}{s'_1}\cdot s'_r - (A+\Delta A)$$

Hence $$s'_r\left[\frac{(A+\Delta A)}{s'_1} + \frac{(A-\Delta A)}{s'_2}\right] = 2A$$

i.e. $$s'_r\left[\frac{(A+\Delta A)}{f(s+\Delta s)}\cdot(s+\Delta s-f) + \frac{(A-\Delta A)}{f(s-\Delta s)}\cdot(s-\Delta s-f)\right] = 2A \qquad (31)$$

Again, since $\frac{(A+\Delta A)}{(s+\Delta s)} = \frac{(A-\Delta A)}{(s-\Delta s)} = \tan\alpha = \frac{A}{s}$,

equation (31) may be simplified to

$$s_r' = \frac{f \cdot s}{(s-f)} \qquad (32)$$

The presence of a pinhole of radius r at a distance s_r' from the lens in the object field will therefore reduce the effective focal volume to the region $(s-\Delta s)$ to $(s+\Delta s)$ and will render the photodetector insensitive to light scattered from any other point in the object field. This is of particular importance in both the Doppler mode, where scattering can occur from any point along the incident laser beam, and the fringe and reference modes where a decrease in SNR will result from scattering outside the focal volume.

2.4.2 Optimum Particle Specifications

In order that an LDV produce a signal, it is necessary that a scattering particle of suitable characteristics be present in the focal volume. If the concentration of such particles is sufficiently high, the probability of there being at least one scattering particle in the focal volume is unity and the output of the LDV is a continuous signal. If this probability is less than unity, the Doppler signal is discontinuous and is characterized by bursts of frequency information. A discussion of the special problems that result from this "signal dropout" is presented in later sections.

For the purpose of producing a suitable Doppler signal, a scattering particle has two main properties. In the first instance, the motion of the particle should accurately represent the localised fluid velocity and secondly, the particle must have a sufficiently high scattering cross section in order that a large SNR may be obtained. The properties of the particle may therefore be discussed in terms of both

fluid dynamic and scattered intensity limitations.

In order that the motion of a particle may accurately describe the turbulent nature of the fluid flow, it must have an inertia that is sufficiently small to allow the time lag between its motion and that of the fluid to be significantly less than the period of the highest frequency component of the fluid turbulence. In contrast to this requirement for small scattering centres, the particles must be sufficiently large to provide negligible spectral broadening due to particle Brownian motion. The optimum particle size for each application is clearly therefore a matter of compromise and has indeed been the subject of a great deal of discussion in the literature.

A resume of the results of Hjelmfelt and Mockros (1966) for the equation of motion of spherical particles in an incompressible fluid is presented by Smits (1974) where, under certain conditions, the motion of the particle may be described by the equation:-

$$\frac{d\,v_p}{d\,t} + \frac{18\nu\rho_f}{d_p^2 \cdot \rho_p} \cdot (v_p - v_f) = 0 \qquad (32)$$

in which v_p represents absolute particle velocity

v_f represents absolute fluid velocity

ν represents fluid kinematic viscosity

d_p represents particle diameter

and ρ_p, ρ_f represent particle and fluid densities respectively.

In transfer-function form, (32) becomes

$$v_p = \frac{1}{1+Ms} \cdot v_f \qquad (33)$$

where $M = \frac{d_p^2 \cdot \rho_p}{18\nu \cdot \rho_f}$ and s is the Laplacian operator.

If it is assumed that the maximum angular turbulence frequency is ω_m, the error generated due to particle inertia may be designated ε and approximated by the following expression:

$$\varepsilon = 1 - \left[\frac{1}{(1+\omega_m^2 M^2)} \right]^{\frac{1}{2}} \qquad (33)$$

This equation may be used to set an upper limit on the particle size for a particular flow application where the particle velocity differs by $\leqslant$ n% from the fluid velocity at the maximum turbulence frequency.

For example, for water droplets in air with a maximum turbulence frequency of 20KHz and an inertial lag of $\leqslant$ 2%, the maximum droplet size is given by:-

$$1 - \frac{1}{(1+\omega_m^2 M^2)^{\frac{1}{2}}} \leqslant 0.02$$

Rearranging this formula and substituting the appropriate values gives $d_{p_{max}} = 1\mu m$. Similar calculations may be performed for other fluid flow applications.

As proposed by Becker, Hottel and Williams (1967), when the size of the particle is comparable with the molecular mean free path, a modification to the constant M in terms of the Cunningham correction factor is required as follows:

$$M = \frac{d_p^{\,2} \rho_p}{18\nu \rho_f} \cdot \left[1 + K \cdot \frac{\ell_m}{d_p}\right] \qquad (34)$$

where K is the Cunningham constant and ℓ_m is the molecular mean free path. This correction can be important in low pressure flows where the mean free path is relatively long.

In general, the lower size limit for scattering particles is determined by the sensitivity of the optical components of the LDV rather than the fluid dynamic limitations, but, if the mean square Brownian displacement of a particle is determined by:

$$\overline{\Delta x^2} = \frac{4\ R\ T}{6\pi N \cdot \eta \cdot d_p} \cdot t \qquad (34)$$

where R is the gas constant,

T is the absolute temperature;

N is Avogadro's number;

η is viscosity;

d_p is the particle diameter;

and t time;

practical investigations indicate negligible spectral broadening for particles with a diameter > 0.2μm.

Although the fluid dynamic restrictions allow a relatively large variation in particle size, the scattering characteristics of particles in the fluid medium, as determined from classical Mie theory, strongly favour the larger scattering centres. Mazumder (1972) summarizes the results of Mie scattering for an optically istropic spherical particle in the expression:-

$$\frac{I(\theta)}{I_o} = \frac{\lambda_o^2}{8\pi^2 \cdot R^2} \cdot (i_1 + i_2) \qquad (35)$$

where $I(\theta)$ is the intensity of the scattered beam at an angle θ from the incident beam I_o; λ_o is the original wavelength; R is the distance to the point of observation and i_1 and i_2 are intensity functions having solutions in the form of an infinite series of Bessel and Hankel functions and Legendre

polynomials of the size parameter (= $\frac{\pi \cdot d_p}{\lambda_o}$); refractive index and the Mie coefficients of the electric and magnetic waves.

Making the approximation that $i_1 = i_2$ for a polydisperse aerosol, equation (35) simplifies to

$$I_{(\theta)} = \frac{\lambda_o^2 \cdot I_o \cdot N_p \cdot \Delta\Omega}{4\pi^2} \cdot [i_1] \qquad (36)$$

where N_p is the number of scattering particles within the sensing volume; $\Delta\Omega$ is the solid angle subtended by the receiving aperture and I_o is the power density of the incident beam at the scattering zone.

For forward scattering at very low angles, i.e.$\theta \simeq 0^o$, an estimation of the scattered intensity at a distance R from the focal volume is given by:

$$I_{(\theta \simeq o)} = \frac{\pi^2 d_p^4 \cdot K_s^2 \cdot N_p}{64\ R^2 \cdot \lambda_o^2} \cdot I_o \qquad (37)$$

where K_s is the scattering coefficient and is a function of the refractive index and the size parameter of the scattering particle. This equation clearly indicates the strong dependence of $I_{(\theta)}$ on particle size and illustrates why it may be assumed that particles that are small enough to be effected by Brownian motion contribute only a negligible amount to the total scattered intensity.

Although this dependence is of significant advantage in reducing the spectral bandwidth for any one measurement, if should also be remembered that the number of particles that are large enough to lag the flow by an appreciable amount should be kept as small as possible because of their disproportionate contribution to the detected signal.

2.4.3 Spectral Broadening

Although it would appear from equation (1) that the Doppler frequency shift for any one particle traversing the focal volume is readily defined in terms of the scattered and incident wave vectors and the particle component velocity, the detected Doppler frequency is, in practice, subjected to significant instrument - broadening. The major sources of this frequency broadening are:-

(1) aperture broadening

(2) spread due to finite signal lifetime.

and (3) frequency spread due to velocity gradients in the focal volume.

As will be discussed in later sections, this spectral broadening is a severe limitation to the accuracy of frequency domain analysis techniques because of the uncertainty in centre frequency determinations. Of the large number of suggestions that have been made for the reduction of these spectral linewidths, the following analyses are pertinent to this investigation.

(a) Aperture broadening:-

Recalling equation (6), it will be remembered that the dependence of f_D on the scattering angle was ignored for the purpose of establishing an equation for the photodetector current, i(t). Dimotakis (1975) has indicated that, in practice, for the reference mode, heterodyning occurs over a small solid angle defined in terms of the reference beam cross section, the photosensitive area of the photodetector and the pinhole aperture size. Equation (6) should therefore

be replaced by an integral over the effective receiver aperture and hence:-

$$i(t) = a\iint_{A} [\tfrac{1}{2}E_r^2(x,y) + E_r(x,y)\cdot E_s(x,y,t,) \cdot\cos(\omega_i t-\omega_s(x,y)\cdot t +\phi)]\cdot dx\cdot dy$$

With the assumptions that $E_r(x,y) \simeq E_r$ and $E_s(x,y,t) \simeq E_s(t)$; for small circular apertures, the solution to equation (38) yields:

$$\frac{\Delta\omega}{\omega_D} = \frac{\Delta f_D}{f_D} \simeq 2\kappa \qquad (39)$$

where $\kappa = \sqrt{\kappa_{/\!/}^2 + \kappa_{\perp}^2}$

$$\kappa_{/\!/} = \tfrac{1}{2}\left(\frac{a_r}{R_r}\right)\cdot\left(\cot\frac{\theta_o}{2} + \cos\psi\cdot\tan\phi\right)$$

$$\kappa_{\perp} = \frac{a_r}{R_r\cdot\sin\theta_o}\ (\sin\psi\ \tan\phi)$$

R_r = receiver distance from scattering volume

a_r = receiver aperture radius

and ϕ, θ and ψ are given by Figure 10.

In practice it is possible to reduce Δf_D to a very small value by reducing the receiver aperture radius a_r, provided that the corresponding reduction in detected signal intensity can be tolerated.

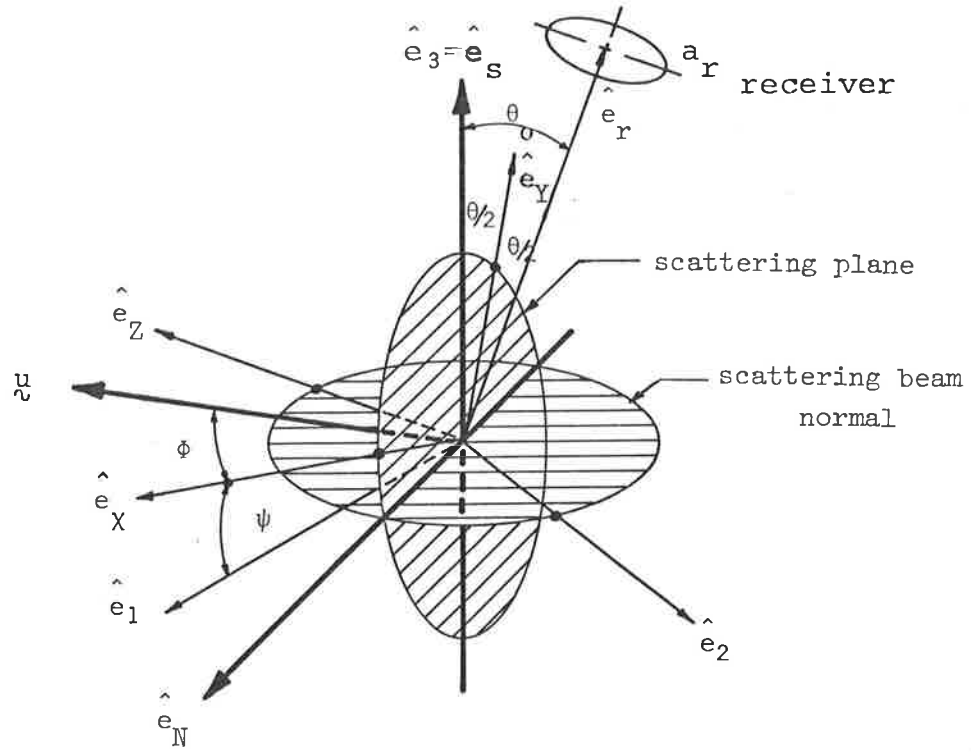

Figure 10: Reference-Scatter Detection Geometry

(From Dimotakis (1975)).

(b) Signal Lifetime

The spectral broadening that results from a finite signal lifetime is, to a large extent, dependent upon the average particle density. If it is assumed that the scattering particle number density is n and the size of the focal volume is V_c, then $nV_c>1$ implies that, on average, more than one particle is present in the focal volume at any one time and $nV_c<1$ implies discontinuous Doppler bursts.

For $nV_c>1$, the signal will, in general, be continuous but, due to phase variations between particles, will exhibit amplitude modulation. In terms of a frequency spectrum, this represents a spectral broadening with a spread of frequencies, Δf_D, equal to twice the maximum modulating frequency, centred on the carrier frequency f_D.

For $nV_c<1$, it is well known that a burst of a single

frequency f_D that is modulated by a slowly varying envelope will have a power spectrum centred on f_D with a frequency spread of $\pm \frac{f_D}{N}$; where N is the number of cycles enclosed by the envelope function.

In both of these cases, it is significant to note that the spectral broadening occurs only as a result of a power spectrum analysis and that the actual detected signal contains only the particle Doppler frequency information. Spectral broadening due to finite transit times for scattering particles through the focal volume is therefore a function of the signal processing elements rather than the scattering process itself.

(c) Velocity Gradients

The frequency spread arising from the finite size of the sensing volume can be determined by a comparison of the effective probe length and the expected average spatial velocity gradient in the fluid at the point of measurement. In order to minimize the spectral broadening due to velocity gradients, the length of the effective focal volume should be significantly less than the small scale turbulence in the flow. If this requirement cannot be met, then it is possible to determine the frequency spread from the following expression:-

$$\frac{\Delta f_D}{f_D} = \frac{(\frac{dv}{dx}) \cdot \ell}{\bar{V}} \qquad (40)$$

where, with reference to Figure (9),

$\bar{V}$ is the average velocity in the Y direction.

ℓ is the effective probe length

and $(\frac{dv}{dx})$ is the change in $\bar{V}$ over the probe length ℓ.

In general, this spectral broadening may often be reduced to a very small value by decreasing the size of the effective scattering volume. However, for high turbulence measurements, where the length of the focal volume may well be comparable with the Kolmogorov lengths, significant broadening may result. It is important to note that, unlike signal lifetime broadening, the spread due to velocity gradients in the focal volume is independent of the signal processing method and must therefore be seen as a possible limitation to the LDV technique.

2.5 DIRECTIONAL ALIASING WITH FRINGE ANEMOMETERS

Although the effects of the three major sources of spectral broadening are not additive and the Doppler line width is dictated by the largest individual source, the conditions required to minimize each of the effects are mutually contradictory in that, to reduce the spectral broadening due to aperture size and velocity gradients in the focal volume, the focal volume should be as small as possible while the spectral broadening due to the finite signal lifetime is proportional to $\frac{1}{N}$ and therefore requires that N, the number of fringes crossed, be as large as possible. Clearly a compromise solution is required and one such technique is to accept only those particles that cross a minimum number of fringes, N_{min}, in the focal volume and to reject all other Doppler signals. This has the advantage of increasing the SNR by rejection of all signals that are either smaller than the acceptance threshold (see Figure 7) or shorter than the minimum allowable signal lifetime such as those that result from a particle just skirting the edge of the focal volume.

It is unfortunate, however, that when the fringes in the focal volume are stationary, this technique also introduces signal aliasing, as can be seen from the following analysis:

Figure (11) represents one half of the focal volume, where:-

t = total thickness

ℓ = total length

w = beam width

d = fringe spacing

and θ = half angle of scattering beam

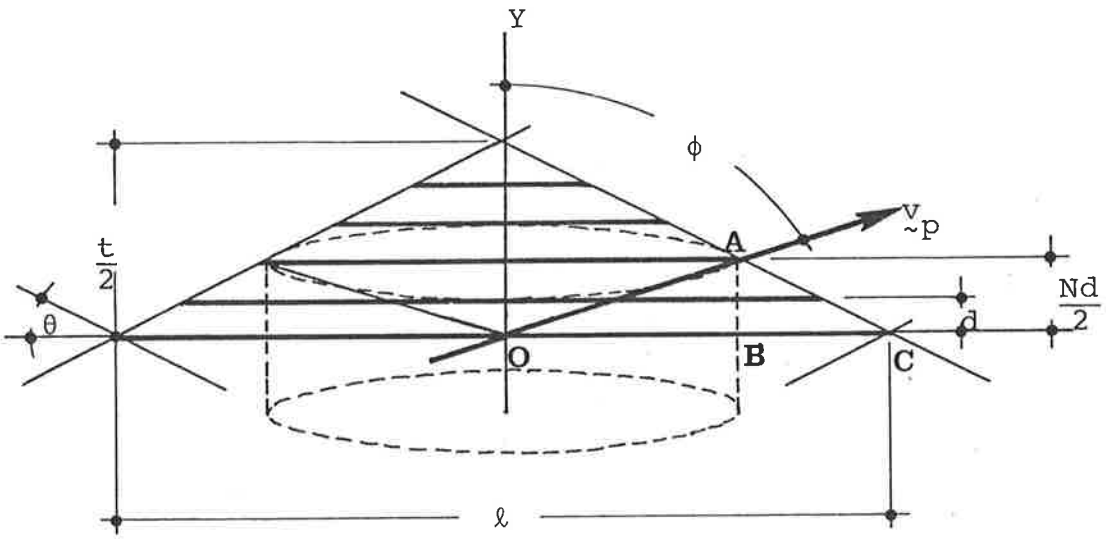

Figure 11. Effective Focal Volume

If a minimum number of N fringes are to be crossed, then the effective scattering volume is reduced to a cylinder of radius OB and height Nd, as shown in the above diagram. Particles that travel through the centre of the focal volume therefore require a sufficiently large y velocity component in order that at least $\frac{N}{2}$ fringes be crossed in the region shown. The angle of inclination between the Y axis and the velocity

vector of a particle, $\underset{\sim}{v}_p$, can therefore be no greater than a maximum value, ϕ_{max}, if the Doppler signal for that particle is to be accepted. The solid angle, Ω will always be less than 2π steradians and it is therefore possible that a measurement of the ensemble average of the y velocity component for the whole of the flow may be biased because the LDV is insensitive to particles that have a longitudinal velocity component less than a preset minimum value.

For any one measurement, an absolute evaluation of the error due to this aliasing is very difficult because it presupposes a knowledge of the distribution of the velocity components. It is reasonable, however, to assume that for turbulent flow, Ω, the solid angle of acceptance should be as close to 2π as possible. With reference to Figures (11) and (12), Ω may be evaluated as follows:-

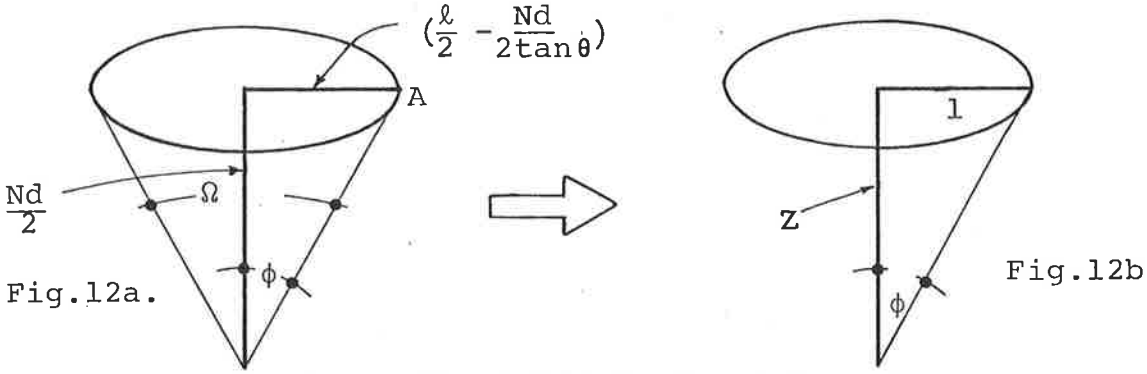

Fig.12a. Fig.12b

Figure 12. Solid Angle of Acceptance

$$AB = \frac{Nd}{2} \; ; \quad \text{hence } BC = \frac{Nd}{2\tan\theta}$$

$$\text{and } OB = \left(\frac{\ell}{2} - \frac{Nd}{2\tan\theta}\right).$$

Ω is therefore defined by the expression:-

$$\Omega = 2\pi \left[1 - \frac{Z}{(1+Z^2)^{\frac{1}{2}}}\right] \qquad (41)$$

$$\text{where } Z = \frac{Nd}{\left(\ell - \frac{Nd}{\tan\theta}\right)}$$

If it is required that Ω be within n% of 2π, the critical beam dimensions may be determined as follows:

For the error to be < n%,

$[1 - \frac{Z}{(1+Z^2)^{\frac{1}{2}}}] \geq (1-n)$, which, by transposition gives:-

$$Z \leq \frac{n}{(1-n^2)^{\frac{1}{2}}} \quad (=k)$$

Hence $$\frac{Nd}{(\ell - \frac{Nd}{\tan\theta})} \leq k$$

i.e. $$Nd\,[\frac{1}{k} - \frac{1}{\tan\theta}] \leq \ell$$

But $\ell = \frac{w}{\sin\theta}$ and $d = \frac{\lambda}{2\sin\theta}$, hence

$$w \geq \frac{N\lambda}{2}\,[\,\frac{1}{k} + \frac{1}{\tan\theta}\,] \qquad (42)$$

where w is the beam width, N is the total number of fringes to be crossed, θ is the half beam angle and $k = \frac{n}{(1-n^2)^{\frac{1}{2}}}$, where n is the aliasing error.

As a sample calculation, for n = 0.02 (i.e. error < 2%), N = 4 fringes; $\theta = 2^{o}$ and $\lambda = 632.8$nm:

$$w_{min} = \frac{4 \times 0.6328}{2}\left[\frac{1}{.02} + \frac{1}{\tan 2}\right] = 100\mu m$$

This implies that the minimum beam width to ensure a solid angle of acceptance equal to 0.98 x 2π steradian is 100μm and that the corresponding minimum focal volume dimensions are:-

$$\ell_{min} = \frac{100}{\sin 2} = 2.86 \text{ mm}$$

and $$t_{min} = \frac{100}{\cos 2} \simeq 100\mu m$$

From this it follows that fringe anemometers that use

stationary fringes in the focal volume will:-

(a) have a low SNR because of the possibility of velocity gradient broadening in a large focal volume,

or (b) be susceptible to significant directional aliasing errors if the effective focal volume is reduced in size,

or (c) suffer significant spectral broadening due to finite signal lifetime if N, the number of required fringe crossings, is reduced.

Although it is possible to compromise these conditions under certain circumstances, the full potential of the laser Doppler technique can only be realized if the fringes in the region of interaction are set in motion and made to scan the focal volume by providing a difference in frequency between the two incident beams. This corresponds to the f_b term in equation (11), where the fringes, with spacing d, have a velocity v_f given by

$$v_f = d \cdot f_b \tag{43}$$

and can be made to scan in the same or opposite direction with respect to the mean flow direction.

If the fringes are made to scan the focal volume, the directional aliasing problem just described may be removed entirely, for even if a particle is stationary in the focal volume, fringes will be crossed at a rate equal to f_b and hence the y velocity components of all particles traversing the focal volume will be detected. With this configuration, it is therefore possible to reduce the size of the effective focal volume to the minimum values indicated in previous

sections and still require that a preset number of fringes be crossed. Optical frequency biasing therefore provides a technique for simultaneously reducing the spectral broadening due to velocity gradients in the focal volume and finite signal lifetimes.

Whereas the requirement for N fringe crossings in the stationary fringe configuration implied that the particle velocity vector must lie within a solid angle of acceptance Ω, the same requirement for the moving fringe configuration can be shown to impose an upper limit to the maximum detectable fluid velocity. Simply stated, this limitation requires that τ, the transit time for a particle crossing the focal volume, be sufficiently long for at least N fringes, moving with a velocity v_f, to be crossed while the particle is within the focal volume. The maximum particle velocity that is indicated by this limitation is also dependent upon whether the fringes are moving in the same or opposite direction with respect to the mean fluid flow.

With reference to Figure (13), for a particle crossing the geometric centre with a specific particle velocity $|\underset{\sim}{v}_p|$, the minimum transit time, τ_{min}, will occur when $\phi = \theta$ and the corresponding maximum particle velocity will be given by

$$|\underset{\sim}{v}_p|_{max} = \frac{\ell'}{\tau_{min}} .$$

Assuming that the distance OB is less than $\frac{Nd}{2}$, if a total of N fringes are to be crossed, the fringe pattern must move a distance BD in the transit time τ, hence

$$\tau_{min} = \frac{\ell^1}{|\underset{\sim}{v}_p|_{max}} = |\frac{BD}{\underset{\sim}{v}_f}|$$

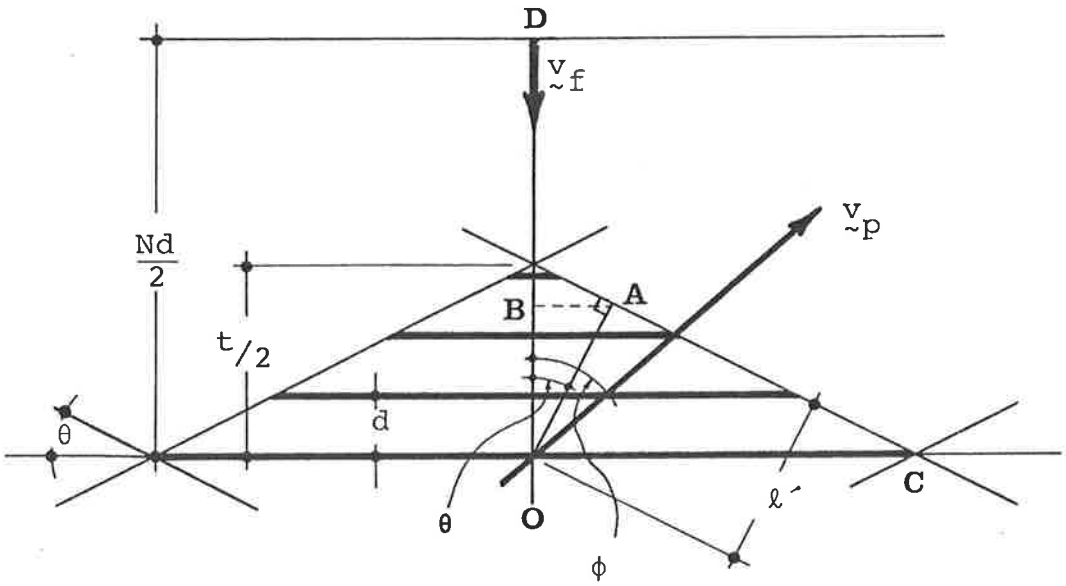

Figure 13. Focal Volume with Moving Fringes

Now OA = ℓ' and $\ell' = \frac{t}{2}\cos\theta$, hence OB = $\ell' \cos\theta = \frac{t}{2}\cos^2\theta$

and BD = $(\frac{Nd}{2} - \frac{t}{2}\cos^2\theta)$

$$\therefore \quad |\underset{\sim}{v}_p|_{max} = \frac{\ell' |\underset{\sim}{v}_f|}{(\frac{Nd}{2} - \frac{t}{2}\cos^2\theta)} \tag{44}$$

Using the relationships $t = \frac{w}{\cos\theta}$, $d = \frac{\lambda}{2\sin\theta}$ and

$v_f = f_b \cdot d$; equation (44) may be rewritten as:

$$|\underset{\sim}{v}_p|_{max} = f_b \left[\frac{w}{N - \frac{w \sin 2\theta}{\lambda}} \right] \tag{45}$$

By way of example, if $\theta = 2^o$, w = 25μm, N = 4; f_b = 30 MHz and λ = 632.8mm

$$|\underset{\sim}{v}_p|_{max} \simeq 600 \text{ m/s}$$

A similar analysis for the configuration where the fringes are moving in the same direction as the mean fluid flow yields the following relationship for the maximum detectable velocity:

$$|\underset{\sim}{v}_p|_{max} = f_b \left[\frac{w}{N}\right] \tag{46}$$

which, under the same circumstances as above, gives

$$|\underset{\sim}{v}_p|_{max} = 30 \times 10^6 \times \frac{25\times10^{-6}}{4} = 187.5 \text{ m/s}$$

Thus it is clear that,if either a large number of fringe crossings are to be counted, or a very small focal volume is required, the bias frequency, f_b, should be as high as possible, commensurate with the frequency response of the processor and the scattered light intensity, in order not to restrict the range of the detector. The maximum practicable bias frequency for these applications may be determined by an analysis of the average scattered light intensity, given by equation (37), as follows:-

Using the example from Section 2.4.2 with water droplets in air, an optimum particle size of $d_p \simeq 1\mu m$ was established. For water particles in the range 0.5 to 1μm, K_s has an approximate value of 2 for λ = 632.8 nm and if R = 50cm, N_p = 1 and the incident laser beam power is 3mW focussed to an airy disc diameter of 100μm, the scattered intensity per particle, $I_{(\theta\simeq o)}$, is approximately 2.4μW/particle. Since the energy of an optical photon at λ = 632.8nm is 3.14×10^{-19} Joules, this average light intensity corresponds to a photon rate of 7.6×10^{12} photons per second. Assuming a typical value of 5% for the quantum efficiency of the detector, the corresponding average photo-cathode current is 3.8×10^{11} electrons per second, i.e. 61nA. Although this average signal current is sufficient for signal detection and demodulation the maximum optical bias frequency is limited by the number of photons collected within any one cycle of the Doppler signal. For the above example, if f_b = 30MHz, the period of the Doppler signal is 30ns, within which an

average of 11,400 photo electrons will be generated. Quantization effects should not therefore be apparent for this application but if back-scatter techniques or sub-micron particles are used a reduction of the scattered light intensity by two to three orders of magnitude may be experienced. An increase in incident laser power or a decrease in the optical bias frequency would therefore be necessary in order to accurately define the Doppler signal, even though the average signal current may appear to be adequate.

From the foregoing discussions, it is obvious that the selection of the operating parameters for an LDV is not a straightforward process and almost invariably involves a compromise between focal volume dimensions; SNR; maximum turbulence frequencies and maximum fluid velocities. However, once a specific application has been delineated, it is possible to optimize the constraints to provide significant advantages over conventional techniques in most practical applications provided that some form of optical frequency biasing is used to reduce the size of the effective focal volume and to allow the resolution of bidirectional or oscillatory flows.

CHAPTER THREE

OPTICAL METHODS OF FREQUENCY BIASING

SUMMARY:

As indicated in the previous chapter, the ability of the LDV to resolve bidirectional velocities constitutes a major advantage of this technique over hot-wire anemometer and other material probe techniques. In addition, the use of moving fringes in the focal volume removes the aliasing problem associated with fringe anemometers and allows the effective probe volume to be minimized without decreasing the SNR. These significant advantages have prompted the research of a number of methods for optical frequency biasing and this chapter provides a summary of some of the currently available techniques together with the results of this author's investigations.

The techniques are broadly categorized as follows:-

Mechanical Systems

Magneto-optic Techniques

Electro-optic Devices

Acousto-optic Devices

and it is concluded that, for high velocity flows, the acousto-optic cell is the most suitable technique, since it offers a high conversion efficiency at suitable bias frequencies for a modest input power requirement.

The design criteria and performance specifications of a 30MHz, water filled Bragg cell constructed by this author are also included in this chapter.

3.1 MECHANICAL SYSTEMS

Although it is the case that any scattering, other than pure reflection, from a moving surface may be used to provide a frequency bias by the Doppler effect, mechanical systems generally use some form of rotating diffraction grating in order to enhance the scattered light intensity in one or more particular directions. Common configurations are shown in Figure 14, where the diffraction grating is either mounted on the periphery of a rotating disc or ruled radially from the centre to form either a transmission or reflection grating. Mazumder (1972) has reported that a high density optical encoder disc may be satisfactorily used as a transmission grating but higher diffraction efficiencies may be achieved if the grating is blazed to enhance diffraction into one particular order.

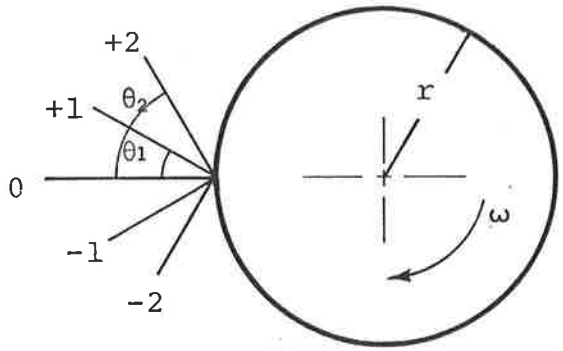

Figure 14a.

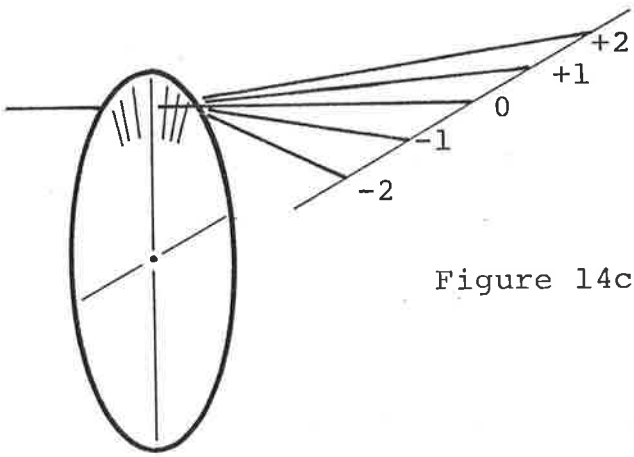

Figure 14c.

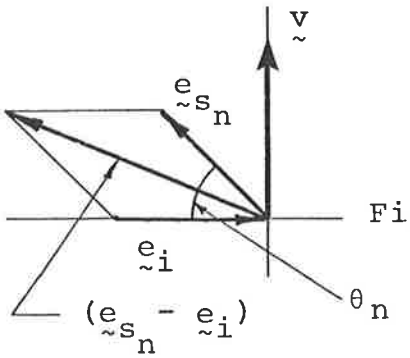

Fig.14b.

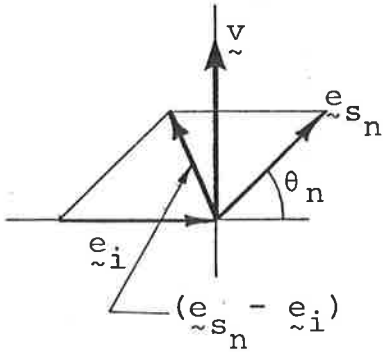

Fig.14d.

Figure 14. Mechanical Systems.

For any diffraction grating, the grating formula:

$$n\lambda = 2d \sin \theta_n \tag{47}$$

is valid, where n is the order of the diffracted beam; λ is the incident wavelength; d is the grating spacing and θ_n is the angle of diffraction of the n^{th} order beam.

For both of the above systems, the Doppler shift between the n^{th} order diffracted beam and the incident beam may be derived from the original Doppler equation, viz,

$$f_D = \frac{1}{\lambda} (\underset{\sim}{e}_{s_n} - \underset{\sim}{e}_i) \cdot \underset{\sim}{v}$$

and shown, from the geometry of the corresponding vector diagram to be

$$f_D = \pm \frac{v \cdot \sin \theta_n}{\lambda} \tag{48}$$

where $\underset{\sim}{e}_{s_n}$ is the unit vector in the direction of the n^{th} diffracted order

$\underset{\sim}{e}_i$ is the unit vector of the incident beam

and $\underset{\sim}{v}$ is the surface velocity of the grating at the point of incidence.

Using the expression for $\sin\theta_n$ as derived from the diffraction grating formula, equation (48) may be rewritten as:

$$f_D = \pm \frac{nv}{2d} \tag{49}$$

or $$f_D = \pm \frac{nr\omega}{2d}$$

where ω is the angular frequency and r the radius of the rotating disc.

The sign of the Doppler shift, as indicated by equation (48) is dependent upon whether the positive or negative diffracted orders are heterodyned with the incident beam. In

practice, significant advantages may be obtained by using both the positive and negative orders since twice the Doppler frequency shift is obtained for a given surface velocity and the symmetry, phase and polarization of the diffracted beams are retained. Other advantages of these mechanical systems include the ability to obtain any bias frequency without changing the orientation of the optical components and the non critical nature of alignment procedures. Furthermore, one major disadvantage of rotating diffraction gratings, i.e. the low power transmission, may be overcome with the use of bleach radial gratings, for which it is now possible to recover and use up to 70% of the input power.

A symmetrical heterodyning system of the type shown in Figure (15) was initially used by the author, where a flexible diffraction grating of line density 13,400 lines per inch was mounted on the periphery of a 7.5 cm diameter, aluminium disc. A small D.C. motor was used to rotate the disc with an angular velocity of 240rpm and a bias frequency of approximately 0.5MHz was observed.

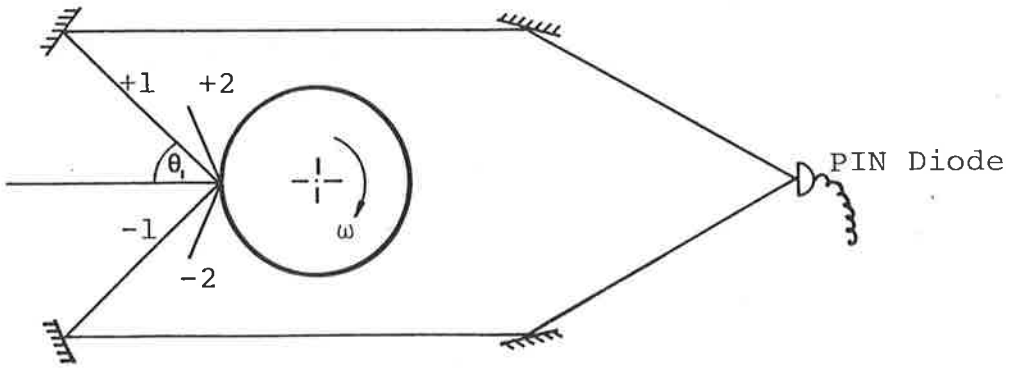

Figure 15. Symmetrical Heterodyning System

Although reasonable success was achieved with this technique, severe problems were experienced with (a) dispersion of the diffracted beam due to irregularities in the grating; (b) very low diffraction efficiency, and (c) lack of stability of the bias frequency due to variations in the angular velocity of the disc. Attempts to stabilize and servo-control the motor speed were moderately successful but since the stability of the bias frequency is the basis of the accuracy of the whole laser Doppler process, the difficulty in achieving a constant reference frequency was considered to outweigh the advantages of this and other mechanical systems.

3.2 MAGNETO-OPTIC TECHNIQUES

Of all the methods for optical frequency biasing investigated here, the use of a longitudinal magnetic field in the laser cavity to produce Zeeman splitting of the spectral lines is perhaps the most interesting and promising method available for producing a constant frequency difference between two coherent laser beams.

In the presence of a weak external magnetic field $\underset{\sim}{H}$, discrete atomic energy levels are split into multiplets, separated in energy by an amount ΔE, given by

$$\Delta E = -\underset{\sim}{\mu} \cdot \underset{\sim}{H} \tag{49}$$

where $\underset{\sim}{H}$ is the external, applied magnetic field and $\underset{\sim}{\mu}$ is the nett magnetic moment vector, determined by the summation

$$\underset{\sim}{\mu} = -\frac{\mu_B}{\hbar} \left[\sum_i \underset{\sim}{L}_i + 2 \sum_i \underset{\sim}{S}_i \right] \tag{50}$$

for all the optically active electrons i. In the expression,

$\underset{\sim}{L}$ is the orbital angular momentum vector; $\underset{\sim}{s}$ is the electron spin angular momentum vector; μ_B is the Bohr magneton $(= \frac{eh}{4\pi mc})$ and $\hbar = \frac{h}{2\pi}$, where h is Planck's constant.

When the external field is significantly less than the atomic magnetic field (typically 1 $Wb/_{m^2}$), the assumptions of the normal Zeeman effect allow equation (49) to be written as:

$$\Delta E = \mu_B \cdot H \cdot g \cdot m_j' \qquad (51)$$

where m_j' is the total angular momentum quantum number and g is the Lande g factor, which may be evaluated from the expression:

$$g = 1 + \frac{j'(j'+1) + s'(s'+1) - \ell'(\ell'+1)}{2\,j'(j'+1)}$$

In the He-Ne laser, the important transition is the Ne $2S_2 \rightarrow 2P_4$ transition and in the presence of a longitudinal magnetic field, the $2S_2$ energy level is split into a triplet and the $2P_4$ energy level is split into a quintiplet, as shown in Figure (16).

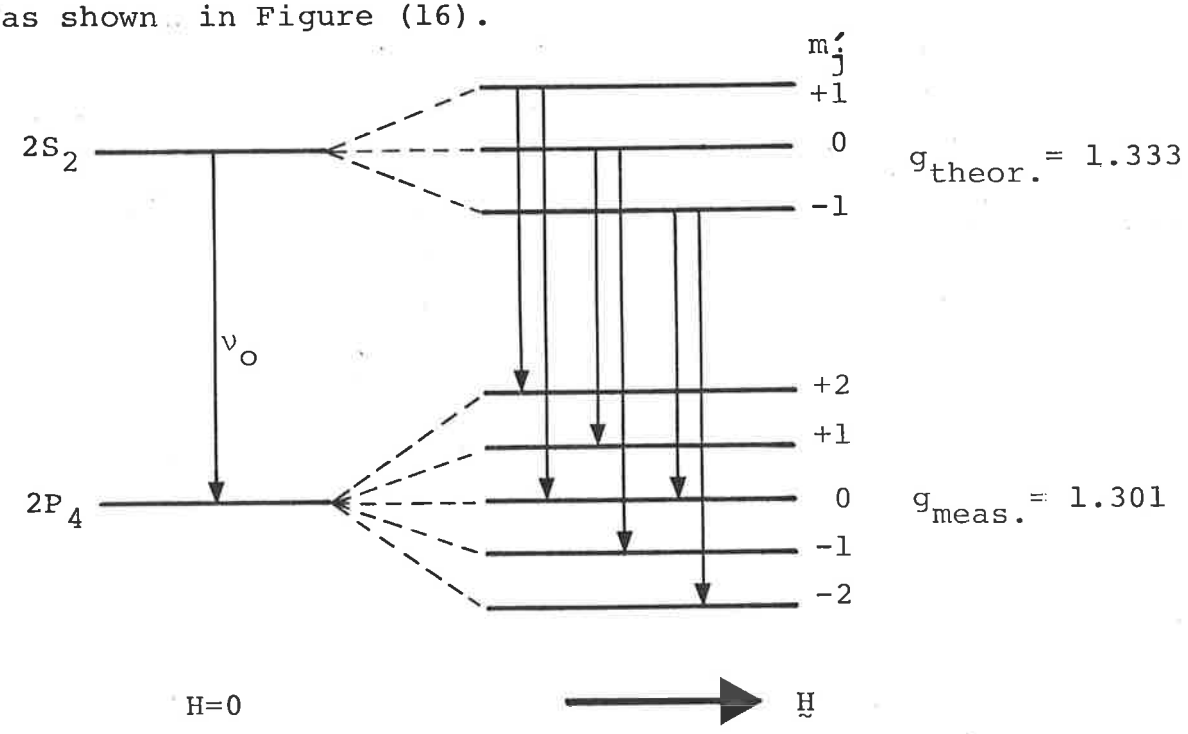

Figure 16. Normal Zeeman Effect in He-Ne Laser Transition

The effect of the Lande g factor is to determine the actual separation of the multiplets for each of the energy levels and since they are approximately equal for the $2S_2$ and $2P_4$ levels in Ne, as reported by Paananen et al (1963), the six transitions shown in Figure (16) that are allowed by the selection rule $\Delta m_j' = \pm 1$ actually result in only two spectral lines, $\nu_o + \Delta\nu$, corresponding to $\Delta m_j' = -1$ and $\nu_o - \Delta\nu$, corresponding to $\Delta m_j' = +1$. When viewed in a direction that is parallel to the axis of the laser cavity, these two lines have opposite circular polarization and the resultant total field is a linearly polarized wave oscillating at the average of the two frequencies with the plane of polarization rotating at half the difference frequency. If observed through a linear polarizer, the resultant wave will therefore appear as an amplitude modulated, linearly polarized wave, independent of the orientation of the linear polarizer and with a frequency given by:-

$$\Delta\nu = \frac{\mu_B \cdot H \cdot g}{h} \cdot \frac{\Delta f_c}{\Delta f_{Ne}} \qquad (52)$$

where Δf_c and Δf_{Ne} are, respectively, the half widths for the laser cavity and Ne $2S_2 \rightarrow 2P_4$ transition frequencies.

Assuming that the induced frequency shift, $\Delta\nu$ is significantly less than the laser cavity mode separation, f_c, given by $f_c = \frac{c}{2\ell}$, where ℓ is the length of the laser cavity and c is the speed of light, inter-mode modulation will not be apparent and the induced frequency shift will therefore be linearly dependent upon the longitudinal magnetic field intensity. Investigations with a Metrologic, 1.5mW, fixed mirror, He-Ne laser indicated that a constant of proportionality of approximately 7.5Hz/AT/m could be achieved when the

laser cavity was enclosed within a long solenoid, through which a relatively small direct current was passed. (These results are consistent with the findings of other workers, for example Paananen, where Δf_{Ne}; Δf_c and g were taken as 10^3MHz; 0.33MHz and 1.3 respectively).

The solenoid used to provide the longitudinal magnetic field consisted of 1000 turns of 22SWG wire, wound on a former 10cm long and 2cm diameter. It was assumed that the axial magnetic field intensity within the solenoid was represented by the relationship:

$$H = \frac{nI}{\ell} \qquad (53)$$

where n is the number of turns on the coil; I the current in amperes; and ℓ the length of the coil in metres. Variation of the field current from 0 to 5A resulted in an observed frequency shift over the range 0 to 375KHz when detected with a linear polarizer and a PIN photodiode. From this it was possible to experimentally estimate the constant of proportionality as 75KHz/A.

To separate the two Zeeman shifted beams, which are initially colinear, a combination of phase retardation and linear polarizing plates was used. The two beams emerge with opposite circular polarization and may be separated by conversion of the circular polarization to linear polarization with quarter and half-wavelength phase retardation plates. The orthogonality of the direction of polarization of the resultant beams enables either one of the beams to be selected by suitable orientation of a plane polarizing plate. This technique resulted in a very high conversion efficiency and would therefore be suitable for either fringe or reference

mode operation.

Although excellent agreement between the theoretical and experimental results was achieved, the Zeeman splitting technique unfortunately suffers the following limitations:

(1) Unless very strong magnetic fields are used, in which case the Paschen-Back effect will disrupt the normal Zeeman separation, the maximum practicable frequency shift is limited to approximately 2-2.5MHz. This would be inadequate for high velocity flows requiring a small focal volume but would be well suited to low velocity flows or acoustics applications.

(2) The requirement for no polarization anisotropy precludes the use of laser tubes with Brewster angle windows and virtually makes the use of internal mirrors mandatory. Since the reflecting surfaces for this type of laser tube are inaccessible, cleanliness and deterioration of the reflective coatings become even more critical considerations and may in practice, prove to be a considerable problem.

(3) The stability of the modulation frequency was found to be very poor because of variations in the laser cavity modes due to thermal fluctuations in the plasma tube. Unless the laser can be stabilized and induced to centre on one particular cavity mode, the relative amplitudes of the two Zeeman shifted beams and the resultant frequency separation may vary in a psuedo-random fashion. This was found to be particularly obvious with the Metrologic laser since the mirrors

were cemented onto the ends of the glass envelope. Investigations with a Fabry-Perot spectrum analyzer showed quite rapid changes in cavity modes for this laser both during the initial warm-up period and after several hours operation.

The gravity of these problems is indicated by the extent of the technological development sustained by Hewlett-Packard in the production of the HP5525A Laser Interferometer system, where single cavity mode operation is achieved by servo-control of the laser cavity length. As reported by Burgwald and Kruger (1970), the difference in intensity of the two Zeeman lines is taken as an error signal and used to adjust the EHT supply for a piezo-electric wafer on which one of the internal mirrors is mounted. In this way, compensation is made for the small changes in the laser cavity length that occur during and after the warm-up period and the laser maintains a single centre frequency.

Although the problem of maintaining single cavity mode operation would appear to present some technological difficulties, it is still considered that the ability to continuously control and vary the frequency shift; the high conversion efficiency; the simplicity with which the Zeeman lines may be separated and the relatively low input power requirements are all significant advantages that recommend this technique as one of the most attractive for providing low frequency optical biasing.

3.3 ELECTRO-OPTIC DEVICES

Electro-optic frequency shifting is based on the principle of the reversal of the direction of rotation of a circularly polarized beam by a half-wave retardation plate. If the plate is rotated at a frequency f, the frequency of the emergent beam is shifted by an amount 2f since the E vector of the emergent beam is related to that of the incident beam by reflection about the axis of symmetry of the retardation plate.

In practice, mechanical rotation of a $\frac{\lambda}{2}$ plate at sufficiently high speeds is impracticable for most applications and the effect is simulated by the production of a rotating electric field in a suitable medium. Kerr cells, such as those described by Buhrer *et al* (1963) and Campbell *et al* (1971) have been successfully used, but the production of a rotating field by means of a single four electrode cell, in which two pairs of electrodes are fed by voltages differing in phase by 90°, has a number of severe practical disadvantages.

Drain and Moss (1972) have suggested that a series of conventional electro-optic cells arranged with various inclinations and electrical phase differences would be a more efficient method of reducing the losses that occur in the unwanted sidebands in the presence of strong electrostatic or r.f. fields. They conducted a computer simulation of the conversion efficiency for a large number of cells with various electrical phase differences and orientations and the results suggested that the most economical combination is a configuration of four electro-optic cells at inclinations of 0°;

45^{o}; 0^{o} and 45^{o}, excited by r.f. fields with phase differences of 0^{o}; 90^{o}; 0^{o} and 90^{o} respectively. Although an efficiency of approximately 92% is predicted for this configuration, the Kerr cells require accurate amplitude and phase regulation of peak voltages in excess of several kV at radio frequencies. These r.f. power requirements may be significantly reduced if liquid Kerr cells are used with a very high D.C. bias voltage (typically 8kV), but the method still requires a high degree of homogeneity in the refractive index of the cell medium to avoid degradation of the spatial coherence of the beam.

The results of experiments conducted by Drain and Moss on two potassium dideuterium phosphate cells, which use the longitudinal Pockels effect, and a specially constructed three cell unit employing the Kerr effect in nitrobenzene indicated disappointingly low maximum nominal efficiencies of 10% and 23% respectively for a frequency shift of 1MHz. Considering the difficulties in phasing and amplitude regulation and the requirement for high alternating voltages, the method is not considered to be a particularly suitable technique for producing the higher bias frequencies (typically 10MHz) required for a high resolution LDV.

3.4 ACOUSTO-OPTIC DEVICES

Diffraction of light by ultrasonic soundwaves was predicted by Brillouin in 1922 and first observed by Debye and Sears in 1932. A great deal of experimental and theoretical work has been done since that time and a large number of investigations have been reported.

Prior to the development of theoretical quantum mechanics, analyses of the observed diffraction effects were mainly geometric in nature and based on the assumption that the travelling sound waves behaved in the same way as a sinusoidally varying phase grating. Willard (1949) reported criteria for the distinction between Debye-Sears (Raman-Nath) scattering and Bragg diffraction, which are the two most important interactions in acousto-optic cells. Figure (17) represents a typical acousto-optic cell, where a travelling ultrasonic sound wave of width W and wavelength Λ is generated in a material whose normal refractive index is η, by a piezo-electric crystal operating at a frequency f_a. The incident laser beam, with free space wavelength λ, is diffracted into positive and negative orders, the number and relative intensity of which are a complex function of interaction length W; angle of incidence ϕ; acoustic wavelength Λ; and the induced refractive index change in the medium $\Delta\eta$.

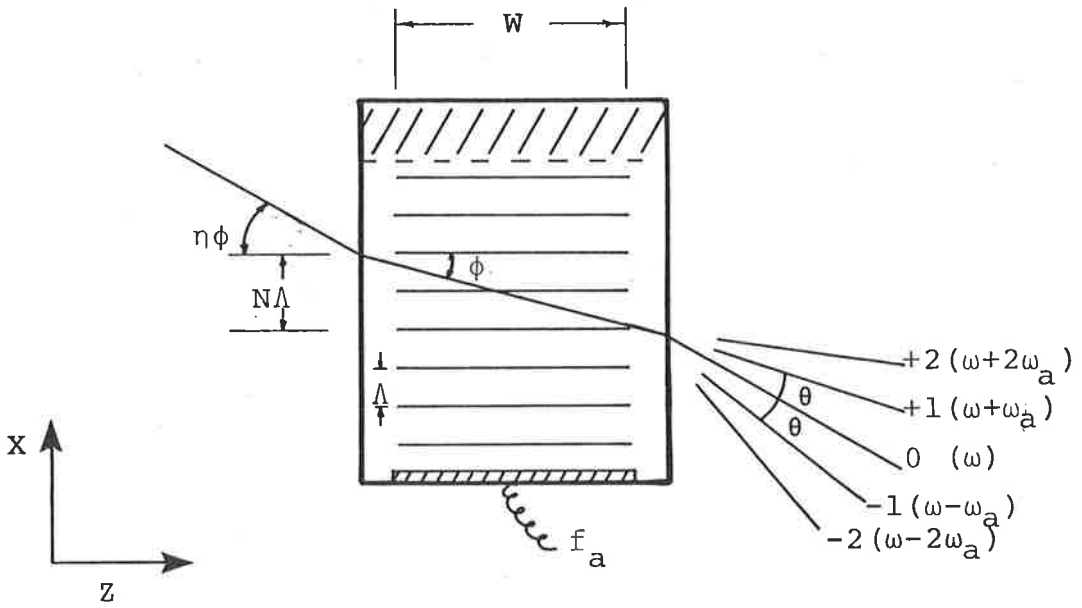

Figure 17. Acousto-Optic Cell

Although the transition from Debye-Sears to Bragg diffraction is not particularly acute, certain conditions can be prescribed for the predominance of one or other of the two scattering modes. In particular, if either $\phi \neq \theta_B$, the Bragg diffraction angle, or N, the number of acoustic wavefronts crossed by the undiffracted (zero order) beam, is less than unity then the Bragg conditions cannot be satisfied and any diffraction that results will be purely Debye-Sears. Conversely, if $\phi = \theta_B$ and N is typically 2 to 3, then Bragg diffraction will predominate.

Bearing in mind that it is possible to concurrently satisfy the conditions for both Debye-Sears and Bragg diffraction, the two may be separately analyzed, as follows:-

3.4.1 Debye - Sears Scattering

For $\phi = 0$, i.e. the incident laser beam parallel to the acoustic wavefronts, the positive and negative orders are equal in number and corresponding orders are of equal intensity. For $\phi \neq 0$, the system is analogous to a spectrometer using an inclined diffraction grating and, for the configuration shown in Figure(17), the positive orders would be enhanced in both number and intensity. In each case, the angle of diffraction of the n^{th} order beam, θ_n, is given by:

$$\theta_n = \text{arc sin } (\frac{n\lambda}{2\Lambda}) \tag{54}$$

which, for small angle approximation, reduces to:

$$\theta_n \simeq \frac{n\lambda}{2\Lambda} \tag{55}$$

One important difference between the diffraction

grating analogy and the acousto-optic cell is that, due to the travelling-wave nature of the phase grating in the cell, the diffracted orders are shifted in frequency by the Doppler effect and the actual frequency for the n^{th} order spectrum is given by:

$$f_n = f_o + n \cdot f_a \tag{56}$$

where f_o is the frequency of the incident laser beam. The diffracted orders are therefore shifted in frequency by integer multiples of the acoustic frequency f_a, as predicted by Raman and Nath (1936) and experimentally verified by Cummins et al (1963).

From Willard, the intensity of light diffracted into the n^{th} order spectral line follows a Bessel function relationship given by:

$$J_n^2(a) = J_{-n}^2(a) = J_n^2\ (2\pi p) \quad \text{for } \phi = 0 \tag{57}$$

and $$J_n^2(ka) = J_n^2(k \cdot 2\pi p) \quad \text{for} \quad \phi \neq 0 \tag{58}$$

including the undiffracted, zero order beam, for which n = 0. In each case, the argument a (=2πp) is the amplitude of the angular phase retardation produced in the sound beam and:

$$p = \frac{W \cdot \Delta\eta}{\lambda} \tag{59}$$

The constant k is given by:

$$k = |\sec(\phi)| \cdot \left[\frac{\sin(N\pi)}{N\pi}\right] \tag{60}$$

where $$N = \left(\frac{W}{\Lambda}\right) \cdot \tan(\phi) \tag{61}$$

To calculate the actual diffracted light intensities, it is necessary to establish a relationship between refractive index change and the amplitude of the material density change, $\Delta\rho$, which Willard reports as:

$$\frac{\Delta\eta}{\eta_1} = \frac{\Delta\rho}{\rho} \qquad (62)$$

where $\eta_1 = (\eta-1)\cdot[(\eta^2+1.4\eta+0.4)\div(\eta^2+0.8\eta+1)]\simeq(\eta-1)$ and ρ is the density of the medium.

Since $\frac{\Delta\rho}{\rho} = \frac{\Delta P}{\rho\cdot v_a^2}$; where ΔP is the hydrostatic pressure change and v_a is the velocity of sound in the medium, the argument of the Bessel function relationships in equations (57) and (58) may be expressed in terms of $\Delta\eta$, $\Delta\rho$ or ΔP and of particular interest is the value of $p = 0.289$, for which J_1^2, the intensity in each of the ±1 orders, first reaches a maximum value of 0.35.

With this particular scattering configuration, Willard derived the following expression for the total acoustic power requirement P_a:-

$$P_a = \left(\frac{\rho\, v^3\, \lambda^2 h}{2\,\eta_1^2\, W}\right) p^2 \quad \text{(watts)} \qquad (63)$$

where h is the height of the acoustic beam (in the Y direction) and all of the other variables have SI units. For sound waves in water, for which $\rho = 1000$ kg/m^3; $v_a = 1500$ m/s and $\eta_1 = 0.347$, equation (63) may be reduced to:

$$P_a = 5.61\ \left(\frac{h}{W}\right)\cdot p^2 \quad \text{(watts)} \qquad (64)$$

for $\lambda = 632.8$nm.

As a point of comparison, the results of Durao and Whitelaw (1974) provide at least order of magnitude agreement between experimental results and the predicted acoustic power requirements given by equation (64). Operating a water filled Bragg cell at 9.22MHz, with an acoustic beam 2.54 cm wide and 0.7 cm high, Durao and Whitelaw reported a maximum diffraction of 76% of the transmitted light intensity into the

+1 and -1 order beams, with approximately 10% in the zero order beam, for an electrical power input to the crystal of 0.56W.

Under similar conditions, i.e. $J_1^2(2\pi p)$ equal to its first maximum value, p = 0.289 and the Bessel function solutions of equation (57) predict diffracted efficiencies for the zero, ±1 and ±2 order beams as 10%, 70% and 20% respectively. Equation (64), with p = 0.289, h = 0.7 cm and W = 2.54 cm predicts an acoustic power requirement of 0.13W.

The differences between the predicted and experimental power requirements could be due to attenuation of the sound beam in the water; conversion efficiency of the quartz crystal or the non inclusion of the electrical power factor in the measurements taken by Durao and Whitelaw. It is, however, obvious from the results of the investigation that Debye-Sears scattering in an acousto-optic cell is a particularly attractive technique for optical frequency biasing since, if both the +1 and -1 orders are used, an optical frequency shift of twice the excitation frequency with a diffraction efficiency of at least 70% may be achieved for a very small electrical input power.

Although it would appear from the above analysis that the electrical input power could be reduced by increasing the interaction length W, this is only true up to a certain maximum value. Adler (1967) indicates that, due to diffraction broadening, a beam will be spread through an angle of $\pm \frac{2\lambda}{\Lambda}$ as it traverses the cell. If the spread of the diffracted beam in the direction of propogation of the sound waves

is $>\frac{\Lambda}{2}$, then destructive interference will result and the light intensity in the diffracted orders will decrease. This may be expressed in terms of the following relationships:

$$W_{max} = \frac{\Lambda^2}{4\lambda} \qquad (65)$$

$$\text{or} \quad \frac{K^2 W_{max}}{\beta} \ll 1$$

where $K(= \frac{\omega_a}{v_a})$ is the propogation constant of the sound wave and $\beta(= \eta\frac{\omega}{c})$ is the propogation constant of the light beam in the cell. Experiments for which this condition holds are said to lie within the Debye-Sears or Raman-Nath regime. For the Durao and Whitelaw investigations,

$$W_{max} = \frac{\Lambda^2}{4\lambda} = (\frac{v_a}{f_a})^2 \cdot 4\frac{1}{\lambda}$$

$$= \left\{\frac{1500}{9.22\text{x}10^6}\right\}^2 \text{ x } \frac{1}{4\text{x}632.8\text{x}10^{-9}}$$

$$= 1.05 \text{ cm}$$

hence their use of a crystal 2.54cm long violated this Debye-Sears criterion and may well have been the reason for the increased power requirement.

Since the maximum interaction length is inversely proportional to the square of the excitation frequency, the conditions indicated by equation (65) are almost invariably violated at higher acoustic frequencies and, in practice, this presents a limitation to the maximum optical frequency shift that can be obtained by this method. Thus it follows that if large diffraction efficiencies for acoustic frequencies in excess of this maximum are to be achieved, then a modification to the Debye-Sears technique is required. This modification is in the form of the Bragg reflection criteria.

3.4.2 Bragg Diffraction

If the orientation of the incident beam is adjusted so that the Bragg diffraction conditions are satisfied,it is possible to diffract a large percentage of the incident light into one particular order and to obtain constructive interference for higher acoustic frequencies than are allowed by the Debye-Sears criteria. With reference to Figure (18), classical geometric constructions may be used to derive the well known Bragg relationship and to verify the induced Doppler frequency, as follows:-

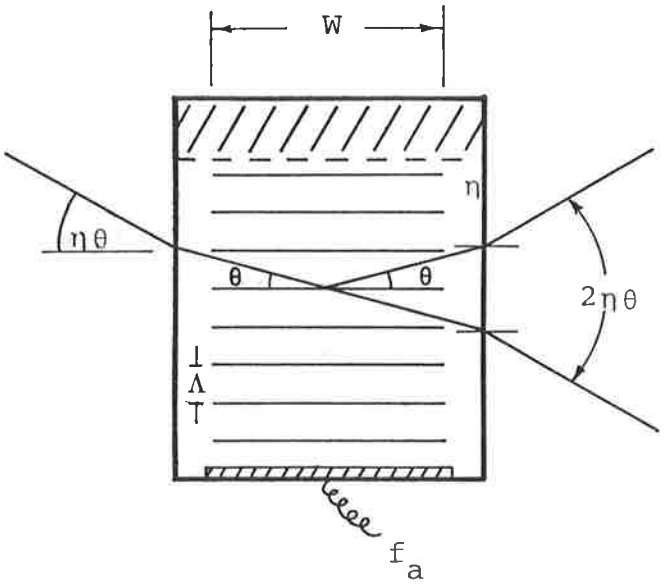

Fig. 18a.

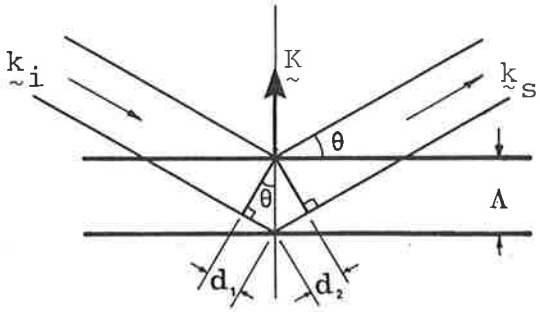

Fig. 18b.

Figure 18. Bragg Cell

When the optical path difference (= $d_1 + d_2$), for incident beams reflected by successive wavefronts, is an integral number of half wavelengths, constructive interference will result.

$$\text{For } n = 1,\ d_1 = d_2 = \frac{\lambda}{2}\ ,\ \text{hence } \sin\theta = \frac{\lambda}{2\Lambda}$$

$$\text{or} \quad \lambda = 2\Lambda \sin\theta, \tag{66}$$

the Bragg diffraction formula.

If $\underset{\sim}{k}_s$ and $\underset{\sim}{k}_i$ are the propogation vectors for the scattered and incident beams respectively and $\underset{\sim}{e}_s$ and $\underset{\sim}{e}_i$ represent the unit vectors in those directions, the Doppler frequency shift in the scattered beam is given by:

$$f_D = \frac{1}{\lambda} (\underset{\sim}{e}_s - \underset{\sim}{e}_i)\cdot\underset{\sim}{v}_a$$

where $\underset{\sim}{v}_a$ is the acoustic beam velocity vector.

The geometry of Figure (17b) gives

$$(\underset{\sim}{e}_s - \underset{\sim}{e}_i)\cdot\underset{\sim}{v}_a = 2\sin\theta\cdot v_a$$

hence

$$f_D = \frac{2v_a}{\lambda}\sin\theta \quad \text{and, since } v_a = f_a\cdot\Lambda,$$

$$f_D = 2\cdot f_a\cdot\frac{\Lambda}{\lambda}\sin\theta$$

Transposition of equation (66) implies that $\frac{2\Lambda\sin\theta}{\lambda} = 1$ and hence $f_D = f_a$, as expected.

An alternative analysis of the operation of the Bragg cell may be obtained by consideration of the photon - phonon interaction indicated in Figure (19).

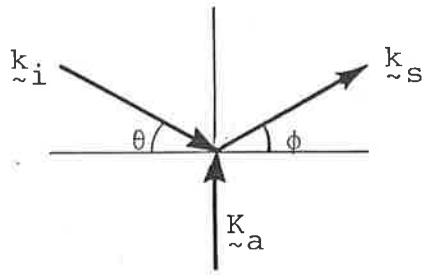

Figure 19. Photon-Phonon Interaction

If $\underset{\sim}{K}_a$ represents the incident phonon wave vector and

$\underset{\sim}{k}_i$ and $\underset{\sim}{k}_s$ are, respectively, the incident and scattered photon wave vectors, Brillouin scattering of the photon will result in the annihalation of the phonon, from which conservation of energy yields

$$\hbar\omega_s = \hbar\omega_i + \hbar\omega_a \tag{67}$$

and conservation of momentum gives

$$\hbar\,\underset{\sim}{k}_s = \hbar\,\underset{\sim}{k}_i + \hbar\,\underset{\sim}{K}_a \tag{68a}$$

Equation (67) reduces to

$$f_s = f_i + f_a, \text{ as expected} \tag{69}$$

and equation (68a) may be resolved into horizontal and vertical components as follows:

$$k_s \cos\phi = k_i \cos\theta \tag{68b}$$

and $$k_s \sin\phi = K_a - k_i \sin\theta \tag{68c}$$

Since $\lambda_s \simeq \lambda_i$, equation (68b) implies $\phi \simeq \theta$ which, when substituted into equation (68c), yields

$$\frac{\sin\theta}{\lambda_i} = \frac{1}{\Lambda} - \frac{\sin\theta}{\lambda_i}$$

i.e. $\lambda_i = 2\Lambda \sin\theta$, the classical Bragg equation.

The Bragg diffraction condition may therefore be represented by the propogation vector diagram of Figure (20), where conservation of momentum produces a scattered photon whose direction is changed by twice the Bragg angle and whose frequency is shifted by an amount equal to the applied acoustic frequency.

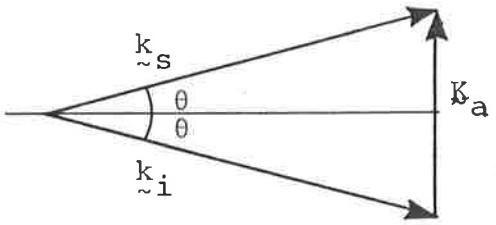

$$\underset{\sim}{k}_s = \underset{\sim}{k}_i + \underset{\sim}{K}_a$$

Figure 20. Propogation Vector Diagram

The determination of the scattered light intensity, as a function of applied acoustic power, for the Bragg regime is a more complicated process than the previous analysis for Debye-Sears scattering. The functional relationship is of the form:

$$\frac{I_1}{I_o} = f(W;M;\ P_a;\Lambda;\lambda) \tag{70}$$

where M is a figure of merit for the scattering medium, and Adler (1967) and Beiser (1974) propose that (70) may be approximated by:

$$\frac{I_1}{I_o} = \sin^2\ (\frac{\Delta\phi}{2})\cdot \tag{71}$$

$\Delta\phi$ is the phase excursion of the light in the medium and is given by:

$$\Delta\phi = \pi\ [\ (\frac{2}{\lambda^2})\cdot(\frac{W}{h})\cdot M\cdot P_a\ ]^{\frac{1}{2}} \tag{72}$$

for which, W is the acoustic beam width; h is the acoustic beam height; P_a is the acoustic power at the point of interaction and M is the figure of merit, defined by

$$M = \frac{\eta^6\cdot p^2}{\rho\cdot v_a^{\ 3}} \tag{73}$$

(here p is the elasto-optic coefficient, defined as the derivative of the reciprocal dielectric constant $\varepsilon_o/_\varepsilon$, for optical frequencies, with respect to s).

Although equation (71) can only be regarded as an approximate relationship, it does indicate that when $\Delta\phi (= \frac{2\pi \cdot W \cdot \Delta\eta}{\lambda_o})$ is equal to π radians, the incident beam is completely diffracted into the selected first order mode. These results are confirmed by the investigations of Kleinhans and Fried (1965) who reported diffraction of up to 90% of the incident beam into the -1 order for a water filled Bragg cell of similar design to that used by Cummins et al in 1963. In general, however, the acoustic power requirements for diffraction efficiencies of this order are much higher than the figures quoted for the Debye-Sears scattering technique. Durao and Whitelaw quoted figures of 20W electrical power at 30MHz for a diffraction efficiency of 88% and Kleinhans and Fried report an applied crystal voltage of 105V r.m.s. for a diffraction efficiency of approximately 90% at 15MHz. Although these power requirements are considerable, they are not prohibitive and are, in fact, significantly less than the power requirement of an equivalent electro-optic system.

It would appear from these results, then, that Bragg diffraction is a very efficient method of optical frequency conversion and it is indeed the case that a number of commercially produced units, such as the DISA model 55LO2, are currently available for flow direction discrimination. The Bragg technique becomes even more attractive when it is considered that the cells may be used in parallel or series combinations, thus allowing the use of the more efficient solid acousto-optic materials and the selection of almost any desired optical frequency bias. Furthermore, the developments of surface acoustic wave oscillator and thin film waveguide modulator techniques, such as those reviewed by Chang et al

(1974), will undoubtedly lead to the evolution of very small and very efficient integrated optical units capable of providing a very wide range of optical biasing frequencies.

Using the design criteria indicated in the foregoing analyses, a water filled acousto-optic cell was constructed by this author for use with the LDV in either the Bragg or Debye-Sears modes of operation. A sectioned view of the cell is included in Appendix B2 and a circuit diagram of the crystal driver is presented in Appendix B1.

A quartz crystal oscillator with a diameter of 3cm and a thickness of 0.298mm was used to generate the ultrasonic sound beam. The crystal was operated at its fundamental,resonant frequency of 9.86MHz for the Debye-Sears mode and at the third harmonic of 29.57MHz for Bragg diffraction. These frequencies were selected because they offer a near optimum compromise between acoustic power requirements, crystal dimensions; interaction length and acoustic absorption coefficient while permitting both modes of diffraction, at suitable bias frequencies, from a single quartz oscillator.

Electrodes for the crystal were formed by vacuum deposition of a 0.5μm layer of gold and, to reduce the acoustic power requirements, the upper electrode was restricted to a strip 0.7cm wide and 2.9cm long. The axis of the strip was parallel to the centre line through the optically flat windows so that, for the analysis used in the previous sections, h = 0.7cm and W = 2.9cm.

Water was selected as the acousto-optic material since

its figure of merit (see equation (73)) is quite high but it was noted that an acoustic attenuation of approximately 2dB/cm was experienced when the cell was operated in the Bragg mode at 30MHz. For this reason, the crystal was aligned with the centre of the windows and maximum diffraction efficiency was achieved when the incident laser beam just cleared the top surface of the crystal.

The 7.5cm column of water on top of the crystal was found to provide sufficient attenuation at 30MHz to prevent the occurrence of standing waves in the cell. As an additional measure, a fine wire mesh, in which the hole size was comparable with the acoustic wavelength in the medium, was mounted near the end of the cell and acted as a sound absorbing material. The requirement for this dispersive medium is much greater at lower frequencies since the attenuation at 10MHz is typically only 0.25dB/cm. These results are consistent with the findings of Pinnow (1970), where the material loss characteristics are designated by $\frac{\alpha}{f^2}$, in which α is the attenuation per unit path length and f is the acoustic frequency.

Modes of Operation

The versatility of the acousto-optic cell can be readily demonstrated by a comparison of the three modes of operation illustrated in Figure (21).

In the first example, Figure (21a), the crystal was driven at 29.57MHz and the cell was operated in the Bragg regime. Analysis of the aforementioned Bragg criteria for these cell dimensions and acoustic frequencies yields:

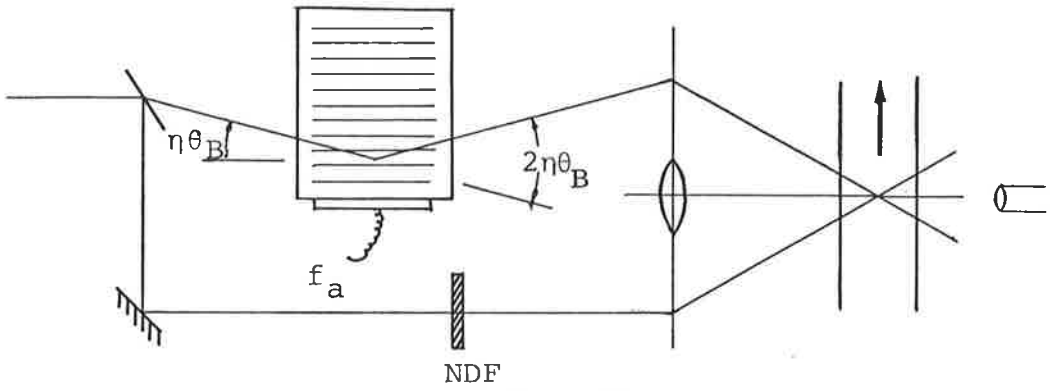

Fig. 21a.

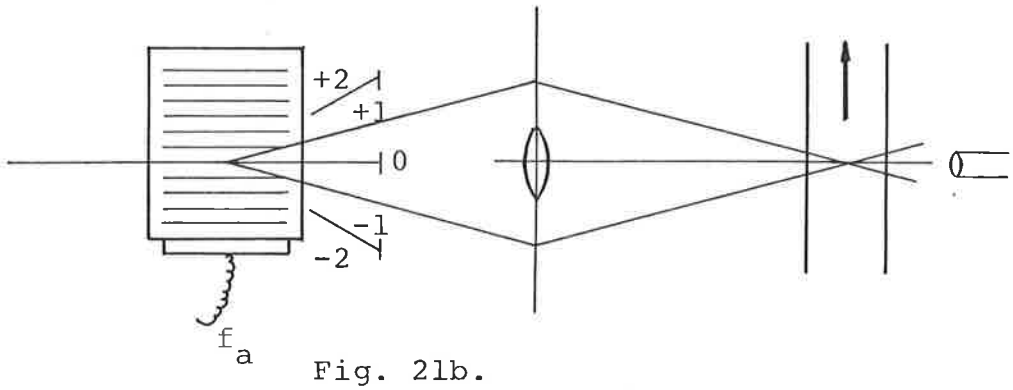

Fig. 21b.

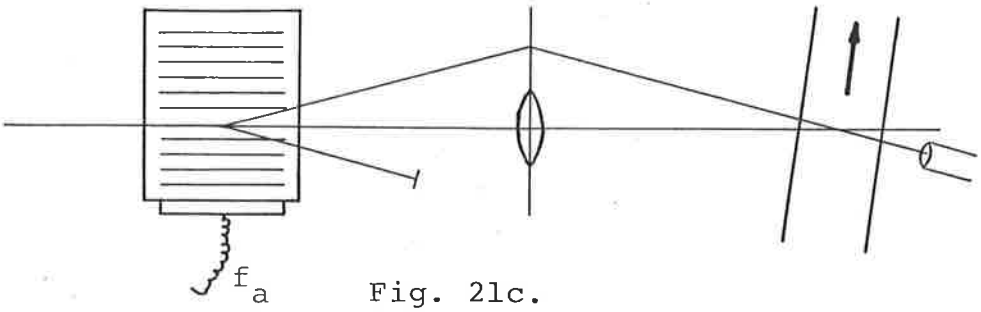

Fig. 21c.

Figure 21: Acousto-Optic Cell - Modes of Operation

$\theta_B = 0.357^o$; N = 3.57 and $\Lambda = 50.7\mu m$

and it was noted that when the incoming beam was incident at a point approximately 2mm above the crystal surface, a diffraction efficiency of better than 70% was achieved with an applied voltage of $125V_{RMS}$ (8.5W electrical power). This configuration was found to be most suitable for providing a high bias frequency (f_b = 30MHZ) for both the fringe

and reference modes of operation. When used in fringe mode, the beams were adjusted to approximately equal intensities by providing maximum input power to the crystal oscillator. For reference mode operation, the intensity of both beams could be independently controlled by either reducing the acoustic input power to the Bragg cell or changing the opacity of the neutral density filter. Although both of these techniques successfully control the intensities of the two beams, a higher overall efficiency is possible if the 50/50 beam splitter in Figure (21a) is replaced with a variable density neutral filter and the incoming laser beam is split into two components with the required relative intensities.

In Figures (21b) and (21c), two possible modes of operation of the cell in the Debye-Sears regime are illustrated. In the first of these, a symmetrical system uses the +1 and -1 diffracted orders and the applied acoustic power is reduced so that the argument of the Bessel function relationship in equation (57) is equal to the value required for the first maximum of $J_1^2(2\pi p)$. Experimentation with the acousto-optic cell revealed a combined diffraction efficiency of approximately 70% when the applied acoustic power was reduced to about 0.5W and, since both the +1 and -1 orders are used, the bias frequency between the two beams was set at 19.72MHz. The symmetry of the diffracted orders in terms of both angular deviation and intensity were found to be significant advantages for this configuration when fringe mode applications requiring a bias frequency of approximately 20MHz were considered.

The second configuration in the Debye-Sears regime,

i.e. Figure (21c), was used for reference mode operation and the acoustic power was further reduced to the point where the intensity of the +1 diffracted order was approximately equal to $0.05I_o$. In this case, the optical bias frequency was equal to the fundamental crystal frequency (9.86MHz) and the configuration was found to be most suitable for flow investigations using reference mode techniques and requiring a low bias frequency.

Of all the methods for optical frequency biasing reviewed in this Chapter, the acousto-optic cell is considered to be the most suitable technique for high velocity flows since it offers a high conversion efficiency, at suitable bias frequencies, for a modest input power requirement. The ease of operation and alignment; versatility and non-requirement for moving parts are additional features that provide practical advantages over other techniques when the cell is incorporated into complex optical configurations.

CHAPTER FOUR

REQUIREMENTS OF AND DESIGN APPROACH FOR A HIGH RESOLUTION LDV

SUMMARY:

Based on the results of the foregoing analyses, this chapter elucidates the important requirements for a high resolution LDV. The essential and desirable characteristics are outlined and the advantages and disadvantages of currently available techniques are discussed.

The important considerations of temporal and spatial resolution; signal dropout; directional aliasing; signal processing and spectral broadening are summarized with reference to both frequency - domain analysis and time-series analysis techniques. For single particle scattering in high turbulence, high velocity flows, it is shown that time-domain methods (using the elapsed time between successive points of equal phase) offer significant advantages over the conventional techniques of frequency-domain analysis.

4.1 REQUIREMENTS OF A LASER-DOPPLER SYSTEM

4.1.1 Optical Frequency Biasing

For the investigation of oscillatory or high turbulence flows in fluid mechanics and the analysis of surfaces vibrating about a mean position in acoustics, the requirement for optical frequency biasing or directional phase determination in an LDV is well understood. Optical biasing also allows a simplification of the demodulation circuitry by the provision of a centre frequency for frequency tracking and phase lock detection systems. Signal to noise ratios are signifi-

cantly improved since narrow bandwidth filters may be used to exclude the inherent low frequency noise in Doppler signals. Greater versatility in the application of the LDV is also provided in that the fringes may be made to scan in the same direction as the mean fluid flow, thereby increasing the range of the instrument, or in the opposite direction to the flow. This ability to compromise between velocity range and resolution is a feature of the LDV that is not so readily incorporated into most other flow detection systems.

In Section 2.4.3 it was shown that optical frequency biasing allowed a reduction of the focal volume dimensions, without a corresponding increase in the spectral broadening due to the finite signal lifetime, while Section 2.5 indicated that the directional aliasing limitations of fringe crossing detectors could be satisfactorily removed, provided that the bias frequency was sufficiently high. For these reasons it is considered that the ability to incorporate a high frequency optical biasing technique is a very desirable feature of an LDV system. This requires that the frequency response of the signal processor be as high as possible in order to demodulate the Doppler signal.

4.1.2 Sample Biasing

All of the preceeding analyses have, by implication, assumed that only a single scattering particle is present in the focal volume at any one time. If this is not the case, random phase variations can result in beat frequencies and amplitude modulation, with a confusion of the Doppler signal beyond an acceptable level. Although it is possible to ensure

that the probability of more than one particle being present in the focal volume at any one time is minimal by having a very sparsely seeded flow, this condition may result in a bias towards the low turbulence frequencies since it is not possible to obtain any information about turbulence frequencies that are much higher than the mean sampling frequency.

Dimotakis (1975) suggests that an optimum condition of:

$$0.1 < n\,V_c < 1.0 \tag{74}$$

(n is the mean particle number density and V_c is the effective scattering volume) is suitable for most single scattering particle applications, and that, if the particles are randomly distributed in the flow,the probability of finding exactly one in the focal volume V_c, is given by a Poisson distribution, as

$$p_1 = n \cdot V_c \cdot e^{-nV_c} \tag{75}$$

and the probability of finding more than one is given by:

$$p_{>1} = 1 - (1+nV_c) \cdot e^{-nV_c} \tag{76}$$

Although these probabilities represent the probability, at any one time, that one or more particles will be present in the focal volume, they do not contain any information about how frequently the flow will be sampled. As Dimotakis has explained, if the scattering particles are randomly dispersed in the medium, the flow rate will be randomly sampled in time. However, since the rate at which scattering particles cross the focal volume is a function of the localized fluid velocity vector, the sampling process is coupled to the measured quantity and individual measurements cannot be treated as

statistically independent.

Furthermore, if there is a dead time associated with the signal processor, i.e. there exists a time interval following a measurement within which a subsequent signal is ignored, the sampling bias may be further complicated since the number of particles that are rejected will be higher when the particle density, i.e. fluid velocity, is high than when the number of particles is low. Any signal processing technique, such as that proposed by Steenstrup (1975), where individual measurements are considered to be statistically independent and average velocity components are determined by summation methods must introduce a sampling bias and, if considered at all, any biasing algorithm that attempts to compensate for the sampling bias will at best be controversial. A far more accurate determination of the statistics of the flow is possible if both the time at which each measurement was made and the velocity information are recorded. For example, in the determination of average velocity,

$$\bar{u} = \frac{1}{\Sigma \Delta t_i} \cdot \sum_{i=1}^{N} \cdot u_i \cdot \Delta t_i,$$ and the auto-correlation function,

$$R(\tau) = \frac{1}{\Sigma \Delta t_i} \cdot \sum_{i=1}^{N} \cdot u(t_i) \cdot u(t_i + \tau + \Delta t_i) \cdot \Delta t_i,$$ the provision of both u_i and Δt_i data allows a complete evaluation of the functions without sampling bias. Alternatively, if both forms of information are recorded, the complete velocity - time history of the signal may be reconstructed and then sampled in a standard and statistically independent way to determine the desired quantity.

This ability to record both velocity and real-time

data, which is considered essential for a high resolution LDV, is not available on any current commercial system.

4.1.3 Spectral Broadening

In Section 2.4.3 it was established that a compromise between the spectral broadening due to the finite signal lifetime and velocity gradients in the focal volume could be achieved if the signal processor only demodulated those Doppler bursts that contained a minimum number of fringe crossings with an amplitude greater than the acceptance threshold. In principle, if the signal processor does not resort to frequency analysis, the Doppler frequency may be obtained by measuring the time between successive points of equal phase. Since the period of the waveform, which is the time of flight from one fringe to the next, cannot depend upon the total number of fringes, the problems due to frequency broadening from discontinuous or amplitude modulated waveforms may be completely removed and the compromise with velocity gradient broadening discharged.

From this it can be seen that the full potential of the laser Doppler technique can only be realised if time-of-flight measurements are used in preference to conventional frequency analysis methods. Such techniques invariably involve the use of digital counting circuitry and associated signal processing methods in contrast to the usual methods of analogue spectrum analysis.

4.2 FREQUENCY DEMODULATION METHODS

In the broadest sense, a distinction may be made between those demodulation techniques, usually analogue systems, that operate in the frequency domain and those that use the time-series signal as a basis for demodulation. The advantages and disadvantages of frequency domain and time domain analysis systems are reported in this section, together with the results of investigations conducted by this author.

4.2.1 Frequency Domain Analysis

In principle, any analogue laser Doppler system that operates in the frequency domain seeks to convert the temporal fluctuations in the Doppler signal frequency to a corresponding voltage or current variation. Once obtained, the demodulated velocity signal may be used as a record of instantaneous fluid or surface velocity or analysed in any one of a number of ways to obtain appropriate statistical information.

Although this appears to be a straightforward problem, the conventional methods of frequency demodulation used in other fields have had only limited success in the demodulation of time - discontinuous Doppler signals because of the rather unconventional characteristics of signals derived from turbulent flows. The most troublesome of these characteristics are (a) large variations in signal frequency and modulation index; (b) discontinuity and/or amplitude modulation of the Doppler signal; and (c) low signal to noise ratios and significant spectral broadening.

In a turbulent flow, the frequency of the Doppler

signal may fluctuate over a range of six to seven orders of magnitude, depending upon the mean velocity of the flow and the LDV system parameters, while the rate of frequency change may vary from a low value to frequencies in excess of 50KHz. The frequency modulation index, β, therefore, which is defined as the ratio of the Doppler frequency deviation to the modulating frequency, f_m,

$$\text{i.e.} \quad \beta = \frac{\Delta f_D}{f_m} \tag{77}$$

may vary from a small fraction to several hundred and in a random fashion. Conventional F.M. demodulation circuits cannot cope with these simultaneous variations in signal frequency and modulation index. A Q spoiled ratio detector or phase shift discrimination may be used for relatively small frequency excursions, but both require a larger SNR than is commonly encountered in laser Doppler systems and a centre frequency for the system which is only present if an optical biasing technique is employed.

A natural progression from these techniques is towards a frequency tracking system such as the phase-locked-loop (P.L.L.). Here again, a centre frequency is required, but modern P.L.L.'s have a hold in range in excess of ± 70% of the centre frequency with excellent linearity in the demodulated output. This ability of the P.L.L. to demodulate over a wide frequency band and its low cost and simplicity combine to make it a very attractive detection system. In the initial stages of the project, this author experimented with a Signetics NE561B P.L.L. to demodulate the Doppler signal obtained from a vibrating mirror in a Michelson interferometer. Frequency biasing of approximately 0.5MHz was obtained with the rotating diffraction grating described in Section 3.1 and a

schematic of the optical configuration and circuit diagram of the detector are shown in Figure (22).

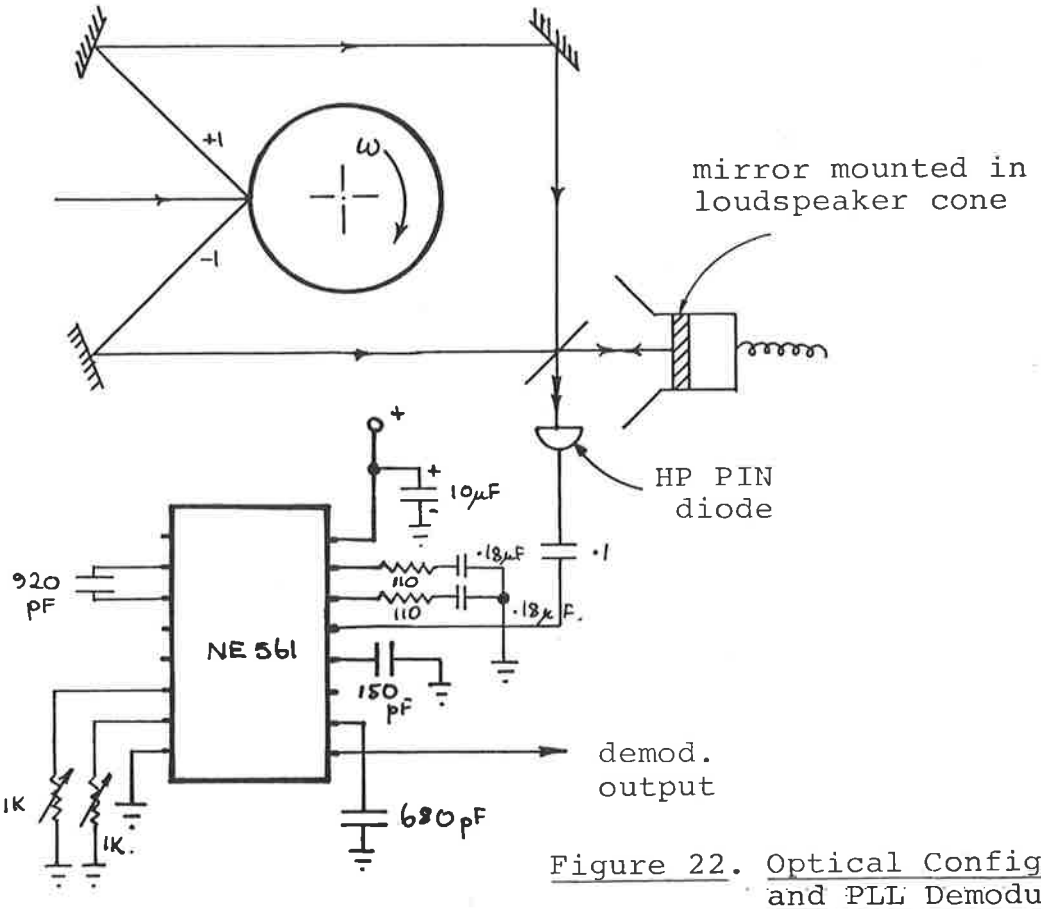

Figure 22. Optical Configuration and PLL Demodulator

While the Doppler frequency excursions did not exceed the tracking range of the loop (approximately ± 150KHz in this case) and the modulating frequency remained below approximately 25KHz, the P.L.L. provided excellent demodulation of the driving signal. However, when either the peak mirror velocity became too large, or the driving frequency became excessive, it was noted that the demodulated waveform became distorted and decreased in signal to noise ratio. These two observations exemplify the inherent disadvantages in the use of phase-locked-loops. In the first instance, exceeding the tracking range of the loop causes dropout, i.e. an uncertainty in the VCO frequency, which will not be recovered until the Doppler frequency re-enters the capture range of the P.L.L. In every case, the capture range is less than, or at best

equal to the tracking range of the loop and hence the signal processor dead time is increased. Secondly, distortion of the output waveform and a decrease in SNR occur when the slew rate limit of the P.L.L. is exceeded. This is most likely to occur when the high frequency components dominate the power spectral density of the Doppler signal and since, in the design of the loop characteristics, a trade-off is made between loop gain and bandwidth, it is clear that no single circuit configuration can provide optimum processor characteristics for all applications.

Further, for the application just described, the Doppler signal was continuous and of relatively constant amplitude. When the laser beam was chopped with a perforated rotating disc, in order to simulate a time discontinuous signal, the output SNR and the uncertainty in the VCO frequency during periods of signal dropout were seriously degraded. This is to be expected since the loop becomes free running in the absence of an input signal and the damping coefficient and loop gain, which are of critical importance, are fixed and can therefore not offer optimum response for all input signals.

From this it should be clear that frequency domain analysis techniques, and in particular, the P.L.L., are best suited for continuous, constant amplitude Doppler signals, such as those that may be obtained in acoustics applications, but will always suffer the severe practical limitations of spectral broadening and sample biasing when applied to the demodulation of discontinuous Doppler bursts, for example, those that are obtained from single particle scattering in high turbulence flows.

4.2.2 Time Domain Analysis

Determination of the instantaneous Doppler frequency by the measurement of the elapsed time between successive points of equal phase will, in principle, allow the effective probe volume to be reduced since the problems due to finite signal lifetime are avoided. This is shown by the analysis of Dimotakis, where the spatial resolution of the LDV is considered in terms of two separate components, the absolute spatial resolution, ℓ_a, and the relative spatial resolution, ℓ_r. For all other velocity measuring systems, ℓ_a and ℓ_r are the same, but, for the LDV, they may be independently controlled in terms of the transmitting and receiving optics and the signal processing technique. In general, ℓ_a is associated with the effective probe volume while ℓ_r may be considered as the minimum length in the focal volume, over which a reliable frequency measurement may be made.

If the LDV signal processor uses any form of frequency domain analysis then the Doppler frequency will be effectively averaged over the whole of the burst and ℓ_a and ℓ_r are essentially the same. If, however, time domain analysis is used and the time of flight of a single scattering particle is recorded, ℓ_r may be reduced to at least the spacing between successive fringes in the focal volume, subject to the measurement resolution of the signal processor. In principle ℓ_r is not limited to the fringe spacing, d, since the Doppler frequency is given by:

$$f_D(t) = \frac{1}{2\pi} \cdot \frac{d\phi}{dt} \qquad (78)$$

where ϕ is the instantaneous phase of the detected signal, and therefore the period of the Doppler frequency may be

obtained by measurement over any fraction of a wavelength. Alternatively, if a frequency biasing technique is employed and the fringes are made to traverse the focal volume, the relative spatial resolution for points of equal phase (e.g. fringe zero crossings) is given by:

$$\ell_r \geq \frac{d}{(\frac{f_b}{f_D} \pm 1)} \tag{79}$$

where d is the fringe spacing; f_b is the bias frequency and f_D is the instantaneous Doppler frequency. The selection of the sign in equation (79) is dependent upon whether the fringes are moving in the same direction (-) or in the opposite direction (+) with respect to the scattering particle but it can be seen that if $\frac{f_b}{f_D}$ is made very large, $\ell_r \to o$, thus providing the incentive for and the limitations to time domain analysis.

Practical limits, in the form of the temperal resolution of the signal processor and the Brownian motion of the particle, may well be experienced, but it is clear that time domain analysis, by removing the problems due to finite signal lifetime broadening and reducing the relative spatial resolution to significantly less than one fringe spacing, is intrinsically a more viable techniquc for the realisation of optimum operating conditions.

Also, since a signal processor operating in the time domain is already recording temporal information, it is a relatively simple extension of the technique to simultaneously record real time information for discontinuous Doppler signals. If the sample time, τ_s, is less than $\frac{1}{f_{max}}$, where f_{max} is the maximum turbulence frequency and measurements are recorded

for a time, T, such that $T >> \frac{1}{f_{min}}$, where f_{min} is the minimum turbulence frequency, the sampling bias discussed in Section 4.1.2 may be totally removed by recording both velocity and real-time data.

A very high speed digital, time-domain signal processor was constructed by this author and designed to incorporate the majority of the foregoing LDV requirements. A description of the principle of operation and the results of experimental investigations are presented in the following chapter.

CHAPTER FIVE

OPERATION OF THE LDV

SUMMARY:

This chapter describes in detail the operation and characteristics of a high speed, digital LDV that uses time-series analysis techniques to determine instantaneous velocity information over a wide range of analogue frequencies.

The system is described, firstly in block diagram, and then in detailed form and it is shown to include the majority of the essential and desirable characteristics indicated in the previous chapter. Of particular significance is the ability of this LDV to record both velocity and real time information within one period of the main clock frequency, a feature that enables a reduction of the digitization error for consecutive measurements and a complete reconstruction of the velocity-time history of the scattering source. These two facilities, which are not available in other instruments, are used to enhance the versatility of the system and to completely remove the problems due to sampling bias.

The acousto-optic cell and signal processor are used to demodulate the Doppler signal from a Michelson interferometer in which a front surface mirror is mounted on the spindle of a shaker.

5.1 INTRODUCTION

The design approach that has been indicated in the previous chapter was utilised in the construction of a high speed, digital Laser Doppler Velocimeter capable of velocity measurements of continuous and discontinuous data in the range 10 mm/s to 600 m/s for analogue frequencies from DC to 100KHz. The system specifications that are listed at the end of this chapter have been made possible by the use of MECL III and MECL 10K series logic components and the ability of the LDV to acquire complete velocity and real time information within a period as short as 100 ns.

Velocity information is derived from the Doppler frequency which is in turn determined within the system by recording the time required to count a preset number of fringe crossings. The time required for each such "measurement" is obtained by latching the output of a free running counter at the beginning and end of the count period and subtracting the two numbers in an arithmetic logic unit. This difference is therefore proportional to the time required for N fringe crossings and may be interpreted as frequency data. Particle or surface velocity is then obtained by application of equation (9) i.e.

$$v_{p_y} = f_D \frac{\lambda_o}{2\sin\theta}$$

5.2 BLOCK DIAGRAM DESCRIPTION

A simplified block diagram of the signal processing elements of the LDV is included as Appendix A2. This diagram indicates that the system may be considered in terms of the following five units:-

U1 - Analogue Unit

U2 - Main Control Unit

U3 - Main Counter Unit

U4 - Buffer Storage Unit

and U5 - D to A Converter Unit

It is the purpose of this section to describe the functional operation of each block, together with the system interconnections and control sequences

Analogue Unit - U1

This unit contains the photo detector, preamplifier and driver, a variable sensitivity Schmitt Trigger and a level detector to authenticate the signal levels. The purpose of this unit is to amplify the photodetector output to suitable logic levels and to provide, by means of the envelope level detector, a verification of adequate signal strength or, alternatively, an indication of signal "dropout" for discontinuous data. The input data is considered to be acceptable when the logic signal $\overline{\text{LEVEL}}$ is LOW.

Main Control Unit - U2

Once amplified and authenticated, the Doppler signal is passed to the Main Control Unit and is counted in the S and B counters as "fringes". The operator of the LDV has front and back panel control over both the number of fringes that will be counted within one measurement (S Counter setting) and the maximum number of measurements that will be recorded within each burst of information (B Counter setting). These facilities are provided to allow an optimization of the

compromise between velocity resolution and maximum detectable analogue frequency.

Output pulses from U2 occur at the beginning ($\overline{\text{INITLP}}$) of the first measurement and at the end (ENDPUL) of each measurement in a burst. These pulses are used to clock the latches L1 and L2 in the Main Counter Unit - U3.

Front panel START; STOP; AUTO STOP and DELAY TIME BETWEEN BURSTS (DTBB) controls are also provided by the Main Control Unit.

Main Counter Unit - U3

The Main Counter Unit consists of a MECL III clock generator; a 32 bit counter chain; two 16 bit latches and a 16 bit arithmetic logic unit wired as a subtractor.

At the beginning and end of every measurement, the latches L1 and L2 are clocked by either $\overline{\text{INITLP}}$ or ENDPUL from U2. L2 is clocked before L1 in order that the output of L1 may be read before it changes to the new value. After settling, the difference between these values, which is determined by the subtractor, is equal to the number of main clock pulses that have been counted in the preceeding measuring interval. This numerical value is then either written into the Buffer Storage Unit - U4 or transferred to the output latch for conversion to an analogue signal in the DAC Unit - U5.

In addition to this data, which may be interpreted as Doppler frequency (i.e. particle velocity), the second 16 bits of the main counter train are recorded at the beginning

and end of every measurement. This provides a record of the "real" time at which each measurement was made thus removing the biasing errors due to the increased probability of finding a particle in the focal volume at higher fluid velocities.

Buffer Storage Unit - U4

When used in conjunction with a Data Acquisition System, the velocity and real time data are each presented as a 16 bit binary word at the back panel output data connector. As it is likely that the maximum measurement rate of the LDV (nominally 10MHz) could exceed the data transfer rate to the Data Acquisition System, a small memory storage is provided by the LDV in U4.

Each memory is a 16 x 16 RAM with RAMs IA and IB used for velocity data, and IIA and IIB for real time information. The memory control unit multiplexes the functions of the parallel RAMs so that while IA and IIA are in the "Write" mode, IB and IIB are in the "Read" mode and vice versa. This ensures that the time lost due to data transfer is minimized and that the system is only disabled by the memory busy signal, $\overline{\text{MEMDIS}}$, when the measurement (Write) rate is greater than the transfer (Read) rate.

Digital to Analogue Converter Unit - U5

Even if the digital output facilities of the LDV are in use, an analogue reconstruction of the velocity information is available at the ouptut of the D to A converter by selection of the most suitable eight of the 16 bits from the output latch. As the latch is updated at the end of each measurement,

it performs the function of a sample and hold and the output of the DAC may be viewed directly with an oscilloscope or recorded on the front panel meter.

Front panel controls for the meter include range and RMS or Peak value selection, but it should be noted that the averaging process of the meter will only be valid when continuous signal information is available at the photodetector.

5.3 DETAILED SYSTEM OPERATION - SIGNAL PROCESSOR

5.3.1 Analogue Unit - U1

Appendix A3 includes a detailed circuit diagram of the three types of photodetector circuits that were constructed for use with the LDV.

The RCA type 8645 photomultiplier tube that is shown in figure U1-a was used for applications involving low scattered light intensities and requiring significant current amplification. The photo anode of the PMT was connected directly to the input of an LM 733C video amp wired as a transconductance amplifier; a configuration that was selected in order to obtain maximum signal to noise ratio. Although difficulties were experienced with amplifier gain - bandwidth product limitations when a Bragg bias frequency of 30MHz was used, the amplifier proved to be very satisfactory for low frequency, low light intensity measurements.

The output of the LM733C was buffered by an LH0033C fast buffer amplifier which provided current drive for up to 20 ft. of coaxial cable without serious distortion or attenuation of the signal waveform. A simple RC high pass filter was

used to decouple the 1.2V D.C. offset on the output of the video amplifier from the input to the buffer.

The other two detector circuits similiarly used the LH0033C as a line driver, but in these two cases, the LM733C was used as a voltage amplifier with an open-loop gain of approximately 42dB (at 30MHz) and the PMT was replaced with a Hewlett-Packard PIN photodiode. U1-b used a single 1KΩ load resistor for transconductance while circuit U1-c employed a two transistor transconductance amplifier with a 15KΩ feedback resistor, as recommended in H.P. Application Note No. 917.

Both of these circuits were found to be well suited to applications offering large reflected or scattered light intensities such as vibration measurements on objects or surfaces with highly reflective coatings.

As reported by Smits (1974), the PIN diode was found to offer the significant practical advantages of smaller size; simplicity of operation; higher SNR and greater frequency response over the PMT and, in general, is far preferable to the PMT for high scattered light intensity applications where the spectral sensitivity of the latter is not required.

LDV Input Amplifier - Schmitt Trigger

The purpose of the input amplifier is to amplify and limit the Doppler signal from the photodetector to logic levels compatible with the input requirements of the signal processor. It consists of three elements of a MECL III 1692L quad line receiver, operating as a variable sensitivity, two

stage video amplifier, followed by a Schmitt trigger, and a MECL 10K inverter. The input is capacitively coupled through a 0.1μF capacitor and has an input impedance of 50 ohms with Schottky diode clamp protection. The input trigger sensitivity has been made adjustable through R1 in order that the amplifier may be made insensitive to the background noise for each particular application. The output from the amplifier is therefore a pulse train of constant amplitude where transitions between the logical 1 and 0 states correspond to variations of the input voltage about the amplifier threshold.

For the typical Doppler signal described in Section 2.1.3, the output of the Schmitt trigger is shown in Figure (23).

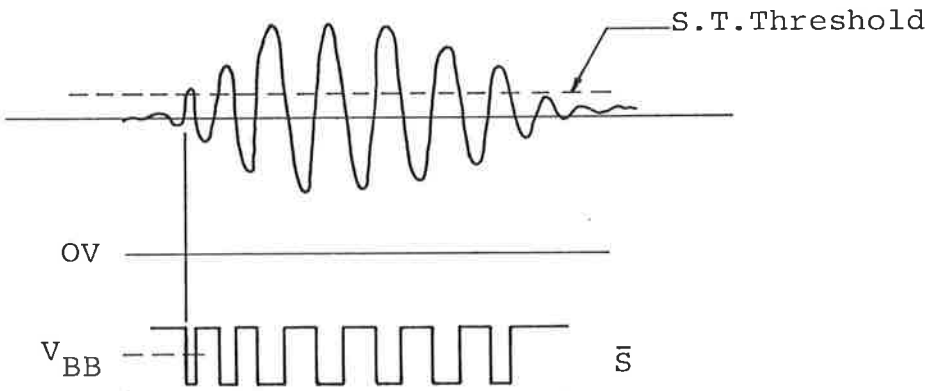

Figure 23: Schmitt Trigger Operation

Tests on the performance of the amplifier with a simulated input showed that it would suitably amplify and limit analogue frequencies in excess of 100 MHz for variations of ± 20mV about the threshold value. These specifications are more than adequate for any of the applications for which the LDV was designed.

In operation it was noted that a slight variation in mark to space ratio occurred in the output waveform due to

the asymmetrical nature of the switching threshold but this in no way limited the operation of the digital counting circuitry that was used in subsequent stages.

Another significant advantage in the use of digital circuitry, as opposed to such analogue devices as the phase-locked-loop, is the inherent insensitivity to amplitude modulation of the input waveform. If the peak value of the waveform exceeds the switching threshold, the waveform is amplified, limited and accepted. If it does not exceed the threshold, the output of A27-3 remains high and the fringe crossings are not counted. Provided, therefore, that some record is maintained of when the input data is acceptable and when it is below an acceptable level, this simple operation provides a solution to the severe problems of amplitude modulation and signal dropout that were shown in Section 4.2.1 to limit the application of P.L.L. and other analogue techniques. This indication of data acceptance is provided in the LDV by the level detector and the logic signal $\overline{\text{LEVEL}}$.

Level Detector

From the circuit diagram, the design and operation of the level detector is seen to be essentially the same as that of the input amplifier. The input to the level detector is similarly terminated and protected but it is also provided with an independent sensitivity control, R_2, which sets the "acceptance level" of the input Doppler waveform. This control is generally adjusted so that the switching threshold of the level detector is greater than the threshold of the input amplifier.

In addition, R_3 and C_1 have been selected so that the level detector will operate as a retriggerable monostable multivibrator. When triggered by the positive transition of a Doppler fringe of acceptable magnitude, $\overline{\text{LEVEL}}$ will go LOW and remain in that state for approximately 50ns after the negative transition of the original Doppler fringe. If the level detector is retriggered within 50ns of this negative edge, $\overline{\text{LEVEL}}$ will remain LOW, indicating that another acceptable Doppler fringe has been received. If the detector is not retriggered within that time, $\overline{\text{LEVEL}}$ goes HIGH, indicating the end of a Doppler burst. This operation is schematically represented in Figure 24.

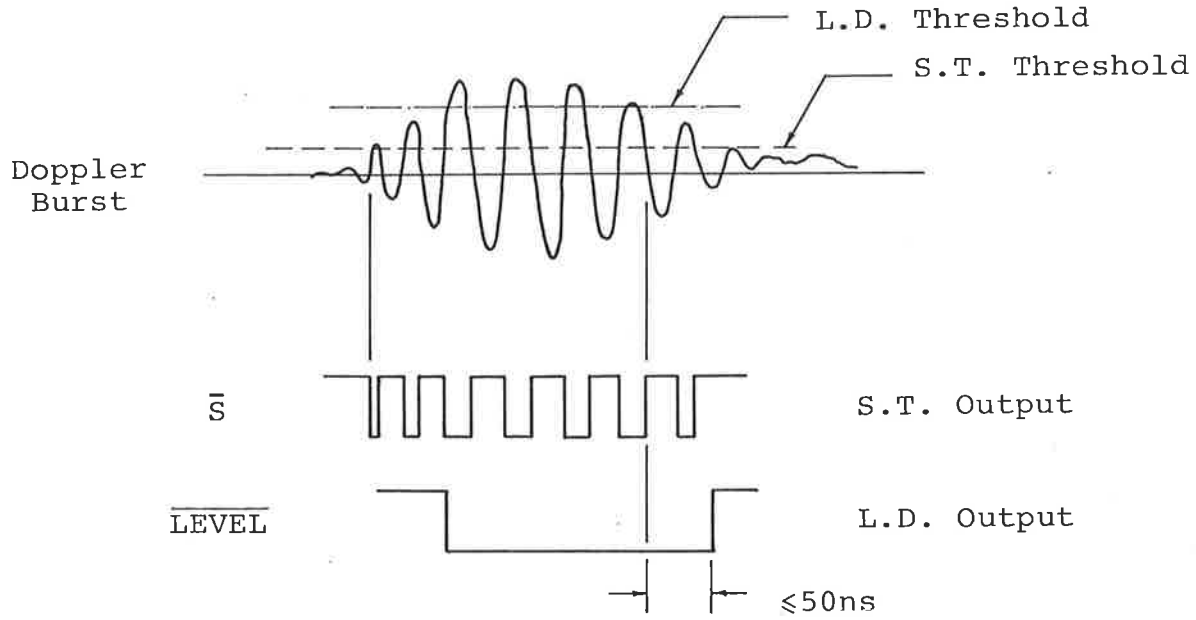

Figure 24: Operation of Level Detector

It was found that, provided a reasonable differential between the input amplifier threshold and the acceptance level was maintained, the one or two extra pulses that could be counted at the end of a burst due to the hold time of the level detector did not create any spurious counting results. It should also be noted that the values stated for R_3, C_1 and the hold time for the level detector presuppose that a centre frequency of approximately 30MHz is provided by means

of the Bragg cell described in Section 3.4.2. If some other bias frequency is used, it would be necessary to modify the values of R_3 and C_1 to suit.

With the ability to independently control the input amplifier sensitivity and the acceptance level for Doppler fringes, the LDV is capable of almost complete noise immunity by selecting only the most reliable information from scattering particles in the focal volume. This facility offers a solution to the noise immunity problems associated with P.L.L. and other analogue techniques while the logic signal $\overline{\text{LEVEL}}$ is used to indicate signal dropout. The other very serious P.L.L. limitations of capture range; tracking range; loop stability and recovery time are not experienced in this, and other, time domain analysis techniques.

5.3.2 Main Control Unit U2

With the exception of the external data transfer commands DATATRANS and TRANSCOMP, the Main Control Unit is the originator of all data control commands within the LDV. Primarily, its functions are to count a preset number of Doppler fringes in the S Counter for each measurement; control the number of measurements that are made during each Doppler burst and to generate a data pulse at the beginning of the first measurement ($\overline{\text{INITLP}}$) and at the end of every subsequent measurement (ENDPUL).

When a Doppler signal of acceptable level is received in U1, the output ($\bar{S}$) of the Schmitt trigger is a pulse train and $\overline{\text{LEVEL}}$ goes LOW. If the other four inputs to B21-2 are also LOW, A21-1 will be clocked on the next positive transition of $\bar{S}$ and the Q output of A21-1 will go LOW. This

constitutes the start of a measurement and the transition of the complementary output $\bar{Q}$ of A21-1, $\overline{\text{INITLP}}$, from LOW to HIGH is used for this indication. Provided that no change occurs at the inputs to B21-2, subsequent fringe crossings are ignored by the latch A21-1 but are gated through A22-3 and recorded in the 8 bit, parallel carry, S Counter. (A17 to A20 and A22 to A24).

The Q outputs of all bits in the S Counter are connected to a 1 of 8 lines multiplexer, A16, and the output of the S multiplexer is gated through A22-1 to reset the S Counter to the all zero state when the selected line undergoes a positive transition. This reset operation immediately changes the state of the selected multiplexer input from HIGH back to LOW and the result, due to propogation delays through the loop, is an 8ns wide pulse (ENDMEAS) at the output of A16. Unless stopped for some other reason, the S Counter will immediately commence another measurement so ENDMEAS is used to indicate both the end of one measurement and the start of the next.

Selection of the number of fringes that are to be counted within one measurement interval is achieved with the S thumbwheel switch on the front panel and is determined according to the relationship:

$$\text{No. of fringes counted} = 2^{(\text{S Setting})},$$

[Maxm No. = 128 fringes]

Every ENDMEAS pulse is also recorded in the B Counter (A29, A30, B21 and B25) and is used as an indication of the number of measurements that have been made in a Doppler burst. The capacity of the B Counter is similarly front panel

selectable with the B thumbwheel switch but, as shown, has a maximum capacity of 16 measurements:

B Setting	No. of Measurements in each Burst
0	1
1	2
2	4
3	8
4	16

TABLE 3: Number of Measurements per Burst

If, at the end of a measurement, the preselected B Counter value is not reached, the S Counter commences another measurement as previously described. If, however, the last ENDMEAS pulse caused the output of the B multiplexer to go HIGH then both the B and S Counters are reset to the all zero condition through A25-3 and A22-1. If the B Counter is reset in this manner, a 7ns wide pulse (ENDBST) is generated to signal the end of a burst of measurements.

In addition to resetting the counters, ENDBST is expanded through B24-1 and B24-3 to form a 100ns wide, one-shot pulse, MINMD, which sets Q on A21-1 HICH and maintains the output of B21-2, and hence the output of A22-3, HIGH for a minimum period of 100ns at the end of every burst of measurements. This was found to be necessary since the propogation delays from U2 to U4 are significantly longer than one fringe period and approximately 60ns is required for $\overline{\text{MEMDIS}}$ to go LOW if the last measurement coincided with the capacity count for the Buffer Storage Unit.

Propogation delays and memory access times also impose a limit on the minimum time interval required for any one measurement. This minimum time interval was initially designed to be 100ns which would provide an acquisition rate of 10MHz in continuous operation. Subsequent tests on the LDV with a simulated input indicated satisfactory operation with measurement times as short as 85ns, however it is recommended that no combination of front panel settings be used that requires a velocity measurement to be made in less than 100ns. This is summarized in Table 4.

Signal Frequency	Minm Fringe Count
DC - 10MHz	1
10MHz - 20MHz	2
20MHz - 40MHz	4
40MHz - 80MHz	8

Table 4: Minm. Measurement Settings.

As previously discussed, the maximum time interval for any one measurement is determined by the S Counter setting and the Doppler signal frequency. If only the S Counter is used, a maximum of 128 fringes is imposed which, for an input frequency of 30MHz, means that the maximum sampling interval is 4.3μs. To provide greater resolution for the analysis of low turbulence frequencies, the outputs of the S and B Counters, ENDMEAS and ENDBST respectively, are multiplexed with the Mode Select control and gates A26 and A27 to form the composite logic signal ENDPUL. This pulse is used to clock latches L1 and L2 in the Main Counter Unit and is expanded from 8ns to 50ns to create $\overline{\text{WRITE}}$ in the MECL

10K one-shot formed by A9-2 and A9-3. For use with the real time counter, ENDPUL is also made synchronous with the main clock frequency to generate the command $\overline{\text{SYNCWRITE}}$ in A14-1 and A14-2.

With the Mode Control in the "Discrete" position, an end pulse will be generated every time the S Counter fills and the LDV may make up to 16 measurements, each of up to 128 fringes in any one Doppler burst. When operated in the "Accumulate" mode, an end pulse will be generated only when the B Counter capacity is reached and it is therefore possible to extend the sampling interval to a maximum of 2048 Doppler fringes. With a Doppler frequency of 30MHz, this setting corresponds to a sampling time of 68.3μs and thus provides a much higher resolution for the analysis of signal frequencies less than approximately 5KHz.

Further control over the distribution of sampling intervals is provided by means of the Delay Time Between Bursts (DTBB) control. When the front panel selector is in any position other than "min", the DTBB counter train is reset by ENBST and the control input to the tristate buffer 13-1-1 goes LOW. This enables an 8MHz clock on the data line to proceed to the input of the counter until the selected output goes HIGH and disables the control gate. During the time that the input gate is enabled and the counter is counting, the logic signal $\overline{\text{DTBB}}$ is HIGH. This signal is sent to the main input gate, B21-1, and is used to disable the LDV for a period of 1μs, 10μs, 100μs, 1ms or 10ms at the end of every burst of measurements. It was found that this facility was particularly useful when the LDV was used in conjunction

with a Data Acquisition System where the time required for data transfer of the total buffer memory contents was approximately 45μs. For applications requiring short measurement intervals, it was possible to use the B and DTBB controls to distribute the measurements evenly over the dead time that resulted from the relatively slow data transfer rate. Although the selection of delay times was adequate for the tests performed, it is considered that a 1-2-5 sequence, with delays of 1μs, 2μs, 5μs, 10μs and 20μs would offer greater flexibility in the distribution of sampling intervals. This modification could be achieved with only minor wiring changes and is therefore recommended.

When set in the "min" position, the DTBB tri-state buffer outputs are all in the Hi-Z mode and $\overline{\text{DTBB}}$ remains LOW. In this instance, the minimum delay between bursts is set by the logic signal MINMD as previously discussed.

The remaining front and back panel controls all relate to the manual and automatic operation of the LDV. Front panel START and STOP push buttons operate in conjunction with latch 17-3-1 to produce the logic signal $\overline{\text{RUN}}$. The complementary command, RUN, is provided at pin 9 of the external control jack and may be used to operate other TTL compatible equipment when the LDV is used in a master role. For slave operation, the LDV is provided with EXT START and EXT STOP inputs on pins 8 and 7, respectively, of the external control jack. A TTL, negative going edge will trigger the LDV in each case and will perform the same operation as the corresponding front panel push button.

For the investigation of transient phenomena it is

often convenient to operate equipment for only a very short time. To this end, the LDV is provided with an Auto Stop selector which may be used to automatically stop the LDV 1ms, 10ms, 100ms, 1s or 10s after a START or EXT START command has been received. In the "man" setting, the LDV requires a manual STOP or an EXT STOP command to reset RUN. The operation of the auto stop circuitry is similar to that of the DTBB counter.

To further extend the versatility of the LDV, it is suggested that hardware additions or modifications could be made to allow a "start after delay" mode of operation. This would be useful for experiments involving significant run up times and could be easily incorporated into the existing operation of the logic signal $\overline{\text{RUN}}$. At present, $\overline{\text{RUN}}$ falls immediately a START or EXT START command is received but this transition could be delayed by a controllable amount to provide the desired operating mode.

The logic signal $\overline{\text{RUN}}$ is sent to the main input gate B21-1 and needs to be a LOW to enable the LDV. Similarly, a HIGH on any one of the other four inputs to B21-2 will disable the input to the S counter and thus inhibit the operation of the LDV.

5.3.3 Main Counter Unit - U3

The system of operation of the latch and counter circuitry within the Main Counter Unit-U3 is the source of some of the unique characteristics of this LDV. In the first instance, the use of a high speed clock and counter train to

record the time taken for a preset number of fringes to be counted allows an increase in temporal resolution given by the ratio of the clock rate to the Doppler frequency. With a clock rate of approximately 150MHz and a Doppler frequency of 30MHz,this results in an increase in resolution by a factor of nearly five times. Secondly, the set up and hold times for the 32 bits of latches L1 and L2 are sufficiently short to enable the state of the first 16 bits of the main counter to be recorded within one clock period. This speed of operation implies complete continuity in the acquired velocity data, a characteristic which, with the aid of supporting software programs may be used to further increase the resolution of the system by the accumulation of the results from any number of consecutive velocity measurements.

Enclosed as Appendix A5 is a detailed circuit diagram of the Clock Generator and Main Control Unit -U3. As shown in the circuit diagram, a MECL III oscillator was used as a clock generator, the output frequency of which was set by the values of parallel tuned circuit components between pins 10 and 12. For the values indicated in the legend to Appendix A5, the output frequency was measured at 142.9MHz ± 0.1 MHz, thus providing a clock period of approximately 7ns. As the nominal set up and hold times of the 10176 Hex latches used in L1 and L2 are respectively 2.5ns and 1.5ns, a clock period of 7ns allows slightly more than ± 1ns variation in the timing of the clock pulses for L1 and L2. Although considerable difficulty was initially experienced in matching the delay requirements for the latch clock pulses and the propogation delays through the main counter train, subsequent tests on the completed circuit module showed satisfactory

operation over a wide temperature range even after any number or all of the integrated circuits had been interchanged or replaced.

The first 16 bits of the counter are composed of 2 D type flip flops, wired as a ripple through counter, followed by 14 $\bar{J}$ $\bar{K}$ flip flops connected as a synchronous counter with parallel carry provided by a combination of OR gates. This configuration was selected to allow a combination of maximum operating speed and approximately constant propogation delays through the major portions of the counter. The 1.6ns, 4.1ns and 3.1ns delay lines shown in L1 are required to match the delays through C_1; C_2-C_7 and C_8-C_{15} respectively.

It will be recalled that at the beginning of a velocity measurement, $\overline{\text{INITLP}}$ from A21-1 in U2 went HIGH. This transition is converted to a 10ns pulse through the one-shot formed by A11-1 and A11-3 and, after a delay of 10ns which is required to match the propogation delay of ENDPUL through the S Counter, is passed through A11-2 to the latch CS1. In response to this clock pulse, the Q output of CS1 goes HIGH and thereby holds the Data input of CS2 HIGH. On the next positive transition of CLOCK, the Q output of CS2 goes HIGH and, after a delay of 11·7ns, resets the Q output of CS1 to a LOW. The next positive CLOCK edge after this transition will then return Q of CS2 to a LOW and remove the RESET command from CS1. The purpose of CS1 and CS2 is therefore to synchronise the logic signals $\overline{\text{INITLP}}$ and ENDPUL to the positive transitions of CLOCK. This operation is essential for the correct timing of clock pulses to latches L1 and L2 and is summarised in the timing diagram shown as Figure 25.

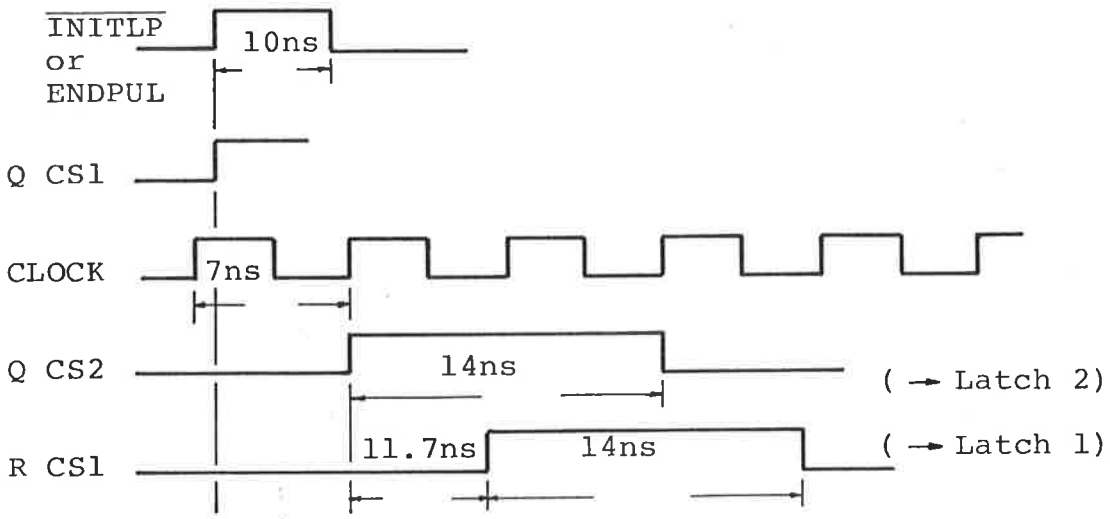

Figure 25. Timing Diagram, CS1 and CS2

Operation of the Latches, L1 and L2

At the beginning of every burst of measurements, $\overline{\text{INITLP}}$ is synchronised with CLOCK, by the operation of CS1 and CS2, to form the two logic signals LATCH1 and LATCH2. As LATCH2 occurs 11.7ns before LATCH1, the old value stored in L1 with be transferred to L2 by the command LATCH2 and the current state of the first 16 bits of the counter will be stored in L1 by the command LATCH1. For the first latch transfer only, the time interval between the end of the last burst of measurements and the start of the current burst is completely random and the old value of the counter, now stored in L2, will therefore bear no relationship to the current value of the counter stored in L1. To remove this erroneous data, $\overline{\text{INITLP}}$ is used to clock L2 a second time after the current state of the counter has been recorded in L1 by LATCH1. This is achieved with the 25ns delay provided by A12, A13 and A15 and has the effect of setting the contents of both L1 and L2 to the value of the main counter at the beginning of the first measurement. It should be noted that this initialization procedure is only necessary at the beginning of every burst and is therefore only generated by a positive transition of $\overline{\text{INITLP}}$.

At the completion of the first measurement, ENDPUL will similarly produce the signal commands LATCH1 and LATCH2 by the operation of CS1 and CS2. As before, LATCH2 will clock the contents of L1 into L2 and LATCH1 will record the new value of the counter in L1. The contents of L2 are therefore the counter status at the beginning of the measurement; the contents of L1 indicate the counter status at the end of a measurement; and the difference between these values represents the number of CLOCK pulses received in the measurement interval. This difference between L2 and L1 forms the Velocity Data Bus and is determined by the four SN74181 arithmetic logic units which, with the SN74182 carry generator, are wired as a 16 bit subtractor.

Assuming that this measurement was not the last in a burst, the next ENDPUL will signal the completion of another measurement. LATCH1 and LATCH2 will again be generated in the same way and the counter status at the completion of the previous measurement will be transferred to L2 and used as the counter status at the beginning of the latest measurement. This process of continually updating the contents of L1 and L2 and interpreting the difference between L1 and L2 as the number of CLOCK pulses recorded during the previous measurement interval will continue until interrupted by a positive transition on any one of the five inputs to the main control gate B21-2 in U2. When the end of a burst is indicated by any such transition, the latch A21-1 resets and a new $\overline{\text{INITLP}}$ will be generated at the beginning of the next burst.

Because it is possible to record the counter status within one CLOCK period, the results obtained from any two consecutive measurements may be added together to give increased resolution without compounding the digitization error inherent to counting techniques. By way of example, five consecutive measurements yielding the results 20, 21, 20, 20 and 21 CLOCK pulses each individually, have an uncertainty of ±1 pulse. The virtue in the operation of this sampling technique is that the accumulated result of 102 pulses still only has an uncertainty of ±1 pulse. This assumption is not valid for other currently available LDV counting systems, such as the DISA LDA, where the counter is rendered inoperative while the data is recorded or transferred.

5.3.4 Buffer Storage Unit - U4

The 1K bit memory within the Buffer Storage Unit, shown in Appendix A6, is arranged as four 16 x 16 bit RAMs, each of which is composed of four SN7489 memory chips. As discussed in Section 5.2, RAMs IA and IB record Velocity Data and IIA and IIB record Real Time Data. The multiplexing function that allows IA and IIA to "Read" while IB and IIB "Write", and vice versa, is achieved with the associated control circuitry, in particular the flip flop 08-5-1.

The RAM Write Enable commands are derived directly from the Q and $\bar{Q}$ outputs of 08-5-1, while the Memory Enable commands are formed by the logic signal $\overline{\text{SYNCWRITE}}$ and the outputs of 08-5-1 through the NAND gates 08-2-1 and 08-2-2. (It will be recalled that $\overline{\text{SYNCWRITE}}$ was made synchronous with the main clock frequency by A14-1 and A14-2 in U2 in order to prevent spurious measurements of the real time

data by asynchronous clocking.)

Whenever a clock pulse is received by 08-5-1, the Q and $\bar{Q}$ states are reversed and the operating modes of the RAMs are interchanged. As can be seen from the circuit diagram, the flip flop will be clocked through 06-5-2 whenever the 4 bit counter 07-1 reaches a terminal count. The input to 07-1 is the logic signal $\overline{\text{WRITE}}$ which is generated in U2 at the completion of every measurement. In summary, therefore modes of operation of the RAMs will be interchanged after every 16 measurements and while a set of measurements are being recorded into one side of the memory (Write mode), the results of the previous cycle are being transferred from the other side to the Data Aquisition System (Read Mode).

Operation of the Memory Control Unit

The two 4bit counters 07-1 and 06-1 are used as RAM address generators for the Write and Read modes respectively with the counter outputs and Q and $\bar{Q}$ from 08-5-1 being multiplexed through gates 06-2 to 06-4 and 07-2 to 07-4. Counter 07-1, the Write address, is incremented by $\overline{\text{WRITE}}$ at the end of every measurement and counter 06-1, the Read address, is advanced by the logic signal TRANSCOMP at the completion of every data transfer operation to the Data Acquisition System. Every $\overline{\text{WRITE}}$ is accompanied by a $\overline{\text{SYNCWRITE}}$ which is used to enable the Write mode of the RAM for approximately 85ns, after the address and data lines have settled. This command enters both the velocity and real time data into the appropriate RAM at the current address generated by the counter 07-1.

As the potential measurement rate of the LDV is greater

than the maximum transfer rate to the Data System, it is possible that 16 measurements may be made before transfer of the previous 16 results is completed. To avoid overwriting the memory, a logic signal $\overline{\text{MEMDIS}}$ is generated by 08-5-2 and 08-1-3 which disables the LDV input until both 06-1 and 07-1 have reached their terminal count. This introduces the possibility of dead time into the measurement record since, at the time of writing, approximately 45μs is required to transfer the complete memory contents to the Data System. Although this initially appears to be a severe limitation to the operating speed of the system, judicious use of the S,B and DTBB controls will ensure that the individual measurements are evenly distributed throughout the measurement interval. For example, if it is assumed that a continuous Doppler signal is to be demodulated and the S,B and DTBB controls are set for 16 fringes, 2 measurements per burst and a mean delay of 5μs respectively, the sample time for a Doppler frequency of 30MHz is approximately 0.5μs and the distribution of measurements can be illustrated by Figure (26).

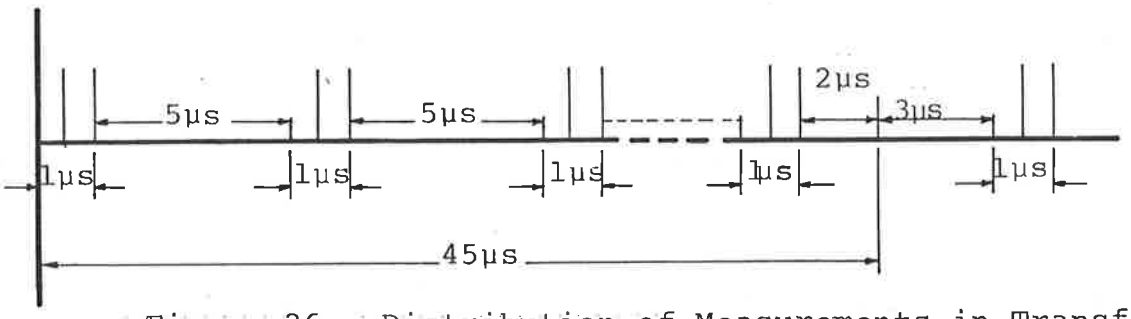

Figure 26. Distribution of Measurements in Transfer Interval

The front panel controls therefore allow operator selection of the individual sampling times and the distribution of those measurements while retaining the capability of an average

measurement rate (355KHz) that is more than adequate for most practical applications.

At the beginning of an acquisition/transfer sequence, 06-1 is reset by a 30ns pulse from the one-shot 16-1. This pulse also clocks 18-5-2 and disables the input to 06-1 through 08-1-1. The negative transition of $\bar{Q}$ of 18-5-2 is delayed by 60ns and sent to the Data System as a transfer command DATATRANS. The Data System responds by sending TRANSCOMP HIGH immediately and returning it to a LOW at the completion of a data transfer. This negative transition clears 18-5-2 and therefore enables a 4MHz clock train to proceed through 08-1-1 to the input of 06-1. The next negative edge of this clock advances 06-1 to the next address and disables 08-1-1 to further pulses by clocking 08-5-2. This generates another DATATRANS and the information in the new RAM address is transferred to the Data System. The process continues in this manner until the information in all 16 channels is transferred and the terminal count is indicated by a LOW on the output of 06-5-1. This LOW disables the input to 06-1 through 08-4-2 and 08-1-1 and the counter remains disabled until reset by 16-1 at the beginning of a new cycle.

The latches 19-5-1 and 19-5-2 record the sequence of terminal counts for the two address counters 06-1 and 07-1 and either reset 06-1 immediately, through 18-5-1, when the measurement rate is very fast, or delay the resetting of 06-1 until 07-1 has been filled during a slow measurement cycle. This operation is designed to allow a minimization of the dead time that results when the time taken to transfer 16 measurements (τ_{trans}) is greater than the time taken to

record 16 measurements (τ_{meas}). The operation is summarized in the timing diagram shown as Figure 27.

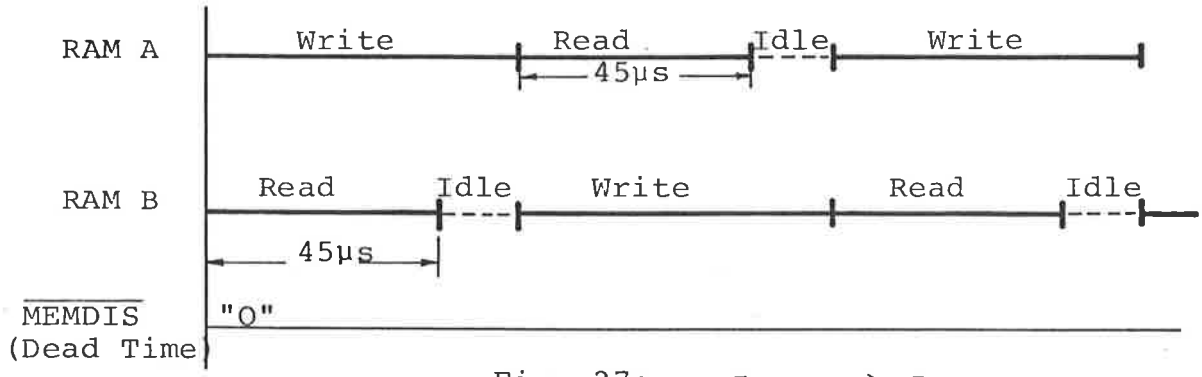

Fig. 27a. $\tau_{meas} > \tau_{trans}$.

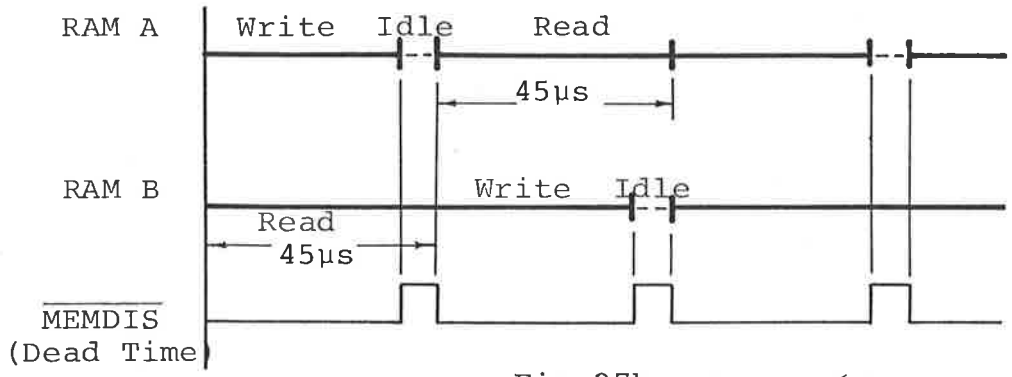

Fig.27b. $\tau_{meas} < \tau_{trans}$

Figure 27. Timing Diagram for RAM Operation

4.3.5 D to A Converter Unit - U5

In addition to being recorded in RAMs IA and IB, the velocity data from the ALU data bus is clocked into the 16 bit output latch OL-0 to OL-3 by the logic signal DACCK. As can be seen from the circuit diagrams in Appendices A6 and A7, DACCK is derived from $\overline{\text{WRITE}}$ in U4 and delayed by approximately 70ns to allow settling time for the ALU outputs. At the end of every measurement, therefore, the velocity data bus is both recorded in the Buffer Storage Unit and presented at the output latch for selection through a back panel connector.

The "any 8 of 16 selector" on the back panel enables the operator to manually select the eight most appropriate

bits of information for each application and therefore enables an increase in resolution or an extension of velocity range, depending upon the particular requirement. Once selected, the eight bits are converted to an analogue current source with an MC1408L, 8 bit DAC and amplified to a 0 to +5V voltage waveform with an LM318H transconductance amplifier. This analogue reconstruction of the velocity data is then available for display, recording or analysis through a BNC connector on the rear panel.

In addition to this external output facility, the waveform is monitored and displayed at the front panel by means of a voltmeter calibrated in "counts". The purpose of this meter is to indicate the number of CLOCK pulses that have been recorded in the 8 selected bits during the previous measurement interval and it therefore has a range from 0 to 256 counts. The other left zero ranges of 0 to 128 and 0 to 64 are obtained by changing the gain of the transconductance amplifier and are selected by means of the Range Control when a more accurate reading of low count numbers is required. The centre zero scales 0 to ± 128, 0 to ± 64 and 0 to ± 32 are employed when the use of the Bragg cell allows demodulation of bidirectional velocities. In such cases, the Offset Adjust control is used to adjust the meter readout to centre zero in order to remove the effect of the bias frequency.

Because the calculation of actual velocities involves a number of other variables, e.g. S, B Counter settings; optical configuration; laser wavelength; etc., the LDV meter output has been left in terms of CLOCK counts. The actual velocity may be determined from equation (80), where

S is the number of fringes counted, C is the main clock rate, N_c is the number of counts recorded, f_b is the bias frequency and f_p is the Doppler frequency due to the particle velocity.

$$f_p = \left(\frac{S \cdot C}{N_c} - f_b\right) \tag{80a}$$

$$\text{hence} \quad v_{p_y} = \frac{f_p \cdot \lambda}{2 \sin\theta} \tag{80b}$$

It should be noted, however, that discontinuities in the Doppler signal will result in a "sample and hold" type operation in the output latches. This may cause significant errors in signal averaging unless a simulataneous record of $\overline{\text{LEVEL}}$ can be maintained and it is therefore far preferable to use the digital output facilities when this condition is present.

5.4 SYSTEM SPECIFICATIONS

From the description of operation of the signal processor, it is possible to see that most of the essential and desirable characteristics detailed in Chapter 4 are available in the LDV system that has been developed as part of this project. The use of digital counting techniques provides excellent noise immunity and a solution to the problem of spectral broadening due to finite signal lifetime while the acousto-optic cell removes the possibility of directional aliasing, permits the demodulation of bidirectional velocity components and allows the relative spatial resolution to be reduced to a very small value without restricting the maximum fluid velocity. The versatility in the modes of operation

of the acousto-optic cell and the ability to select both the number of fringe crossings per measurement and the number of measurements per burst are features of the LDV that permit a compromise between maximum turbulence frequency, maximum fluid velocity and temporal resolution to be achieved for most practical applications. The speed of operation of the latching circuitry permits an accumulation of the results of successive measurements without an increase in digitization error, while the simultaneous recording of real time and velocity information may be used to reconstruct the complete velocity-time record of the information. This record may then be analysed in a statistically independent way to determine ensemble averages, thus avoiding the sampling bias errors that plague other psuedo-single particle anemometer techniques.

Specification of the range, accuracy and maximum observable turbulence frequency for the LDV is a difficult task because, as has been shown in previous sections, these characteristics are not independent and, in addition, are functionally related to the optical configuration; bias frequency; mean sample time and detected Doppler frequency. These relationships may be summarised in the following equations, where τ_s is the sample time; f_p is the Doppler frequency due to the particle; f_D is the observed Doppler frequency and $\Delta\tau_s$, Δf_D and Δv are, respectively, the temporal, frequency and velocity resolution of the LDV:-

Equations 80(a) and 80(b) gave

$$f_p = \left(\frac{SC}{N_c} - f_b\right) \quad \text{and} \quad v_{py} = \frac{f_p \cdot \lambda}{2 \sin\theta} \ ,$$

in which $\frac{SC}{N_C} = f_D$, the observed Doppler frequency, and, since:-

$$\tau_s = \frac{S}{f_D} = \frac{N_C}{C} \tag{81a}$$

then: $$\frac{\Delta\tau_s}{\Delta f_D} = -\frac{\tau_s}{f_D} \tag{81b}$$

i.e.: $$\Delta f_D = -\frac{\Delta\tau_s}{\tau_s} \cdot f_D \tag{81c}$$

The temporal resolution of the LDV, $\Delta\tau_s$, is equal to $\pm \frac{1}{C}$, where C is the main clock frequency, hence

$$\Delta f_D = \pm \frac{1}{C\tau_s} \cdot f_D \tag{81d}$$

and the velocity resolution may be defined as:

$$\Delta v = \pm \frac{\Delta f_D \cdot \lambda}{2 \sin \theta} \tag{81e}$$

These equations are graphically presented in Figure 28, where the frequency resolution (Δf_D) and the maximum resolvable turbulence frequency are plotted against τ_s, the mean sample time.

By way of example, if a bias frequency of 10MHz is used and N_C = 1524 when $\theta = 2^o$; λ = 632.8nm; C = 142.9MHz and S = 128 fringes, v_{py} is given by equation (80a) as

$$v_{py} = \left(\frac{128 \times 142.9 \times 10^6}{1524} - 10^7\right) \times \frac{632.8 \times 10^{-9}}{2 \sin 2}$$

$$= 18.15 \text{ m/s}$$

and τ_s may be evaluated from equation (81a) as

$$\tau_s = \frac{N_C}{C} = \frac{1524}{142.9 \times 10^6} = 10.66\mu s$$

Figure (28) may now be used to determine the frequency resolution and maximum resolvable turbulence frequency (allowing

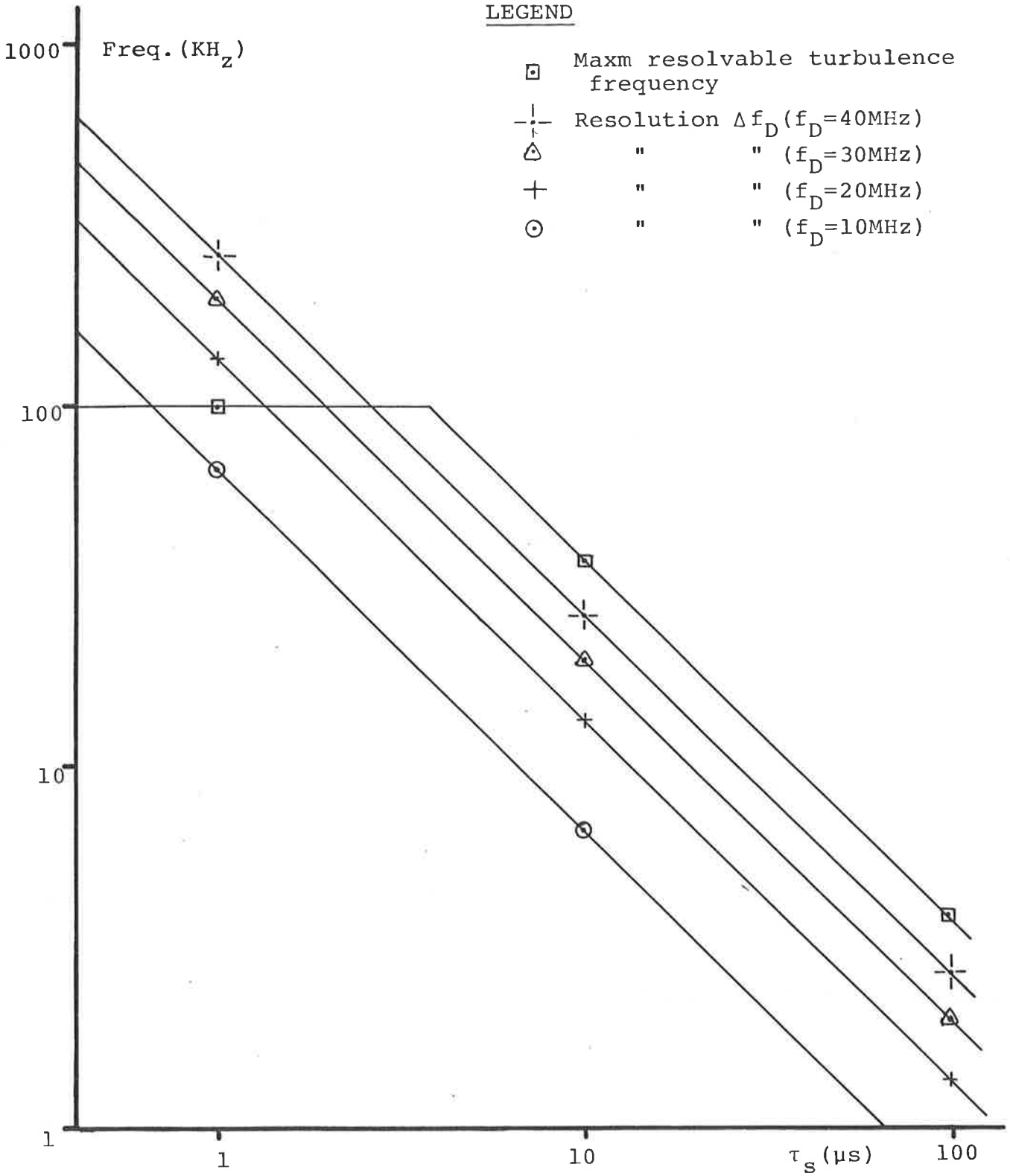

Figure 28. LDV Specification

for a minimum of three samples per period) and for this example are, respectively, 8KHz and 33KHz.

$$\text{Since} \quad \Delta f_D = \pm 8\text{KHz}$$

$$\Delta v = \pm \frac{8\text{x}10^3\text{x}632.8\text{x}10^{-9}}{2 \sin 2} = \pm 0.07 \text{ m/s}$$

therefore, $v_{py} \simeq 18.2 \pm 0.1$ m/s, giving a measurement accuracy of approximately ± 0.5%. From this example it is clear that, for most applications, an accuracy of typically ± 0.5% may be achieved for turbulence frequencies up to 100KHz in the velocity range 10mm/s to 600m/s.

Other system specifications may be summarised as follows:-

(i)	Minimum Sample Time (τ_s)	100ns
(ii)	Maximum Detectable Doppler Frequency (f_D max)	≈100MHz
(iii)	Maximum Average Sample Rate	16 Measts in 45µs
(iv)	Main Clock Rate	142.9 ± 0.1MHz
(v)	Fringe Counting Modes	
	(a) Discrete - up to 16 measts, each of up to 128 fringes.	
	(b) Accumulate - 1 meast of up to 2048 fringes	
(vi)	DTBB Settings	1µs, 2µs, 5µs, 10µs, 20µs
(vii)	Available Bias Frequencies	9.86MHz; 19.72MHz; 29.57MHz.

5.5 APPLICATIONS

To demonstrate the application of the LDV in the analogue output mode, the acousto-optic cell and signal processor were used in a modified Michelson interferometer

to detect the vibration of a front surface mirror mounted on the spindle of a shaker. A schematic diagram of the configuration is shown as Figure (29) and the results of the investigation are presented as Figure (30). The acousto-optic cell was operated in the Bragg mode at a frequency of 30MHz with a diffraction efficiency of approximately 50% and the control settings on the LDV were adjusted as follows:-

S Counter	:	7 (32 fringes per meast)
B Counter	:	4 (16 meast per burst)
Mode Control	:	Accumulate
DTBB	:	Min.

In the first demonstration, Fig. 30a, the shaker was excited with two sine waves of approximately equal amplitude but with frequencies of 30Hz and 60Hz respectively. The bottom trace of Fig. (30a) shows the resultant driving signal, where the vertical sensitivity is 5V/cm and the time base is 10ms/cm. The top trace of the same photograph, for which the vertical sensitivity is 1V/cm, is the demodulated output from the LDV signal processor. With the exception of minor phase variations, the demodulated output is seen to closely approximate the driving signal and, from the control settings previously indicated, it is possible to estimate the peak velocity of the mirror as 0.69m/s.

Figure (30b) illustrates the response of the same shaker to a square wave input. The driving signal (bottom trace) had an amplitude of ±4V and a frequency of approximately 50Hz. As expected, the demodulated output from the LDV exhibited low frequency distortion due to the frequency response of

the shaker and the derivative nature of the velocity waveform.

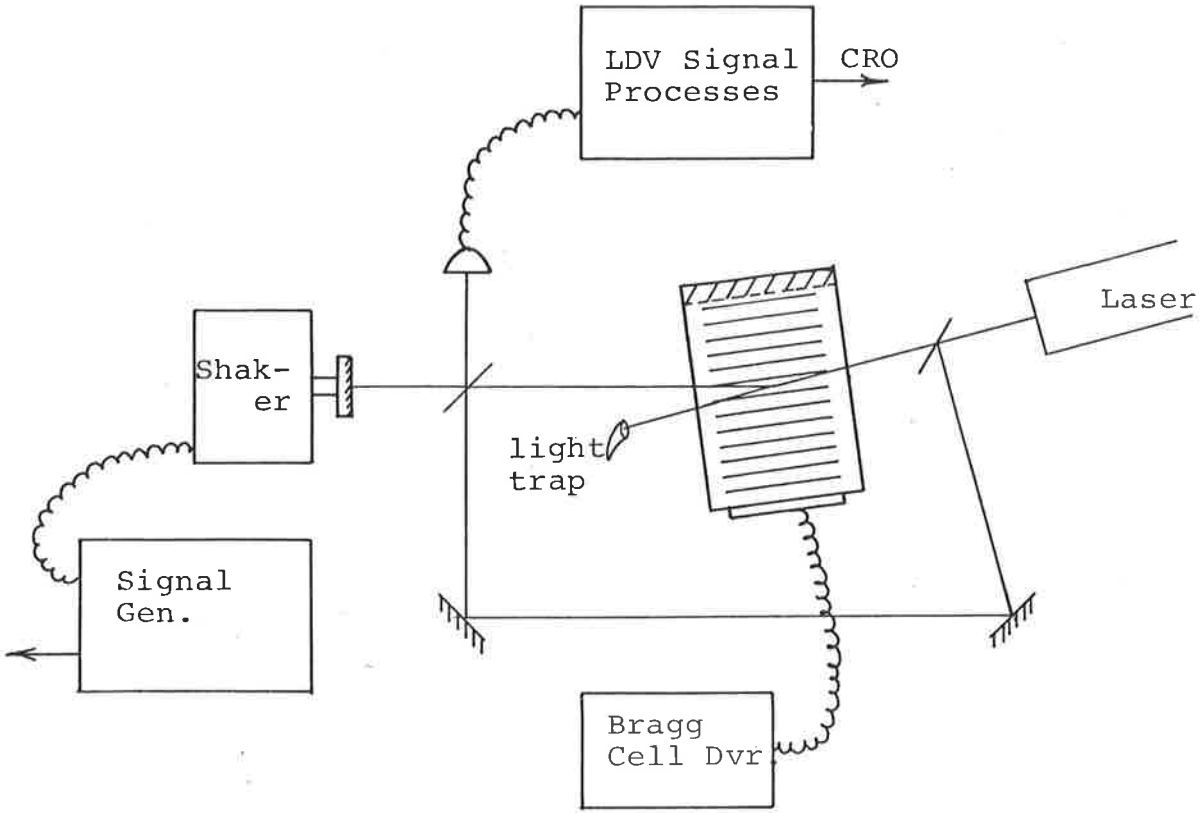

Figure 29. Michelson Interferometer

Using the vertical sensitivity of 1V/cm for the output trace, the peak velocity in this example was calculated as 0.73m/s. For both of these applications, further analysis of the output waveforms in terms of mean square velocity determinations or power spectral analysis would have been possible but was not considered necessary for this demonstration.

The results of the investigations clearly indicate that this LDV system is an extremely versatile instrument, well suited to a very large number of fluid mechanics and acoustic applications. The ability to provide either analogue or digital output data permits either stand alone or computer peripheral type operation when a continuous Doppler signal is available. When used with discontinuous Doppler information, the LDV has been shown to be capable of negating the

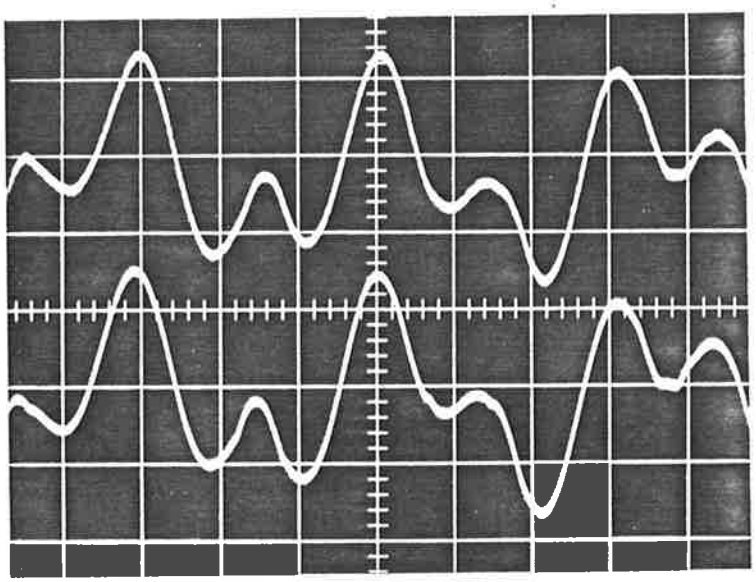

LDV Output

1V/cm; 10ms/cm.

Driving Signal

5V/cm; 10ms/cm.

Figure 30a.

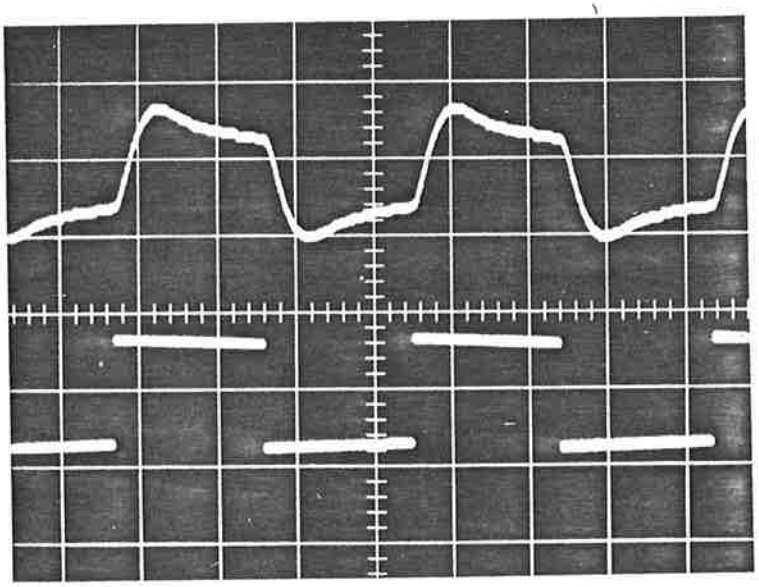

LDV Output

1V/cm; 10ms/cm

Driving Signal

5V/cm; 10ms/cm

Figure 30b.

FIGURE 30: Experimental Results

major objections to currently available signal processing systems. Although time did not permit a diversity of applications in this study, further single particle scattering and noise and vibration investigations are currently being considered and will be the subject of future publications.

SUMMARY OF CONCLUSIONS

Conventional methods of velocity determination in fluid mechanics and acoustics are inadequate for many current research investigations. The laser Doppler velocimeter, while embodying a number of the essential characteristics of the ideal instrument, offers, in some areas, significant advantages over traditional techniques. It should be remembered, however, that spectral broadening, low SNR, signal dropout and sample biasing have long been problems with LDV signal processing systems.

To remove directional aliasing and directional ambiguity a system of optical frequency biasing must be employed. Further, to reduce the effective focal volume size and to increase the SNR, the biasing frequency should be as high as the frequency response of the signal processor will allow. Of the techniques investigated in this study, the acousto-optic cell would appear to be the most efficient, convenient and versatile method for optical frequency shifting.

Spectral broadening due to the finite lifetime and amplitude modulation of the Doppler signal can only be avoided if power spectral analysis techniques are rejected in favour of time-domain methods. In addition, the sampling bias due to the distribution of scattering particles and the processor dead time requires, for complete alleviation, a simultaneous record of velocity and real time information.

The laser Doppler system that has been devised for this project incorporates all of the foregoing characteristics and, as such, is a significant development in the field of instrumentation for research applications.

APPENDIX A1

LOGIC MNEMONICS

LOGIC SIGNAL	LOGIC NAME	EXPLANATION
ADRA	ADDRESS A	Address for memories A
ADRB	ADDRESS B	Address for memories B
CLOCK	MAIN CLOCK	Main clock frequency
DACCK	D to A CONV.CLOCK	Clock signal for output latches
DATATRANS	DATA TRANSFER COMMAND	Trans. comd. to ext. data system.
$\overline{\text{DTBB}}$	$\overline{\text{DELAY TIME BETWEEN BURSTS}}$	See section 5.3.2
ENDBST	END OF BURST	B Counter filled
ENDMEAS	END OF MEASUREMENT	S Counter filled
ENDPUL	END PULSE	Output of mode control multiplexer.
EXT START	EXTERNAL START	External control comd.
EXT STOP	EXTERNAL STOP	External control comd.
$\overline{\text{INITLP}}$	$\overline{\text{INITIAL PULSE}}$	Start of first measurement
LATCH1	LATCH 1	Clock for first latch
LATCH2	LATCH 2	Clock for second latch
$\overline{\text{LEVEL}}$	$\overline{\text{LEVEL}}$	See section 5.2
MEA	MEMORY ENABLE A	Memory enable pulse for memories A.
MEB	MEMORY ENABLE B	Memory enable pulse for memories B.
$\overline{\text{MEMDIS}}$	$\overline{\text{MEMORY DISABLE}}$	System disabled due to memory overflow.
MINMD	MINIMUM DELAY	See section 5.3.2
RESET	RESET	Reset for CS1, CS2.
RTCLOCK	REAL TIME CLOCK	Clock input to R.T. Counter
$\overline{\text{RUN}}$	$\overline{\text{RUN}}$	System operating
$\overline{\text{S}}$	$\overline{\text{SCHMITT TRIGGER OUTPUT}}$	Doppler information
$\overline{\text{SYNCWRITE}}$	$\overline{\text{SYNCHRONOUS WRITE}}$	$\overline{\text{WRITE}}$ made synchronous with RTCLOCK
TRANSCOMP	TRANSFER COMPLETED	Comd. from ext.data system.
WEA	WRITE ENABLE A	Write enable pulse for memories A.
WEB	WRITE ENABLE B	Write enable pulse for memories B.
$\overline{\text{WRITE}}$	$\overline{\text{WRITE}}$	Write command to memories.

LDV-FUNCTIONAL BLOCK DIAGRAM

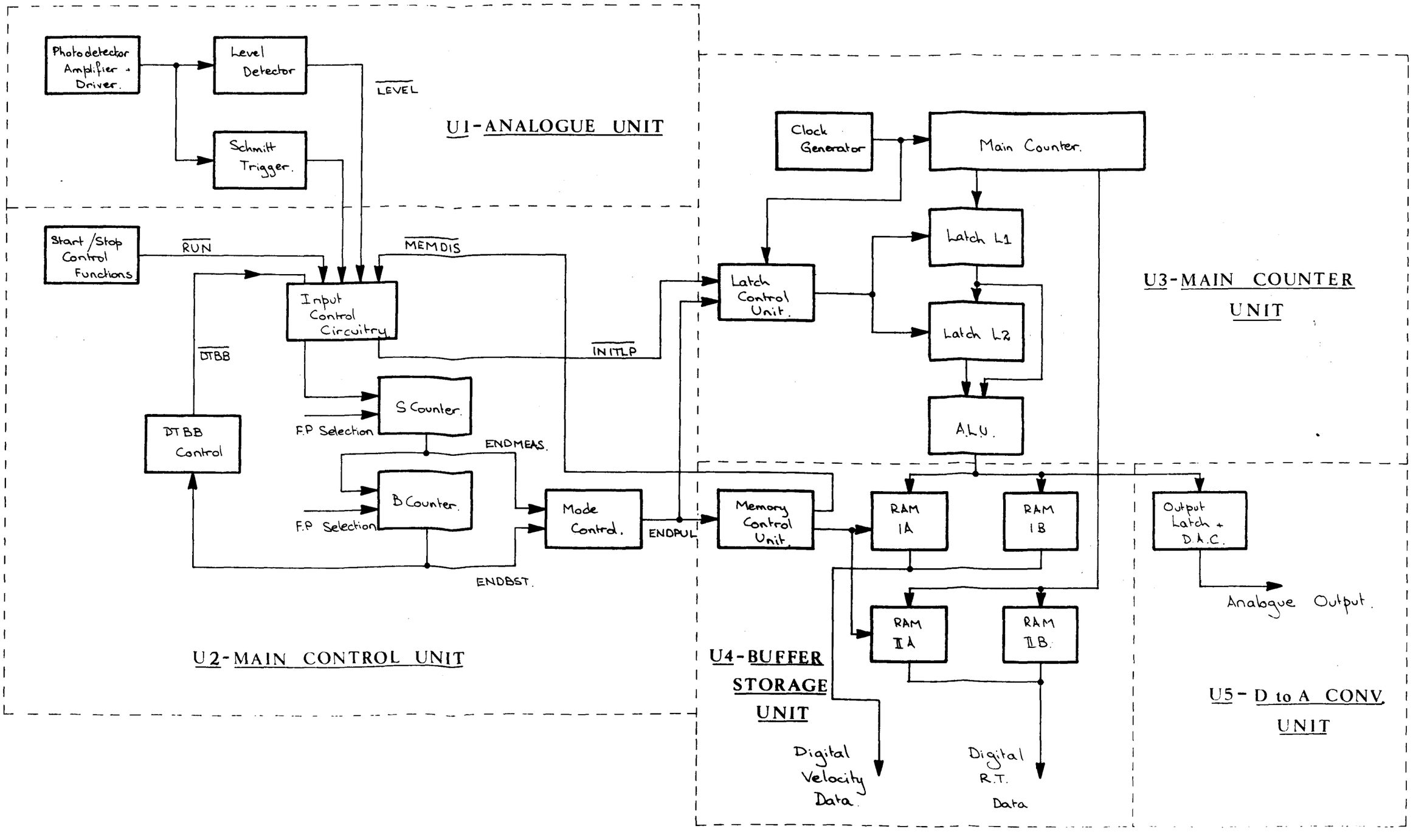

U1-a

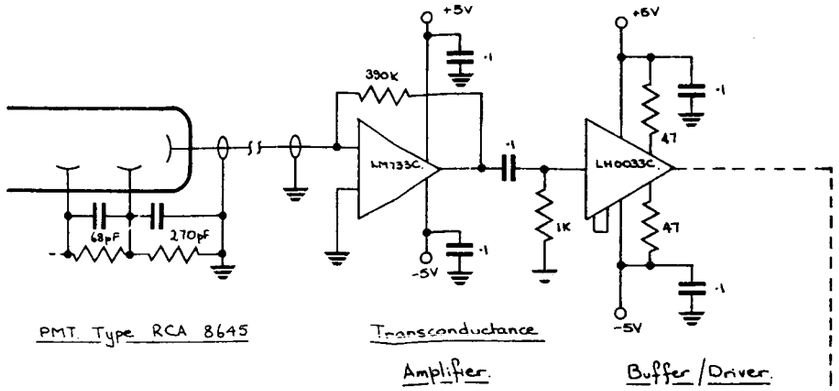

PMT. Type RCA 8645

Transconductance Amplifier.

Buffer/Driver.

U1-b.

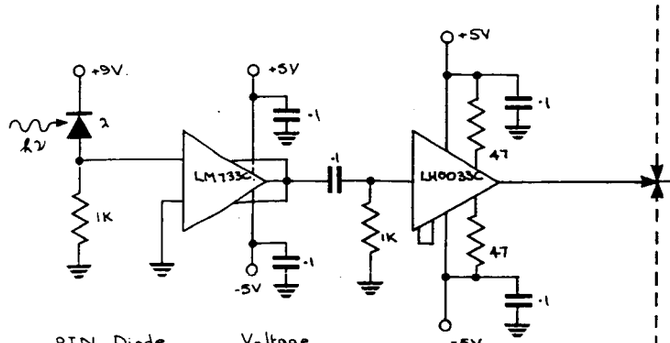

PIN Diode Detector

Voltage Amplifier.

Buffer/Driver.

U1-c.

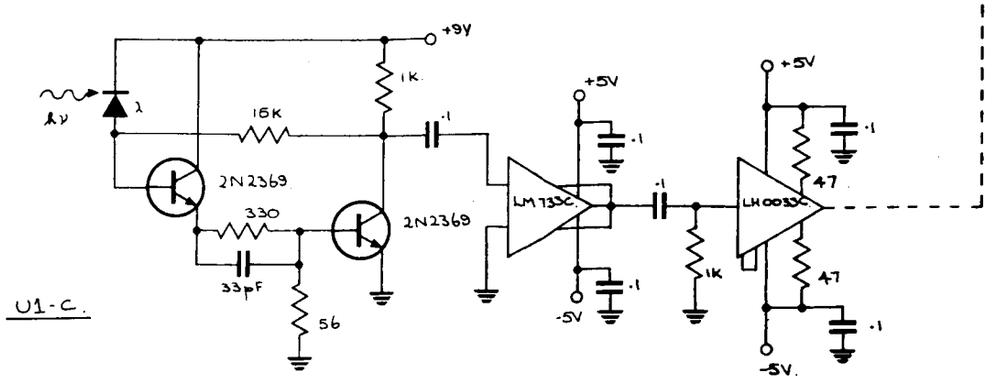

Transconductance Amplifier

Voltage Amplifier

Buffer/Driver.

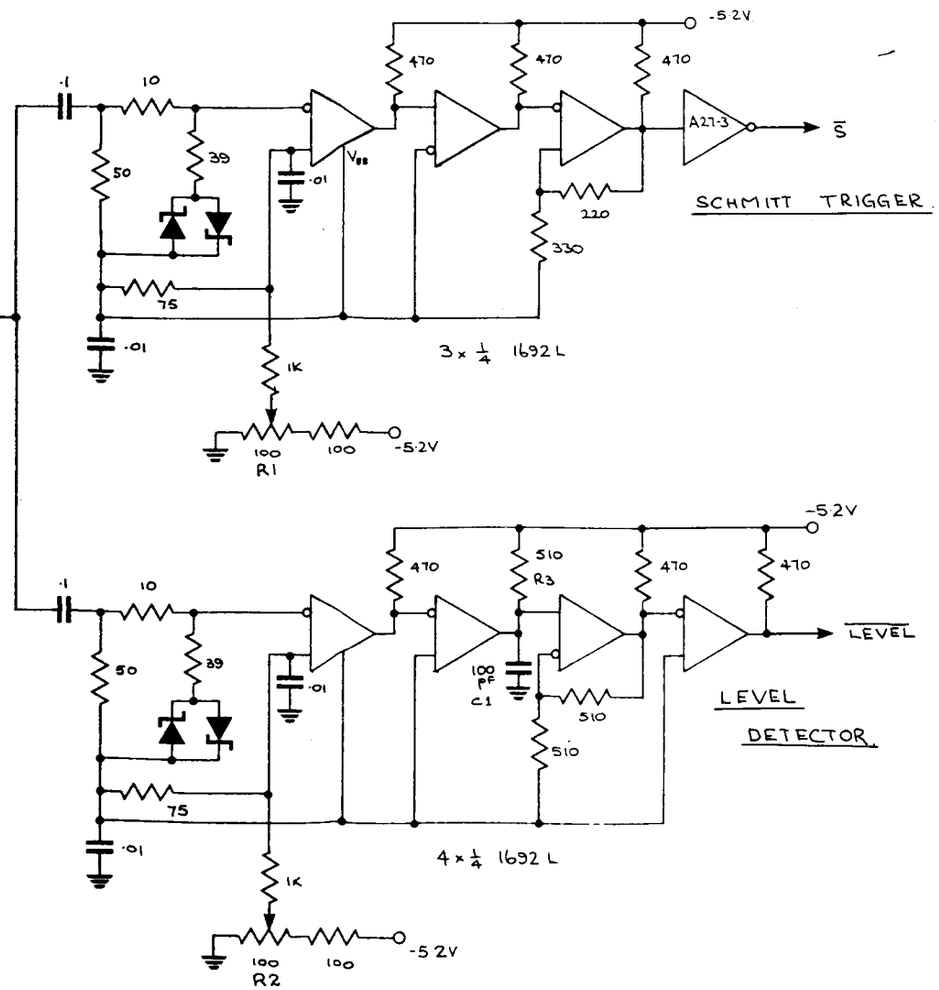

APPENDIX A3

ANALOGUE UNIT-U1

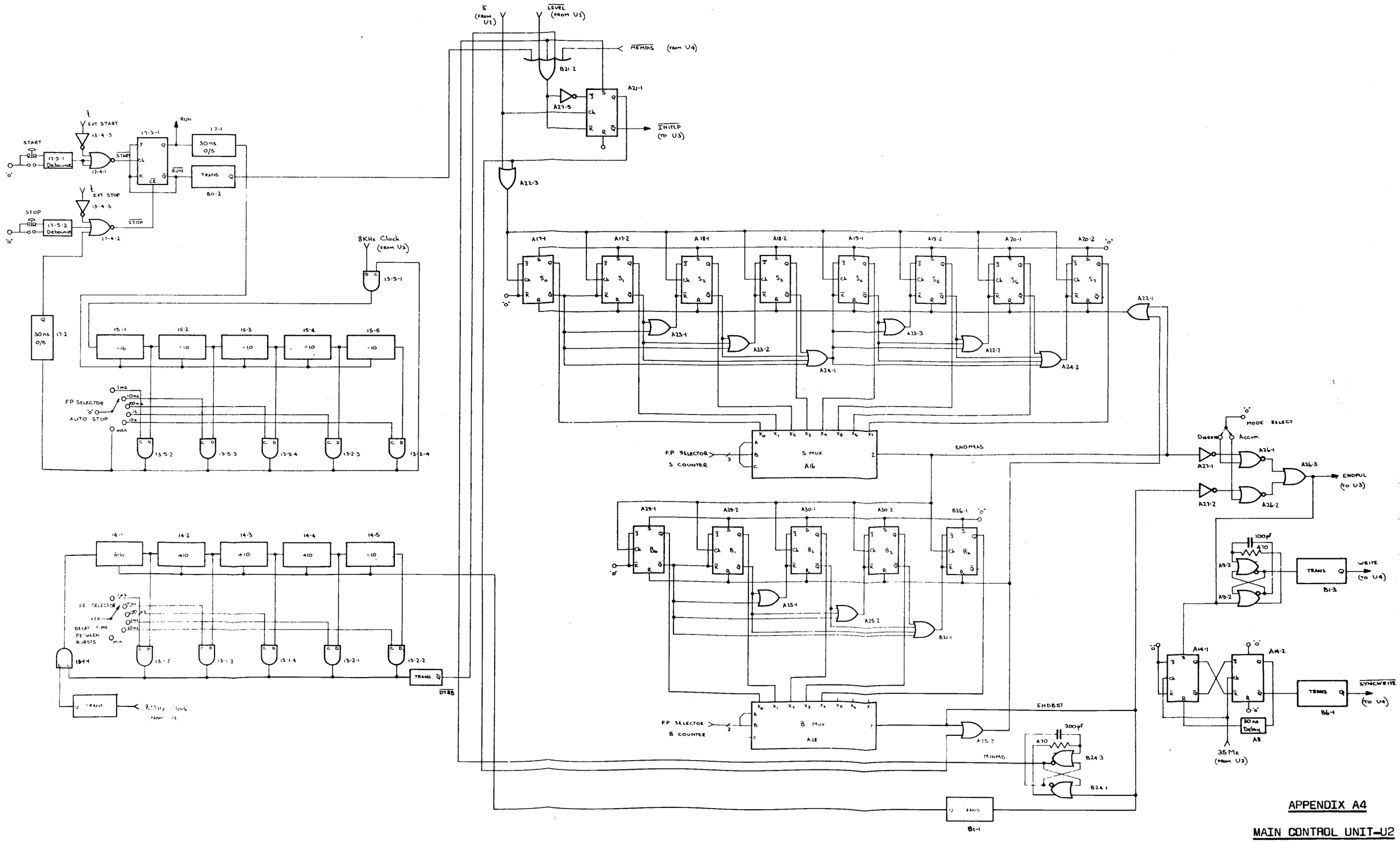

APPENDIX A4

MAIN CONTROL UNIT-U2

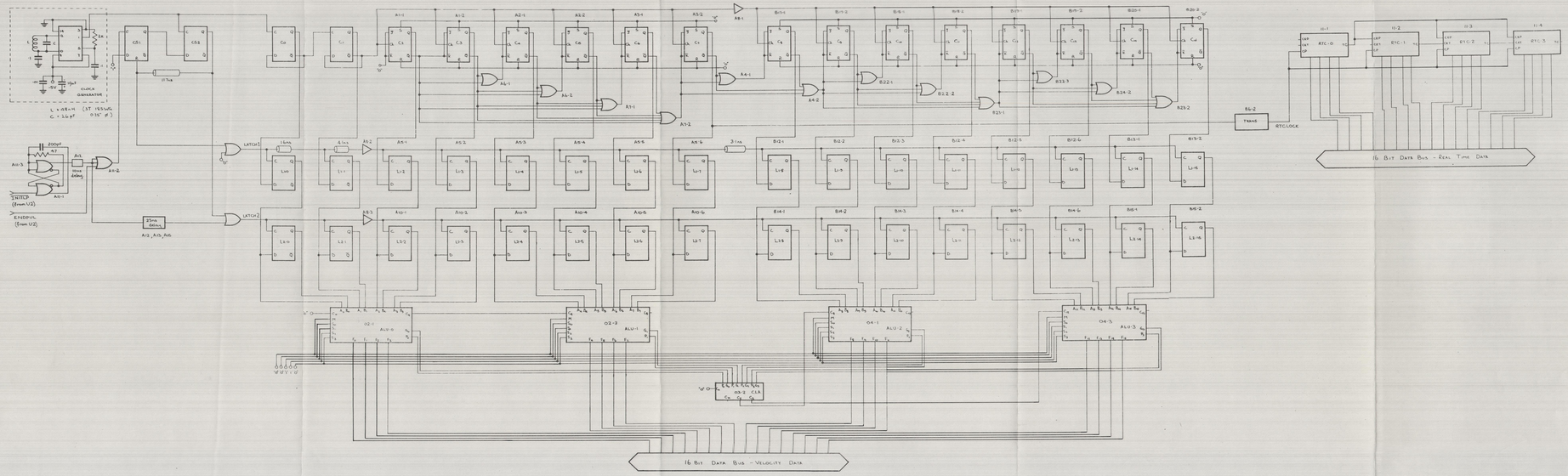

APPENDIX A5

MAIN COUNTER UNIT-U3

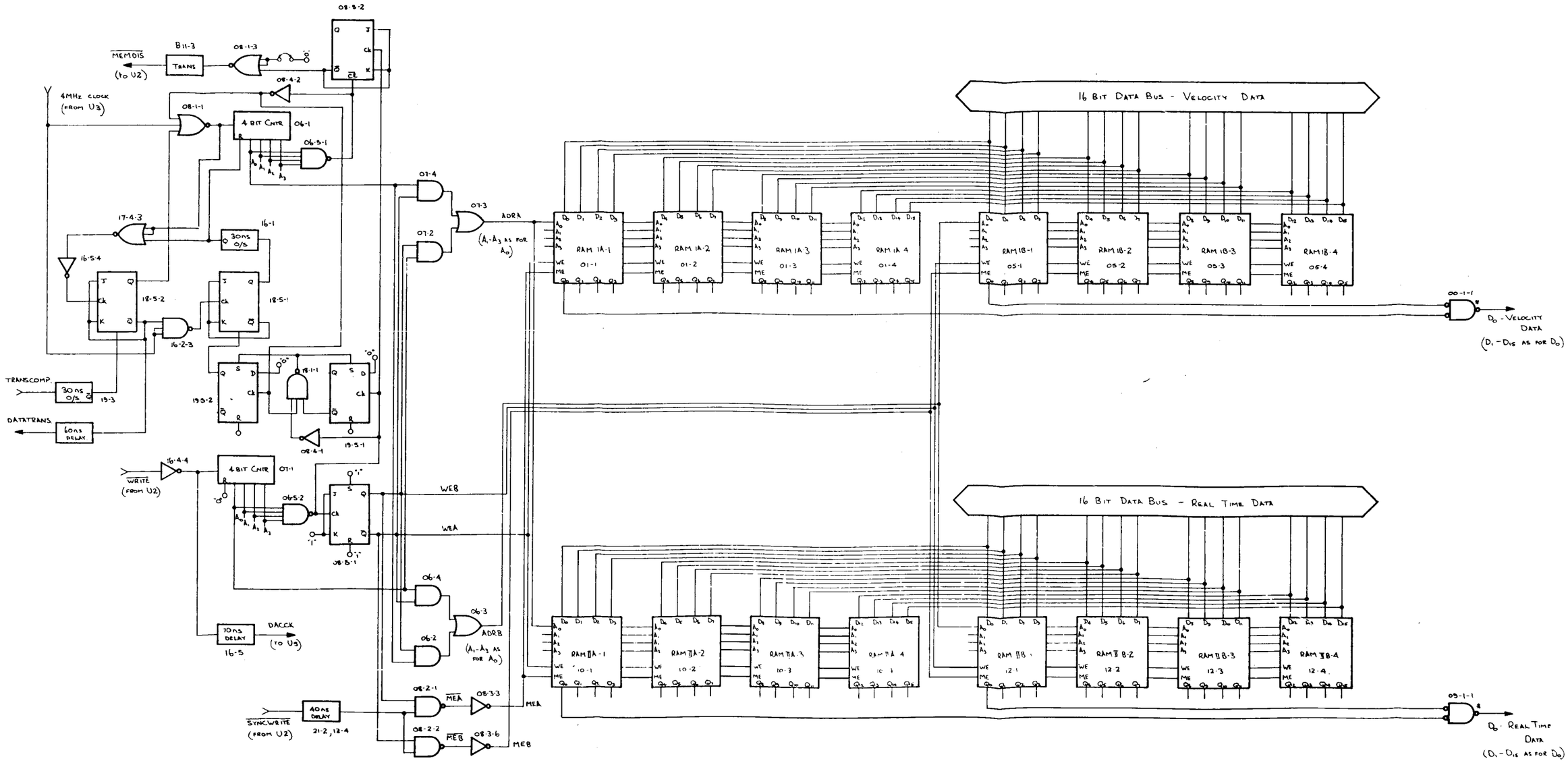

APPENDIX A6

BUFFER STORAGE UNIT-U4

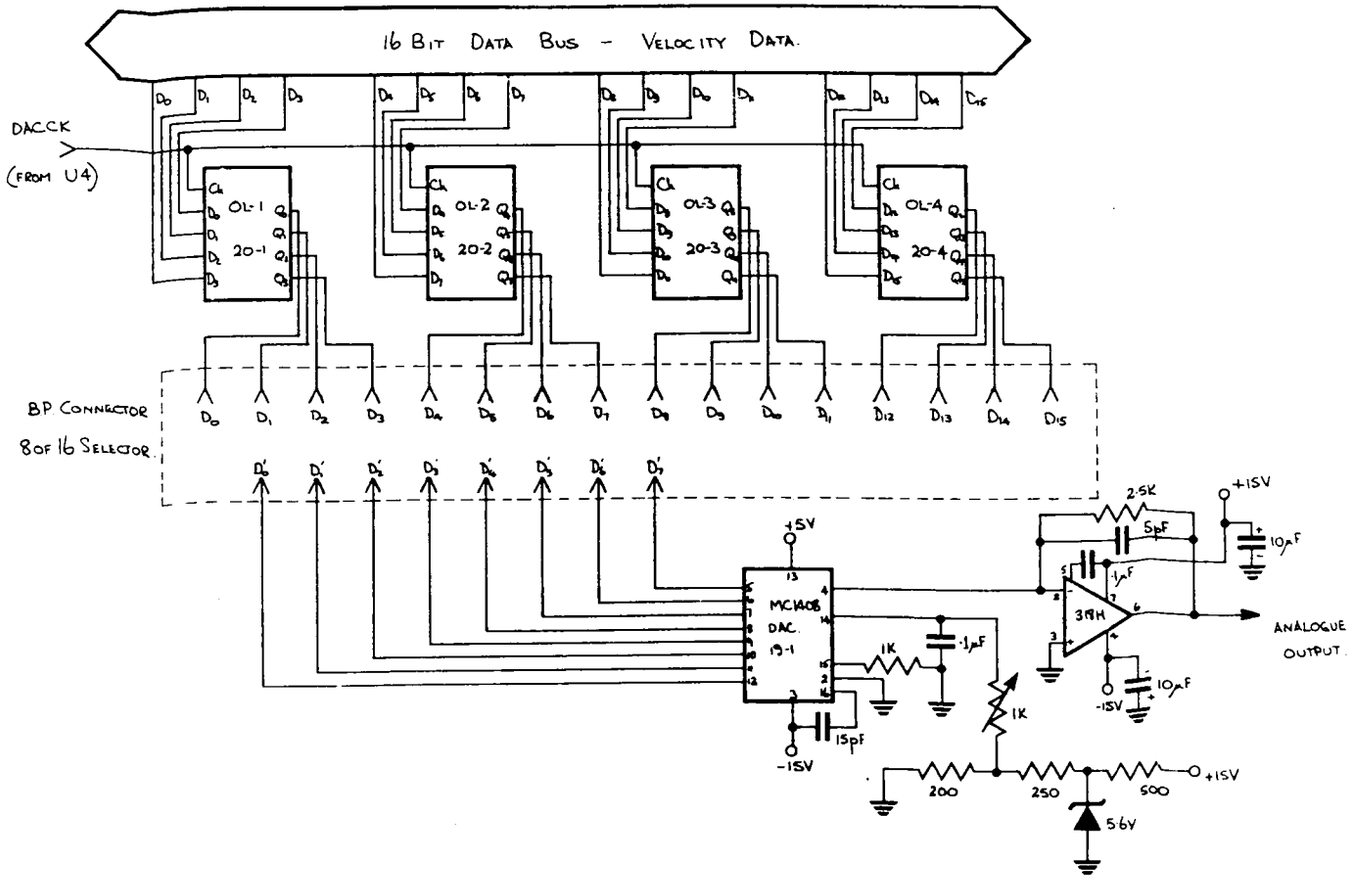

APPENDIX A7

DAC UNIT-U5

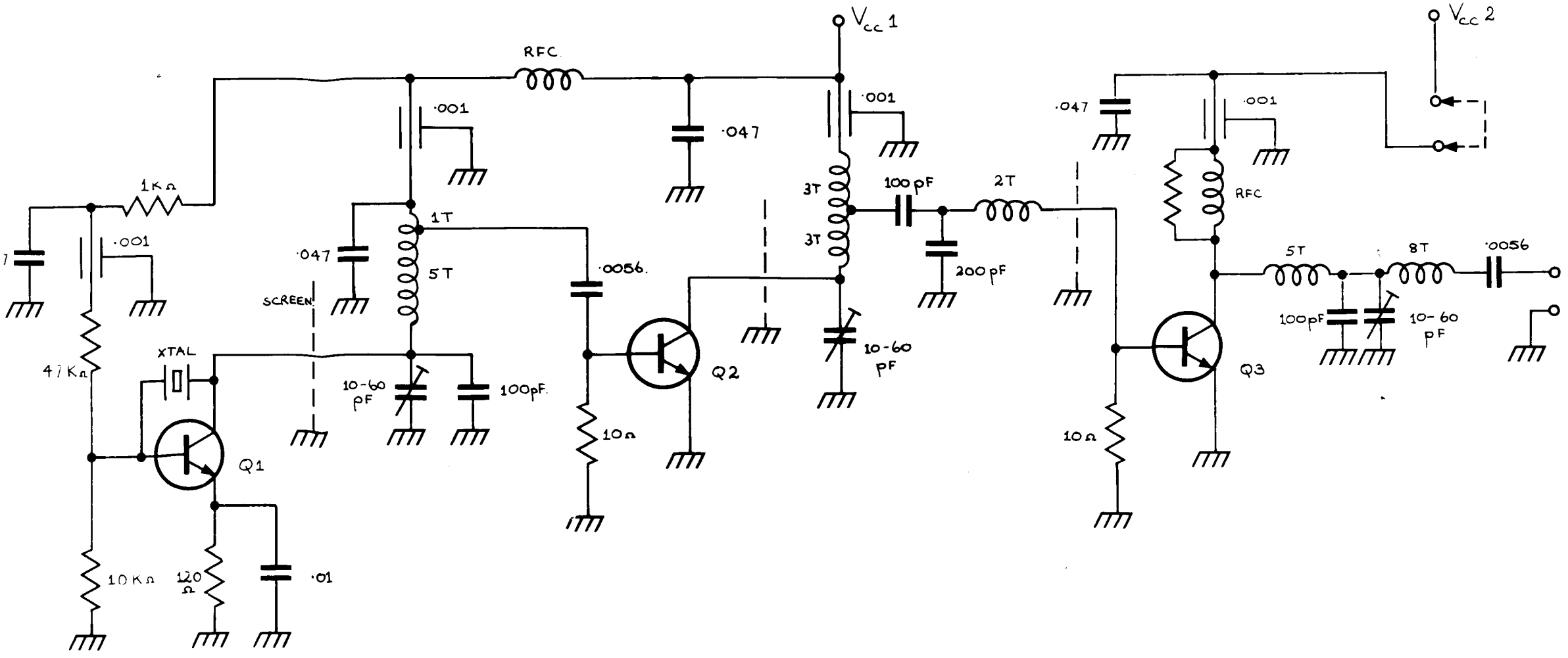

APPENDIX B1

BRAGG CELL DRIVER CCT


LASER DOPPLER VELOCIMETER
LASER DOPPLER VELOCIMETER
A D DATA SYSTEM
A D DATA SYSTEM

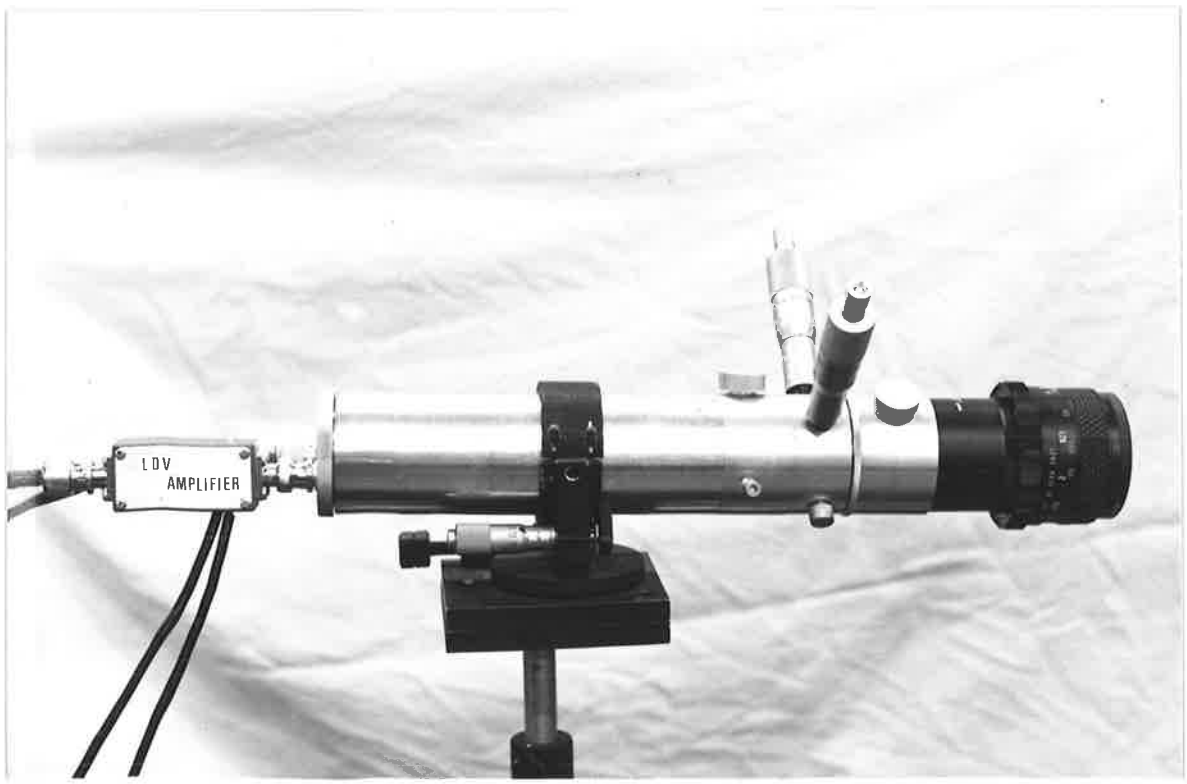
LDV
AMPLIFIER

REFERENCES

ADLER, R. (1967), IEEE Spectrum 4, p.42.

BAK, T.A. (1964), "Phonons and Phonon Interactions", Benjamin Inc. p.314.

BECKER, H.A.; HOTTEL, H.C.; and WILLIAMS, G.C. (1967), J.F.M. V30, part 2, p.259.

BEISER, L., (1974), "Laser Applications" - Vol. 2. Academic Press Inc., - ed. Monte Ross., p.115.

BUHRER, C.F.; BLOOM, L.R. and BAIRD, D.H. (1963). Applied Optics 2, p. 839.

BURGWALD, G.M. and KRUGER, W.P., (1970), H.P. Jnl. 21, p.14.

CAMPBELL, J.P. and STEIER, W.H. (1971), IEEE Jnl. of Quant. Electronics QE7, p.450.

CHANG, W.S.; MULLER, M.W.; and ROSENBAUM, F.J., (1974) "Laser Applications" - Vol. 2, Academic Press Inc. -ed. Monte Ross, pp. 305-332.

CUMMINS, H.; KNABLE, N; GAMPEL, L.; and YEH, Y. (1963) Applied Physics Letters 2 (3) p.62.

DIMOTAKIS, P. (1975), Manuscript to be published.

DRAIN, A.E. and MOSS, B.C. (1972), Opto-electronics 4, p.429.

DURAO, D.F. and WHITELAW, J.H. (1974), Dept. of Mech. Eng. - Imperial College - Internal Report # HTS/74/21.

DURST, F. and WHITELAW, J.H. (1969), Prog. Heat Mass Transfer, 4, p.1971.

DURST, F. and WHITELAW, J.H. (1971), Proc. R. Soc. A324, pp. 137-157.

HJELMFELT, A.T. and MOCKROS, L.F. (1966), Appl.Sc.Res. 3,p.149.

KLEINHANS, W. and FRIED, D.L. (1965), App.Phys. Letters 7(1) p.19.

LAUFER, J. (1975), "Trends in Experimental Turbulence Research", Annual Review of F.M. 7, p.307.

MAZUMDER, M.K., (1972), NASA C.R. 2031.

MULLER, A., (1974), Institut fur Hydromechanik und Wasserwirtschaft ETH., Zurich - Ph.D. Thesis.

PAANANEN, R; TANG, C.L. and STATZ, H., (1963), Proc. IEEE 51, p.63.

PINNOW, D.A., (1970), IEEE Jnl. of Quant. Electronics 6(4), p.223.

RAMAN, C.V. and NATH, N.S. (1936), Proc. Ind. Acad. Sc. Sect. A. 3, p.75.

REFERENCES (Continued)

STEENSTRUP, F.V. (1975), DISA Info. No.18, p.21.

SMITS, A.J. (1974), University of Melbourne - Ph.D. Thesis.

WILLARD, G.W. (1949), Jnl.Acoust.Soc.America. 21 p.101.

YEH, Y. and CUMMINS, H.Z. (1964) Appl. Phys. Letters 4 p.176.

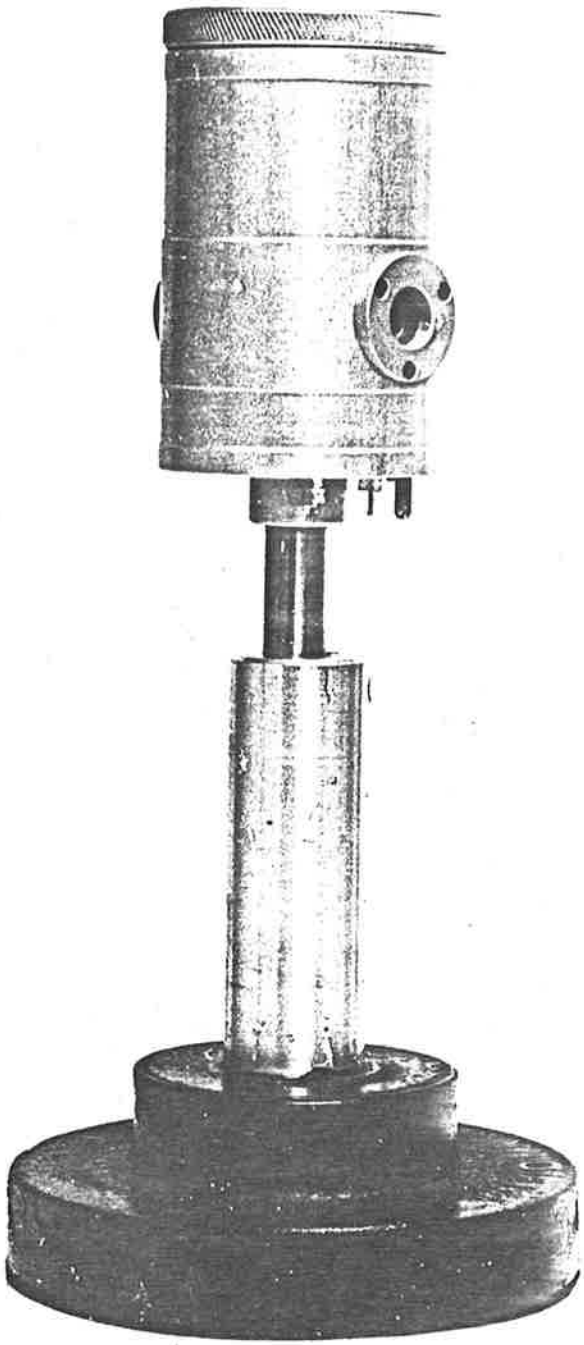

APPENDIX B2 - ACOUSTO - OPTIC CELL

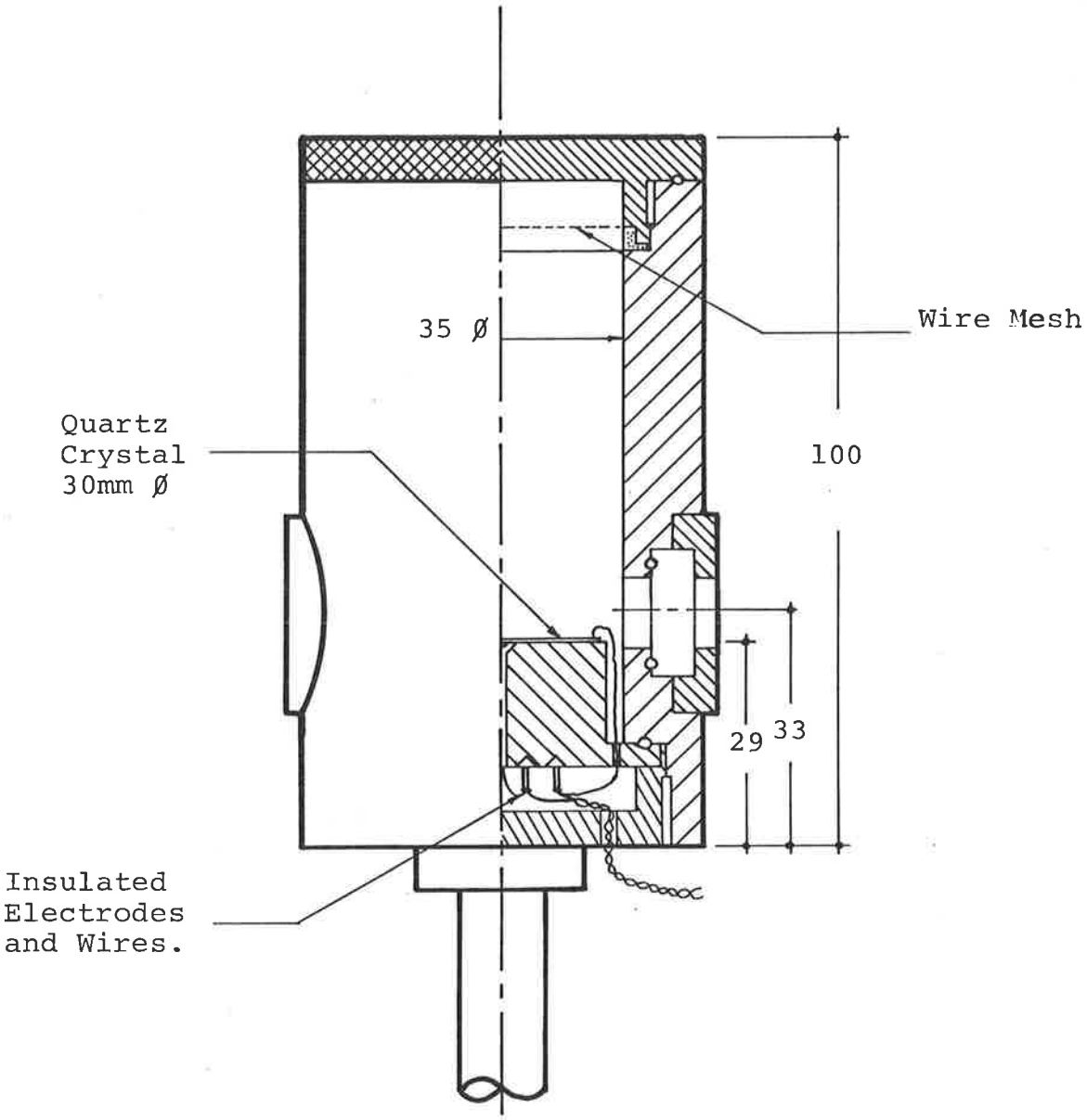

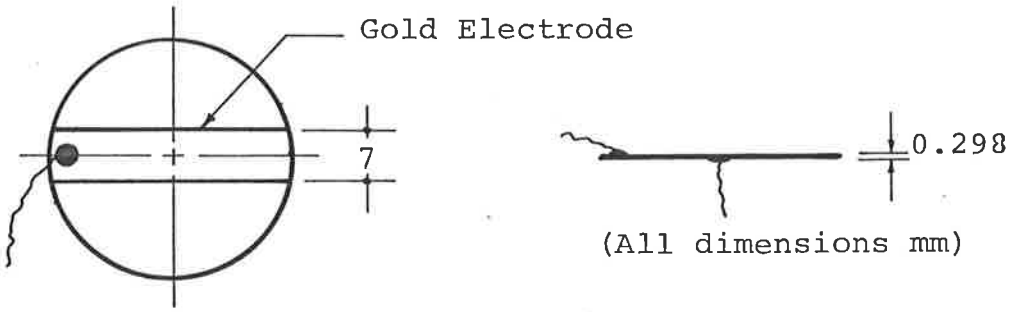

APPENDIX B2

ACOUSTO - OPTIC CELL


LASER DOPPLER VELOCIMETER
N_c

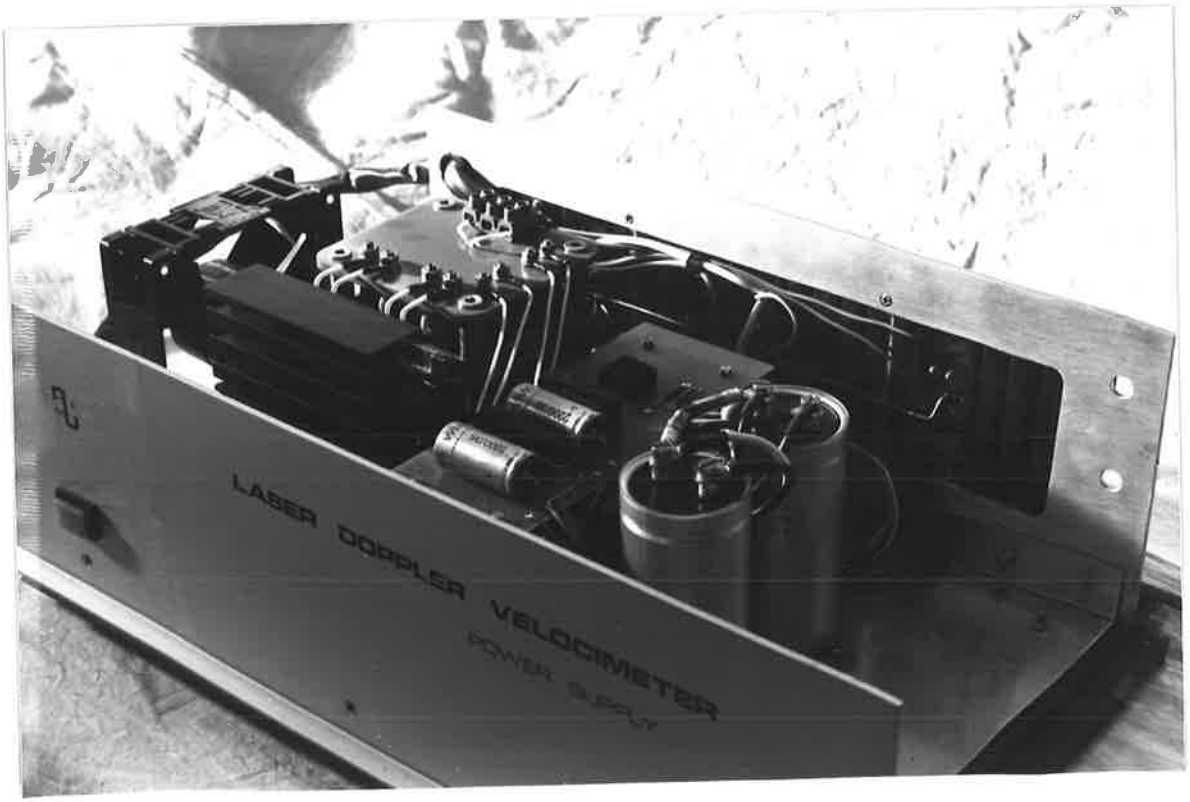
LASER DOPPLER VELOCIMETER
POWER SUPPLY